NTNU

Norwegian University of
Science and Technology

Improved Burst Model for Casing and Tubing Design

Eilen Bauge

Kristian Wilhelmsen

Petroleum Geoscience and Engineering
Submission date: June 2018
Supervisor: Sigbjørn Sangesland, IGP
Co-supervisor: Bjørn Brechan, IGP

Norwegian University of Science and Technology
Department of Geoscience and Petroleum

Summary

Casing and tubing design for burst are performed by requiring a safety margin against yield under internal overpressure. Today's design process uses design limit plots, consisting of Barlow's and the approximate von Mises equation. Embedded in the strength formulas are a wall tolerance factor of 12.5 %, that was introduced in the 1960's due to the inaccuracy in the casing manufacturing process. Unnecessary steel costs are generated by these conservative assumptions and old-fashioned theories. The goal of this thesis was to investigate theories from the literature to develop a more up to date engineering model for designing casing and tubing against burst.

The improved burst model removes Barlow's uniaxial equation, as it was found to obsolete for its theoretical background and for its lack of validity. The approximate von Mises ellipse is replaced with the exact ellipse, to include external pressure. The model also allows the wall tolerance to be specified, as the manufacturing process has improved since the 1960's. Most importantly, ductile rupture is included, to visualise the actual pressure required to rupture the pipe. Comparing the more accurate yield with the limit for loss of pressure integrity, opens up for a much better understanding of the burst tolerance.

The results showed that the ductile rupture formula predicts loss of pressure integrity accurately, when compared to measured rupture pressure. A mean difference and standard deviation of - 0.44 % and 4.48 % respectively, was observed.

The case study performed showed that a shallow water well with a low casing grade resulted in a large plasticity zone. The new design methodology reduced the steel weight from 40 ppf to 36 ppf. For a midwater well, with a small plasticity zone, no weight reduction was recommended. The improved burst model allowed the steel weight to reduce from 59.4 ppf to 53.5 ppf for a deepwater well.

The results from the improved burst model are presented such that the industry can start to implement the cost-saving measures immediately. Before the ductile rupture equation is used, more tests including axial stress and external pressure should be performed.

Sammendrag

Dagens krav til et foringsrørs maksimale burst-trykk er gitt av Barlow og den forenklede von Mises likningen for flyt. En toleranse i veggtykkelsen på 12.5 % er inkludert. Toleransen er basert på 1960-tallets fremstillingsprosess av foringsrør, ettersom datidens veggtykkelse varierte mye. Industristandarden er konservativ for dagens fremstillingsprosess og fører til økte stål kostnader. Målet med denne hovedoppgaven var å undersøke nye teorier fra litteraturen, for å utvikle en mer moderne modell som designer foringsrør mot burst.

I den forbedrede modellen er det mulig å spesifisere maksimal variasjon i veggtykkelse, i henhold til dagens fremstillingsprosess. Dette øker nøyaktigheten i styrkeberegningene. En ny ligning for duktilt brudd er også inkludert i den nye modellen. Ligningen visualiserer nødvendig sprengningstrykk som fører til brudd og dermed tap av trykkintegritet.

Barlow's endimensjonale ligning ble påvist å være mangelfull når det kom til faktiske trykk og spenningsforhold i en brønn. Den nye modellen tar i bruk det nøyaktige von Mises/Lamé-kriteriet for flyt, der industrien i dag bruker en forenklet versjon. Dette sikrer at ytre trykk blir inkludert i beregningene. En bedre forståelse for det faktiske sprengningstrykket til et foringsrør, ble oppnådd ved å plotte resultatene med den nøyaktige flytformelen og bruddformelen sammen.

Bruddtester ble sammenlignet med den duktile bruddformelen. Ligningen stemte best av de undersøkte formlene for sprengningsbrudd, med en gjennomsnittsforskjell og standardavvik på henholdsvis - 0.44 % og 4.48 %.

En studie bestående av tre brønner med forskjellige vanndyp viste et stort forbedringspotensial for foringsrørsdesign. En brønn på grunt vann med lav foringsrør styrke hadde et stort plastisk område. Dermed tillot den nye modellen å redusere stål vekten fra 40 ppf til 36 ppf. For en dypvannsbrønn ble en mulig reduksjon fra 59.4 ppf til 53.5 ppf observert. Brønnen på middels vanndyp fikk en høyere sikkerhetsfaktor, men ingen stålreduksjon ble anbefalt.

Resultatene fra den forbedrede modellen er presentert slik at industrien kan starte med å implementere de kostnadsbesparende tiltakene umiddelbart. For å ta i bruk den duktile

brudd formelen, må flere tester under aksiell spenning og ytre trykk utføres.

Acknowledgment

This thesis is carried out at the Norwegian University of Sciency and Technology (NTNU) at the Department of Geoscience and Petroleum.

We would like to thank our supervisor Bjørn Brechan for valuable inputs and enthusiasm. His experience in the industry gave us an insight to the practical applicability of casing and tubing design. The technical support provided during all stages of this thesis are gratefully appreciated. A special gratitude goes to our other supervisor professor Sigbjørn Sangesland at NTNU, for valuable feedback and good discussions. Last, we would like to thank both our supervisors for their availability and interest.

Contents

Abstract i

Sammendrag ii

Acknowledgment iv

List of Figures **ix**

List of Tables **xiii**

1 Introduction **1**

2 Theory **5**

2.1 Industry Practice 5

2.1.1 Elasticity 5

2.1.2 Deterministic burst model 6

2.1.3 Design Factor 7

2.2 Historical API burst limit 7

2.3 Triaxial yield 9

2.3.1 Triaxial yield criterion without bending and torsion 10

2.3.2 Industry Practice - Triaxial yield 13

2.4 Through-wall yield criterion 17

2.5 ISO - Ductile Rupture 19

2.5.1 Combined Loads - Necking 23

2.5.2 Combined Loads - Wrinkling 24

2.6 Casing Wear with burst 26

3 Wilhelmsen&Bauge - Improved Burst Model **27**

3.1 The Software 28

3.2 User instructions 29

3.2.1 Start - Tab . . . 29
3.2.2 Input Casing properties - Tab . . . 30
3.2.3 Design Factors - Tab . . . 32
3.2.4 Input Load Data - Tab . . . 32
3.2.5 Casing Wear - Tab . . . 34
3.2.6 Design Limit - Tab . . . 34
3.2.7 Minimum Safety Factor - Tab . . . 36
3.2.8 End Design Inputs - Tab . . . 36
3.2.9 End Design Limit Plot - Tab . . . 37
3.2.10 Additional menu options . . . 38

4 Results **39**
4.1 Comparison of models and pipe rupture data . . . 39
4.1.1 ISO models . . . 40
4.1.2 Through-wall yield . . . 40
4.1.3 Performance of ductile rupture in tension . . . 42
4.1.4 Sensitivity analyses . . . 44
4.2 Results - Case study . . . 50
4.2.1 Shallow water (100 m) - Production Casing . . . 51
4.2.2 Midwater (305 m) - Production Casing . . . 53
4.2.3 Deepwater (1524 m) - Production Casing . . . 55
4.3 Casing Wear On The Deepwater Well . . . 57

5 Discussion **59**
5.1 New Design Elements . . . 59
5.2 Case Study . . . 63
5.2.1 Shallow Water . . . 64
5.2.2 Midwater . . . 67
5.2.3 Deepwater . . . 69
5.3 Engineering basis . . . 72

6 Conclusion **75**

7 Further Work **79**

Abbreviation **81**

Nomenclature **82**

Bibliography **87**

A Additional Information **89**

A.1 Thick-walled cylinders 89

A.1.1 Lamé's equation 89

A.1.2 Axial stress 89

B Test Data **91**

B.1 Complete data set of 106 pipe rupture test from ISO 91

B.2 Tresca vs. von Mises 92

C Casing Wear **93**

C.1 Casing Wear 93

C.1.1 Casing Wear Model 93

D Load cases - well information **99**

D.1 Shallow water well 100

D.2 Midwater well 102

D.3 Deepwater well 104

E Burst Load Cases **107**

E.1 Drilling Loads 107

E.1.1 Displacement to Gas 107

E.1.2 Green Cement Test 108

E.1.3 Pressure Test 110

E.2 Production Load 111

E.2.1 Tubing Leak 111

F Through-wall yield **115**

List of Figures

2.1 Stress-strain curve (Kazanowski and Dickson, 2012, 333). 6
2.2 Free body diagram of cylindrical pressure vessel. 8
2.3 The von Mises failure ellipse. Blue part indicates the positive part of the equation, while the red indicates the negative part (Wilhelmsen, 2017, 8). 10
2.4 The von Mises circle limited to burst area. 12
2.5 The exact von Mises ellipse limited to burst area. 13
2.6 Capped-end and open-ended pipe that are free to move axially. 15
2.7 Comparison of capped-end and open-end. 17
2.8 A typical Power law fit to actual stress-strain data to determine n_R (Klever et al., 2010). 22
2.9 Visualisation of necking. 23
2.10 Illustration of wrinkling compared with ductile rupture(ISO/TR, 2007, 27). . . . 25

3.1 Menus and Tabs 29
3.2 Start-Tab 30
3.3 Input Casing Properties-Tab 31
3.4 Input Load Data-Tab 33
3.5 Button group. Screenshot form WellCat. 34
3.6 Casing Wear Factor tab 34
3.7 Design Limit Tab window when von Mises exact ellipse is chosen. 35
3.8 Design Limit Tab window when von Mises industry approximation is chosen. . 35
3.9 Minimum Safety Factor tab 36
3.10 End Design inputs tab 37
3.11 End Design Limit Plot tab 38

4.1 Ductile rupture, Barlow and von Mises burst limits compared with measured rupture pressure from ISO. 40
4.2 Comparison of through-wall yield model performed in Lin et al. (2014). 41
4.3 Ratio of test result to the through-wall yield model with embedded wall reduction factors ($p_{i-TWY_{paper}}$) and without (p_{i-TWY}). 41
4.4 Ductile rupture and reproduced calculation of the through-wall yield model compared with the measured rupture pressure from ISO. 42
4.5 Ductile rupture model compared with test results. 43
4.6 Influence of increasing external pressure on the von Mises failure ellipse for a thin-walled pipe. 44
4.7 A 13 3/8" casing with weight and grade given by 61 ppf and K-55 respectively. The difference between minimum yield strength and ultimate tensile strength = 40 000 psi. 45
4.8 A 13 3/8" casing with weight and grade given by 68 ppf and C-90 respectively. The difference between minimum yield strength and ultimate tensile strength = 10 000 psi. 46
4.9 Percentage difference with and without k_{wall}. 47
4.10 Percentage difference in predicted rupture pressure with and without the recommended ISO value for the hardening index factor ($n_R = 0.1$). 48
4.11 Predicted Rupture Pressures dependence on the burst strength factor (k_a). . . . 49
4.12 Percentage difference in predicted rupture pressure vs. crack depth. 50
4.13 Burst load case from the shallow water example plotted with approximate solution of von Mises and the historical API burst limit in WellCat. The weight and grade were 40 ppf and K-55 respectively. 52
4.14 Burst load case from the shallow water example well plotted with exact solution of von Mises and ductile rupture. The wall tolerance was chosen as 12.5 %. Weight and grade were 36 ppf and K-55 respectively. 52
4.15 Burst load case from the shallow water example well plotted with exact solution of von Mises and ductile rupture. The wall tolerance was chosen as 9.4 %. Weight and grade were 36 ppf and K-55 respectively. 53

4.16 Burst load case from the midwater example well plotted with approximate solution of the von Mises and the historical API burst limit in WellCat. The weight and grade were 58.4 ppf and C-90 respectively. 54
4.17 Burst load case from the midwater example well plotted with exact solution of von Mises and ductile rupture. The wall tolerance was chosen as 6.4 %. Weight and grade were 53.5 ppf and C-90 respectively. 54
4.18 Burst load case from the deepwater example well plotted with approximate solution of the von Mises and the historical API burst limit in WellCat. The weight and grade were 59.4 ppf and C-90 respectively. 56
4.19 Burst load case from the midwater example well plotted with exact solution of von Mises and ductile rupture. The wall tolerance was chosen as 6.4 %. Weight and grade were 53.5 ppf, C-90 and 6.4 % respectively. 56
4.20 The effect of 20 % casing wear on the final deepwater well design. 57
4.21 The effect of 20 % casing wear on the final deepwater well design when the grade was increased to P-110. 58

5.1 Design limit plot for the Wilhelmsen&Bauge model with casing weigh and grade of respectively 40 ppf and K-55. The model has an allowable wall tolerance of 12.5 %. 65
5.2 Design limit plot for the Wilhelmsen&Bauge model with casing weigh and grade of respectively 36 ppf and K-55. The model has an allowable wall tolerance of 12.5 %. 65
5.3 End Design limit plot for the shallow well example. 67
5.4 Design limit plot for the Wilhelmsen&Bauge model with casing weigh and grade of respectively 58.4 ppf and C-90. The model has an allowable wall tolerance of 6.4 %. 68
5.5 Design limit plot for the Wilhelmsen&Bauge model with casing weigh and grade of respectively 58.4 ppf and C-90. The model has an allowable wall tolerance of 12.5 %. 69
5.6 Burst load cases from deepwater example well plotted with approximate von Mises. The weight and grade are 58.4 ppf and C-90 respectively. 70
5.7 Minimum safety factors for the 9 5/8" production casing. Limiting load is green cement test. 70

5.8 Design limit plot for the Wilhelmsen&Bauge model with casing weigh and grade of respectively 58.4 ppf and C-90. The model has an allowable wall tolerance of 12.5 %. 71

B.1 Ductile Rupture, Barlow and von Mises burst limits compared with test results 91
B.2 Percentage difference from actual burst pressure predicted by Tresca criterion, von Mises criterion and an average of both criterion's 92

C.1 Cross-Section of Crescent-Shaped Wear Groove, (Hall Jr et al., 1994, 2) 94
C.2 Casing-wear at dogleg, (Hall Jr et al., 1994, 2) 94
C.3 Undetected dogleg, (Hall Jr et al., 1994, 4) 96

D.1 Well sketch for the shallow water load case 100
D.2 Pore,Mud weight and fracture plot for shallow water load case 101
D.3 Well sketch for the midwater load case 102
D.4 Pore,Mud weight and fracture plot for the midwater load case 103
D.5 Well sketch for the deepwater load case 104
D.6 Pore,Mud weight and fracture plot for the deepwater load case 105

E.1 Displacement to Gas 108
E.2 Green Cement Test 109
E.3 Pressure Test 110
E.4 Tubing Leak below tubing hanger, differential pressure acting on tubing 112
E.5 Tubing Leak below tubing hanger, differential pressure acting on production casing 113

F.1 The ratio of test result to the through-wall yield model presented and the reproduced through-wall yield model. 116

List of Tables

1.1 Overview of models investigated in this thesis. 1

2.1 Design factors 7
2.2 Burst strength factors (k_a) recommended by ISO(ISO/TR, 2007, 23). 18
2.3 Hardening index factors for different casing grades recommended by ISO (ISO/TR, 2007, 22). 22
2.4 API casing grades with their corresponding minimum yield and tensile strength (Bellarby, 2009a, 476). 23

4.1 Input values when the minimum wall thickness is measured. 39
4.2 Statistical evaluation of ISO models. 40
4.3 Test pipe properties(Cernocky, 2005, 11). 43
4.4 Comparison of ductile rupture and test data in tension. 43
4.5 API casing grades with corresponding minimum yield and ultimate tensile strength. 45
4.6 Recommended casing design for shallow water well. 51
4.7 Recommended casing design for midwater load case. 53
4.8 Recommended casing design for deepwater load case. 55

B.1 Statistical evaluation of Tresca, von Mises and the average assumption 92

F.1 Input values used in calculations of the reproduced through-wall yield model . 115

Chapter 1

Introduction

Casing design against burst is related to internal overpressure not surpassing the yield point. This means that the models used today predicts yield, not rupture and loss of pressure integrity. The objective of casing and tubing design is to establish well integrity, which ensures containment, safe operations and profit.

The investigated models in this thesis is summarised in Table 1.1.

Table 1.1: Overview of models investigated in this thesis.

Models	**Assumptions**	**Axis variables**	**Predicts**
Current Industry Practice			
Barlow	Uniaxial	p_i vs F_a	Yield
Approximate von Mises	$p_o = 0$, Lamé	p_i vs F_a	Yield
Wilhelmsen&Bauge Model			
Exact von Mises	Lamé	Δp vs $\sigma_z + p_o$	Yield
ISO Ductile Rupture	Capped-end	Δp vs $\sigma_z + p_o$	Rupture
Other			
Through Wall Yield	Capped-end	p_i vs F_a	Rupture

Today, casing design is performed by using the industry leading software (ILS), where design limit plots and safety factors towards yield are calculated. Design limit plots are graphical representation of the tubulars strength and are plotted as internal pressure vs. axial force for the two upper burst quadrants. Barlow's equation for burst strength is recommended by the American Petroleum Institute (API). Several shortcomings have been identified, the most severe being the lack of ability to take axial stress and external pressure into account. Alongside the industry accepted API equation, the approximate triaxial von Mises yield criterion with Lamé is used in the design limit plot. The major shortcoming being the assumption of zero

external pressure. This assumption causes an inconsistency between the visualised triaxial design limit and the calculated triaxial safety factor, which includes the external pressure. Embedded in the yield formulas used in ILS are also an allowable wall tolerance of 12.5 % of the nominal wall thickness. The tolerance was specified due to the inaccuracy in the manufacturing process in the 1960's. The manufacturing process has improved and the allowable wall tolerance should therefore be updated.

An important aspect with the tubular burst strength is lost by only considering yield. Information regarding the tubulars ability of plastic deformation before rupture and loss of pressure integrity is not a part of the casing design considerations today. Especially two situations could benefit from the knowledge of true rupture. For materials that have a low margin between the yield strength and the ultimate tensile strength, the safety factor against true rupture can be too small. In addition, for materials where the margin between the yield strength and the ultimate tensile strength is large, the safety factor against true rupture can be unnecessary excessive. Therefore, including true rupture in the design process can ensure both a safe and economical design.

Several models for calculating the true burst limit pressure have been proposed to the industry. A few references are listed (Hill, 1998), (Klever et al., 1998), (Lin et al., 2014) and (Klever et al., 2010). The ductile rupture formula provided in ISO:10400, predicts the most accurate rupture pressure.

Another important failure mechanism is brittle failure. This is the dimensional criterion if the formation fluids are corrosive. However, this topic is not the scope of this thesis. Therefore, it is assumed that the pipe material has sufficient toughness in its environment, so that the governing failure mechanism is ductile and not brittle.

The presented industry practice is based on old theories and assumptions. Even though, the standard for casing and tubing design (ISO:10400) was significantly revised in 2007 based on extensive testing of burst and collapse capacity of tubulars. The same software models are used today as before the revision of the standard. Therefore, the objective of this thesis is to investigate the theories in the latest standard and the literature to develop a more up to date

engineering model for designing casing and tubing. The task is limited to burst.

Chapter 2 is meant to give the reader sufficient theory and background knowledge about the industry and the new improved burst model presented, also referred to as the Wilhelmsen&Bauge model. In Chapter 3, the Improved Burst Model software and its features are presented. Chapter 4 describes the obtained results from testing of the improved burst model and of the current industry practice. A sensitivity analysis and results from a case study consisting of three different wells with water depths of 100 m, 305 m and 1524 m are also presented. Chapter 5 presents a discussion on the implications of the results obtained throughout this thesis, as well as the new models applicability. Concluding remarks are presented in Chapter 6, while recommendations for further work are given in Chapter 7.

Chapter 2

Theory

Today's casing and tubing design software uses a combination of one-dimensional and tri-axial theory to calculate the design limit for burst. The most conservative model is dimensioning for the design. Hence, it is essential to understand the theory behind these models and how they are applied in the software, to create a safe and cost-efficient design.

This chapter presents the theoretical background for the current industry practice for burst, together with the resulting formulas for the burst design limits. The following chapter is based on ISO (ISO/TR, 2007, 82-94).

2.1 Industry Practice

2.1.1 Elasticity

As an industry practice, it is established that casing and tubing strings are limited to the elastic stress-strain regime. In example, the design is limit to yield as seen in Figure 2.1. This criterion is used to avoid permanent plastic deformations.

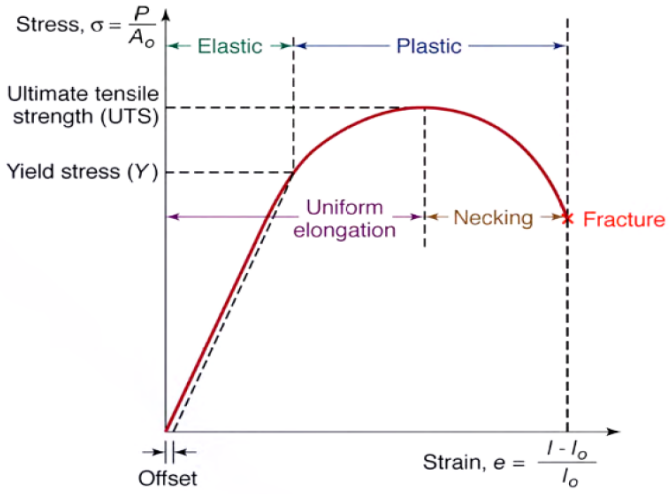

Figure 2.1: Stress-strain curve (Kazanowski and Dickson, 2012, 333).

On the other hand, Figure 2.1 indicates that the actual material strength is greater than the yield strength. How to include this extra plastic strength area in burst design is presented in section 2.4-2.5.2.

2.1.2 Deterministic burst model

Strength design for casing and tubing are mostly based on deterministic models. "A deterministic model assumes that all of the factors are known with absolutely certainty and that the equation used to calculate the strength are exact" (ISO/TR, 2007, 119). The method is favourable in casing and tubing design, as it results in a single, deterministic predicted pressure for each set of input parameters. The deterministic burst limit uses the minimum allowable values for the pipe, in order to ensure a safe value for the expected strength. Accordingly, all of the presented burst models below uses the minimum value for yield strength and wall thickness. The background for the minimum wall thickness used in the industry is described in the section below.

2.1.2.1 Pipe wall reduction factor (k_{wall})

In the 1960's it was difficult to obtain a uniform wall thickness during manufacturing of seamless casings. This is why API and ISO implemented a maximum allowance of 12.5 % in pipe wall thickness, due to manufacturing processes. Consequently, the deterministic burst models presented below have all embedded a wall reduction factor (k_{wall} = 0.875), to account for the minimum allowable wall thickness.

2.1.3 Design Factor

Design factors are applied in casing and tubing design to ensure that the anticipated loads never surpass the yield strength of the pipe. "The definition of a design factor is the minimum acceptable safety factor, where safety factor is given as the component specific yield strength divided by the design load" (Wilhelmsen, 2017, 6). In this thesis the values given in Table 2.1 have been used as design factors.

$$\text{DF} = \text{SF}_{min} \leq \text{SF} = \frac{\text{yield strength}}{\text{design load}}$$

Table 2.1: Design factors

Design Factors	**Casing**	**Tubing**
Burst	1.1	1.1
Tension	1.4	1.2
Compression	1.4	1.2
Triaxial	1.25	1.25
Ductile Rupture	1.25	1.25
Necking	1.25	1.25

2.2 Historical API burst limit

The historical API burst-pressure rating is based on Barlow's one-dimensional equation for pipe yield. The equation can be derived from an isotropic linear elastic model for thin-walled ($D/t > 15\pm$) cylinders. The model is valid under the following conditions (PA, 2013, 185):

- the material is isotropic
- the strains resulting from the pressures are small
- the wall thickness of the pressure vessel is much smaller than the diameter

The model evaluates the tangential stress from an equilibrium analysis of the free body diagram in Figure 2.2.

$$-\sigma_\theta 2tL + dLp_i = 0 \tag{2.1}$$

Which gives

$$\sigma_\theta = \frac{p_i d}{2t} \tag{2.2}$$

$$p_i = 2\frac{\sigma_\theta t}{d} \tag{2.3}$$

The current industry practice uses the outer diameter instead of the inner diameter, to increase the safety factor towards yield. This reduces equation (2.3) to equation (2.4).

$$p_i = 2\frac{\sigma_\theta t}{D} \tag{2.4}$$

where

σ_θ = tangential stress for a thin-walled cylinder
L = length
t = nominal wall thickness
p_i = inner pressure
D = outside diameter

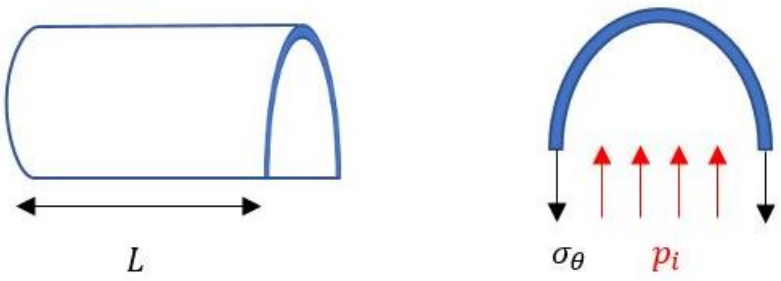

Figure 2.2: Free body diagram of cylindrical pressure vessel.

Barlow's equation calculates the internal pressure that makes the tangential stress equal to the minimum yield strength for a thin-walled pipe. The API burst pressure rating also adds a reduction factor to account for the maximum allowable pipe wall tolerance. By inserting $\sigma_\theta = \sigma_{y,min}$ and $t_{min} = k_{wall}t$ into equation (2.4), the deterministic API burst-pressure rating becomes (ISO/TR, 2007, 93)

$$p_{iAPI} = \frac{2\sigma_{y,min}k_{wall}t}{D} \tag{2.5}$$

where

k_{wall} = pipe wall reduction factor ($k_{wall} = 0.875$)

$\sigma_{y,min}$ = minimum yield strength

p_{iAPI} = internal pressure at yield for a thin pipe

Equation (2.5) is the API recommended approach for estimating the burst pressure limit for tubulars and the approach is still in use today. The recommended burst limit is only valid for zero axial stress and external pressure.

2.3 Triaxial yield

The triaxial yield criterion is based on the von Mises equivalent stress equation, where the radial and tangential stress are expressed by Lamé's elastic equation (A.1) for a thick-walled cylinder. The equivalent stress is given by (ISO/TR, 2007, 84)

$$\sigma_e = \sqrt{\sigma_r^2 + \sigma_\theta^2 + (\sigma_z + \sigma_b)^2 - \sigma_r\sigma_\theta - \sigma_r(\sigma_z + \sigma_b) - \sigma_\theta(\sigma_z + \sigma_b) + 3\tau^2} \tag{2.6}$$

where

σ_e = equivalent stress

σ_r = radial stress

σ_θ = tangential stress

σ_z = axial stress

σ_b = bending stress

τ = torsional stress

Tubulars are in the elastic stress regime when the equivalent stress is lower than the yield strength, $\sigma_e < \sigma_y$. Onset of yield is reached when the equivalent stress equals the yield strength, $\sigma_e = \sigma_y$.

By substituting σ_e with σ_y in equation (2.6), onset of yield for a thick-walled cylinder is calculated.

$$\sigma_y = \sqrt{\sigma_r^2 + \sigma_\theta^2 + (\sigma_z + \sigma_b)^2 - \sigma_r\sigma_\theta - \sigma_r(\sigma_z + \sigma_b) - \sigma_\theta(\sigma_z + \sigma_b) + 3\tau^2} \tag{2.7}$$

The von Mises failure criterion is often represented as an ellipse. By solving equation (2.7) for $\frac{\sigma_\theta - \sigma_r}{\sigma_y}$ results in the quadratic equation

$$\frac{\sigma_\theta - \sigma_r}{\sigma_y} = \pm\sqrt{1 - \frac{3}{4}\left(\frac{\sigma_z - \sigma_r}{\sigma_y}\right)^2} + \frac{1}{2}\frac{\sigma_z - \sigma_r}{\sigma_y} \tag{2.8}$$

Plotting equation (2.8) results in the von Mises ellipse given in Figure 2.3.

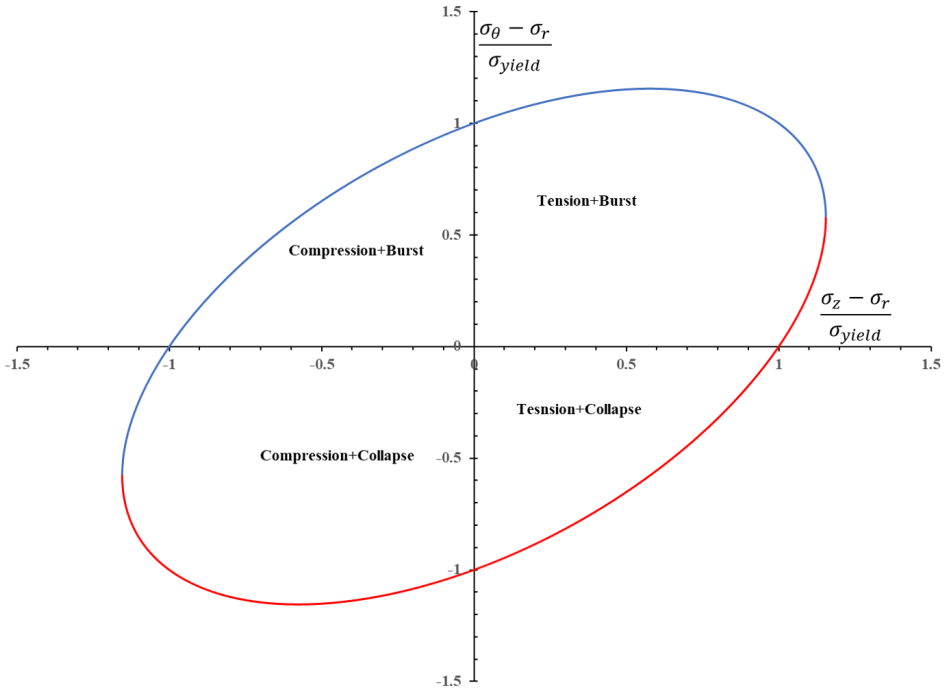

Figure 2.3: The von Mises failure ellipse. Blue part indicates the positive part of the equation, while the red indicates the negative part (Wilhelmsen, 2017, 8).

2.3.1 Triaxial yield criterion without bending and torsion

Equation (2.7) reduces to the following when both bending and torsion are zero

$$\sigma_y = \sqrt{\sigma_r^2 + \sigma_\theta^2 + \sigma_z^2 - \sigma_r\sigma_\theta - \sigma_r\sigma_z - \sigma_\theta\sigma_z} \tag{2.9}$$

Yield will always occur at the inner wall (r = r_i) in the absence of bending and torsion. Inserting Lamé's equation for radial and tangential stress (A.1) at the inner wall, into equation (2.9) results in

$$\sigma_y^2 = \left[\sigma_z - \frac{p_i d^2 - p_o D^2}{D^2 - d^2}\right]^2 + 3\left[\frac{(p_i - p_o)D^2}{D^2 - d^2}\right]^2 \tag{2.10}$$

where

p_o = outer pressure

d = inner diameter; d = D-2t

From this point forward equation (2.10) will be referred to as the exact von Mises equation. The exact von Mises equation can be graphical represented as both a circle and an ellipse.

2.3.1.1 Exact triaxial yield criterion with Lamé - Circle

The circle representation can be performed by expressing the exact von Mises equation in terms of the effective stress, σ_{eff}. The equation is given by (ISO/TR, 2007, 88)

$$\sigma_y^2 = \sigma_{eff} + \frac{(p_i - p_o)^2 D^4}{(D^2 - d^2)^2} \tag{2.11}$$

where

$$\sigma_{eff} = \sigma_a - \frac{p_i d^2 - p_o D^2}{D^2 - d^2} \tag{2.12}$$

The exact triaxial yield criterion can then be graphical represented by a circle, where the axis are given by

$$X_{circle} = \frac{\sigma_{eff}}{\sigma_y} \tag{2.13}$$

$$Y_{circle} = \sqrt{3}\frac{D^2}{D^2 - d^2}\frac{p_i - p_o}{\sigma_y} \tag{2.14}$$

resulting in the circle equation

$$1 = X_{circle}^2 + Y_{circle}^2 \tag{2.15}$$

Plotting equation (2.15) results in the von Mises circle given in Figure 2.4.

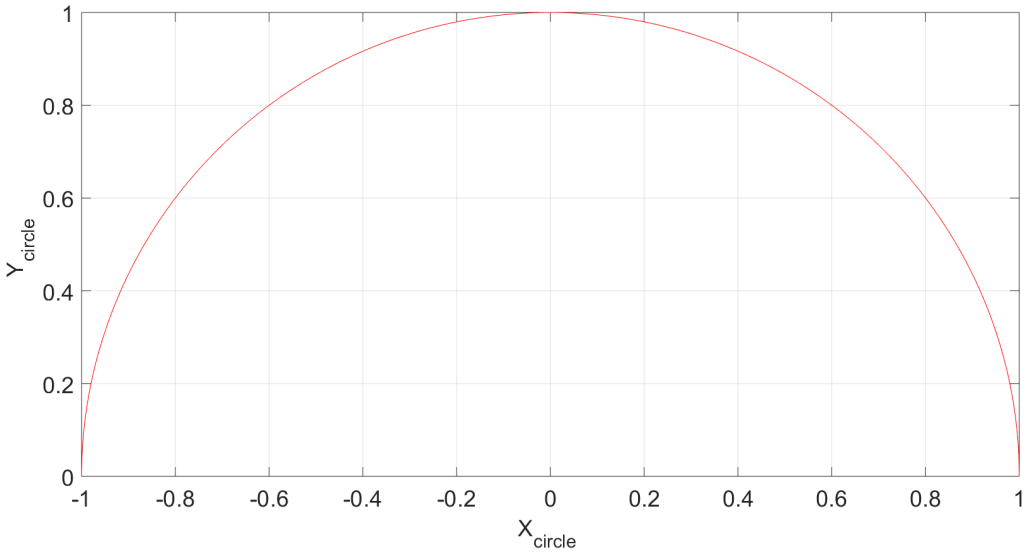

Figure 2.4: The von Mises circle limited to burst area.

The exact von Mises circle can show load cases relative to the von Mises yield criterion from an entire well, since the axis are dimensionless. Therefore, the final casing design for the whole well can be represented in a single plot.

2.3.1.2 Exact triaxial yield criterion with Lamé - Ellipse

The exact von Mises representation, equation (2.10) can be solved for the differential pressure, $\Delta p = p_i - p_o$. The differential pressure is given by (Hall et al., 8)

$$\Delta p = \frac{r_o^2 - r_i^2}{2r_o^2}\left[\left(\sqrt{\frac{1}{j} - \frac{0.75}{j^2}\left(\frac{\sigma_z + p_o}{\sigma_y}\right)^2} + 0.5\frac{k}{j}\frac{\sigma_z + p_o}{\sigma_y}\right)\sigma_y\right] \tag{2.16}$$

where

$$\begin{aligned} j &= \frac{3 + k^2}{4} \\ k &= \frac{r_i^2}{r_o^2} \end{aligned} \tag{2.17}$$

r_i = inner radius

r_o = outer radius

The exact triaxial yield criterion can then be graphical represented by an ellipse, where the axis are given by

$$X_{ellipse} = \sigma_z + p_o \tag{2.18}$$

$$Y_{ellipse} = \Delta p \tag{2.19}$$

Plotting equation (2.16) results in the exact von Mises ellipse given in Figure 2.5.

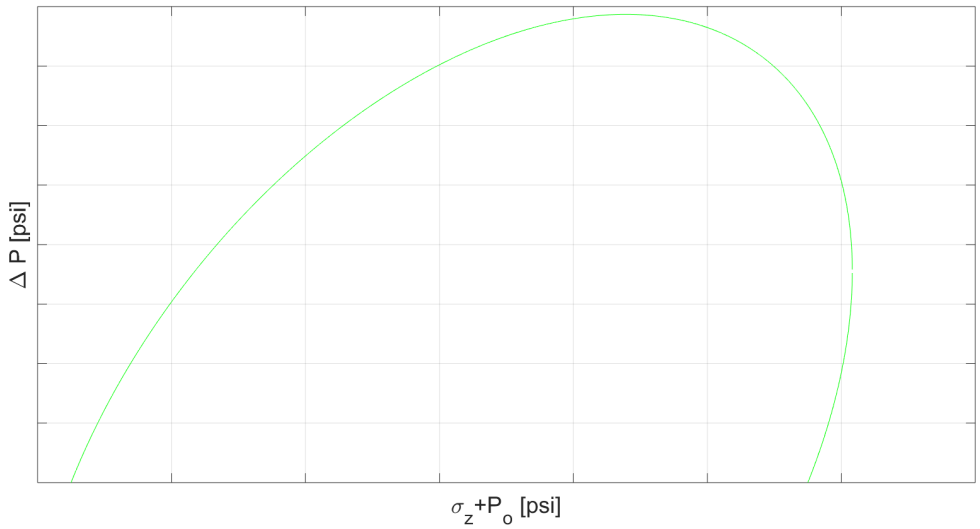

Figure 2.5: The exact von Mises ellipse limited to burst area.

The exact von Mises ellipse can only show load cases relative to the von Mises yield criterion for one casing or tubing string at the time. The reason is that the y-axis is dependent on specific pipe parameters. Therefore, the final casing design for the whole well must be presented in individual plots for each pipe.

2.3.2 Industry Practice - Triaxial yield

The current triaxial design ellipse used in casing and tubing design are constructed from a simplified version of the von Mises triaxial yield criterion. For the top burst part of the ellipse the external pressure is assumed zero, while the internal pressure is assumed zero for the lower collapse part. The approximate solution for the top burst part are found by setting the external pressure equal to zero in equation (2.9). The difference in predicted burst strength for the approximate and exact triaxial solution is given in Figure 4.6.

The approximate ellipse can be plotted together with Barlow's equation, as the axis-variables are the same. The exact von Mises ellipse does not have this possibility, because the axis differs as seen in Table 1.1.

2.3.2.1 Deterministic triaxial yield criterion

The current industry practice uses a deterministic triaxial yield criterion, section 2.1.2. The deterministic model can be derived for the von Mises criterion from the following steps:

1. Account for minimum wall thickness due to manufacturing processes in Lamé's equations for radial and tangential stress (A.1).
   (a) Replace t with k_{wall}t
2. Insert the minimum value for the yield strength.
   (a) Replace σ_y with $\sigma_{y,min}$

The deterministic triaxial yield criterion are presented under open-end and capped-end conditions in (ISO/TR, 2007, 90). Below are a list explaining when the different conditions are valid.

1. Open-end
   (a) Zero axial stress
2. Capped-end
   (a) Closed-end with axial stress due to internal pressure acting on the end cap

Both of the presented conditions are only valid for pipes that are free to move axially, as illustrated in Figure 2.6.

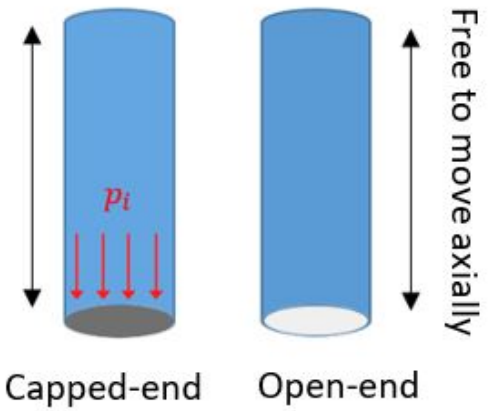

Figure 2.6: Capped-end and open-ended pipe that are free to move axially.

For the capped-end conditions to be valid, one end of the pipe must be free to move in relation to the other end. Normally, this condition only applies to the casing when the top wiper plug is bumped during cementing. After the cementing operations the casing has fixed ends, by the wellhead at top and the cement at bottom (Byrom, 2015).

The derivation of the different formulas and their assumptions is explained step wise for the two conditions. In the end, a comparison of the two formulas without axial stress is presented.

1. Open-end conditions

Internal pressure at yield for an open-end pipe when external pressure, axial stress, bending and torsion equal zero can be derived from the following steps:

1. Set $\sigma_z = 0$ (open-ends conditions)
2. Set $p_o = 0$ in equation (2.10)
3. Insert minimum values as specified in section 2.3.2.1

The equation is given by (ISO/TR, 2007, 92)

$$p_{iYOE} = \frac{\sigma_{y,min}(D^2 - d_{wall}^2)}{\sqrt{3D^4 + d_{wall}^4}} \tag{2.20}$$

where

p_{iYOE} = internal pressure at yield for an open-end thick pipe

d_{wall} = inside diameter based on k_{wall}t; d_{wall} = D-2k_{wall}t

2. Capped-end conditions

The internal pressure at yield for a capped-end pipe when external pressure, bending and torsion equal zero can be derived from the following steps:

1. Set $p_o = 0$ in equation (2.10)
2. Insert minimum values as specified in section 2.3.2.1

The difference from open-end condition is the additional axial stress that is generated by the internal pressure acting on the ends of the sample. The equation is given by (ISO/TR, 2007, 91)

$$p_{iYCE} = \frac{\sigma_{y,min}}{\sqrt{\frac{3D^4+d_{wall}^4}{(D^2-d_{wall}^2)^2} + \frac{d^4}{(D^2-d^2)^2} - \frac{2d^2d_{wall}^2}{(D^2-d^2)(D^2-d_{wall}^2)}}} \tag{2.21}$$

where

p_{iYCE} = internal pressure at yield for a capped-end thick pipe

Comparison of capped-end and open end conditions

Lamé's/von Mises equation for open-end (2.20) and capped-end condition (2.21) are compared in Figure 2.7. The difference between the two equations are plotted as a percentage

$$\frac{p_{iYOE} - p_{iYCE}}{p_{iYCE}} * 100\%$$

Two significant results are observed for the given range of diameter to thickness ratio:

- A pipe with capped-end conditions predicts a higher internal pressure resistance than for an open-ended pipe.
- The difference between the predicted pressure limits are less than 12 % for the range of D/t-ratios typical of oil field tubulars, e.g. $D/t \geq 4.9$ (ISO/TR, 2007, 93).

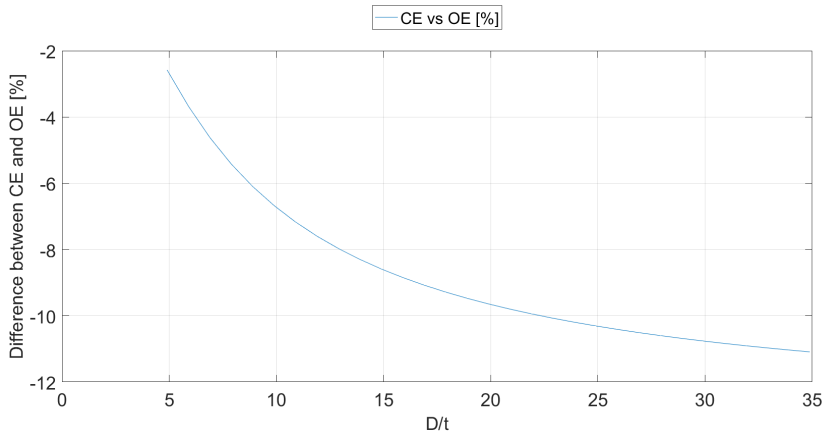

Figure 2.7: Comparison of capped-end and open-end.

2.4 Through-wall yield criterion

The previous presented strength models in section 2.2-2.3 are based on that yield on the inner surface of the pipe causes failure, even though the cross-sectional area of the pipe is still in an elastic state and capable of carrying loads. Therefore, these failure criterion's does not result in loss of pressure integrity or initiation of permanent plastic deformation.

As the internal pressure increases and the stresses on the inside of the casing wall surpasses the yield strength, a plastic region will be formed. The plastic region will increase with increasing internal pressure and when the whole wall has reached a plastic state, a plastic limit load can be obtained. In the paper presented by Lin et al. (2014) a new burst strength model is proposed based on yield through the whole casing wall. Equation (2.22) is derived from equilibrium equation of plastic mechanics, Lamé's equation for thick-walled cylinders and the twin shear unified strength theory.

$$p_{iR-New} = \frac{4}{3}\sigma_y ln(\frac{D}{d}) \tag{2.22}$$

where

d = inner diameter; d = (D-2t)

p_{ir-New} = internal pressure for through-wall yield

Considering the acceptable manufacturing variations in wall thickness (k_{wall}) and the maximum depth of a crack-like imperfection that could reasonably be missed by the pipe inspec-

tion system, the equation for inner diameter becomes

$$d = D - 2(tk_{wall} - k_a a_N) \tag{2.23}$$

where

a_N = maximum depth of a crack-like imperfection

k_a = burst strength factor

The information required in the equations given above are normally not listed in most published material for pipes. The factor a_N accounts for imperfect depth associated with a specified inspection threshold. Meaning the maximum depth of a crack-like imperfection that could reasonably be missed by the pipe inspection system. This value depends on the inspection system, but in this report a 2.5% imperfection threshold of the average thickness is chosen as reasonable ($a_N = 0.025 \times t$).

The burst strength factor is directly related to the material toughness. When a crack of size a_N is present in a casing, the limiting pressure will be altered. How much a crack will decrease the predicted pressure is dependent upon the material toughness of the casing steel. Higher materiel toughness yields a lower burst strength factor, causing a higher rupture pressure.

The burst strength factor (k_a) can be determined through testing. In this report the following ISO recommended values have been used for unknown material, quenched and tempered (Q&T) and chrome (Cr) tubulars.

Table 2.2: Burst strength factors (k_a) recommended by ISO(ISO/TR, 2007, 23).

Pipe Material	k_a **-value**
Unknown	2
Q&T	1
13Cr	1

Equation (2.22) uses the yield strength to calculate the burst strength. This is not representative for all cases as "the real tubing and casing wall will undergo the hardening stage and large plastic deformation from inner wall yield to whole wall yield (Lin et al., 2014, 4)". Hence, the flow stress are recommended to use instead of the yield strength. Analysis of the proposed empirical formulas for the flow stress (2.24) indicates that the ratio of yield to tensile strength

has a large influence on the burst strength (Lin et al., 2014). The flows stress equations are given by (Lin et al., 2014, 4)

$$\begin{aligned}\sigma_f &= 1.1\sigma_y \\ \sigma_f &= \sigma_y + 10(kpsi) \\ \sigma_f &= \sigma_y + 0.8(\sigma_{uts} - \sigma_s) \\ \sigma_f &= \frac{\sigma_{uts} + \sigma_y}{2}\end{aligned} \tag{2.24}$$

From this a new burst strength model is proposed for capped-end conditions by considering the ratio of yield to tensile strength, manufacturing imperfections, crack defects, material hardening and hardness increase under plastic deformation. The new burst strength formula is given by (Lin et al., 2014, 4)

$$p_{iR-New} = \begin{cases} \frac{4}{3}\sigma_f ln(\frac{R}{r}), & \sigma_f = \sigma_y,\ 0.8 \leq \frac{\sigma_y}{\sigma_{uts}} \leq 1, \\ \frac{4}{3}\sigma_f ln(\frac{R}{r}), & \sigma_f = \sigma_y + 10(kpsi),\ 0 \leq \frac{\sigma_s}{\sigma_{uts}} \leq 0.8. \end{cases} \tag{2.25}$$

2.5 ISO - Ductile Rupture

The equations used in the industry today uses yield as the failure criteria. It is doubtful that tubular casing strings rupture when yield is reached. "If the casing material were perfectly plastic, it would quickly yield all the way through the wall thickness as the pressure is increased and rupture, but that is not the way most tubulars behave" (Byrom, 2015, 156). This means that a casing could in theory handle more load than predicted by Barlow's equation (2.5) and von Mises criteria (2.6).

The ductile rupture model (ISO/TR, 2007) created by Klever and Steward predicts rupture and loss of pressure integrity. The model is based on both the von Mises and Tresca plasticity failure models. The von Mises model is known to overpredict the burst pressure limit by 7 %, while the Tresca model underpredict the limit by 8 %, see Table B.1. The model suggest that the burst differential pressure limit should be chosen as the minimum of equation (2.27) based on the von Mises model and the average of equation (2.27) and (2.34). The latter equation is based on Tresca plasticity failure model.

The ductile rupture equation under combined loads (ISO/TR, 2007, 26) is given by:

$$\Delta p_{iRa} = \min\left[\frac{1}{2}(p_M + p_{ref,t}), p_M\right] \tag{2.26}$$

with

$$p_M = p_{ref,M}\left[1 - k_R\left(\frac{F_{eff}}{F_{uts}}\right)^2\right]^{\frac{1}{2}} \tag{2.27}$$

$$F_a = \pi t\,(D-t)\,\sigma_a \tag{2.28}$$

$$F_{eff} = F_a + p_o \pi t\,(D-t) - \frac{\pi p_M t\,(D-t)\,[D-2(k_{wall}t - k_a a_N)]^2}{4\,[(k_{wall}t - k_a a_N)\,(D - k_{wall}t + k_a a_N)]} \tag{2.29}$$

$$F_{uts} = \pi t\,(D-t)\,f_{umn} \tag{2.30}$$

$$p_{uts} = 2 f_{umn}\frac{k_{wall}t - k_a a_N}{D - (k_{wall}t - k_a a_N)} \tag{2.31}$$

$$p_{ref} = \frac{1}{2}\left(p_{ref,M} + p_{ref,T}\right) \tag{2.32}$$

$$p_{ref,M} = \left(\frac{2}{\sqrt{3}}\right)^{1+n_R}\left(\frac{1}{2}\right)^{n_R} p_{uts} \tag{2.33}$$

$$p_{ref,T} = \left(\frac{1}{2}\right)^{n_R} p_{uts} \tag{2.34}$$

$$k_R = \frac{4^{1-n_R} - 1}{3^{1-n_R}} \tag{2.35}$$

where

p_M	=	von Mises pressure
$p_{ref,T}$	=	Tresca pressure
F_a	=	axial force
f_{umn}	=	minimum tensile strength
F_{eff}	=	effective axial load
n_R	=	hardening index for rupture

"The dimensionless hardening index (n_R) is a measure of the ability of a metal to strain harden; the larger its magnitude, the greater the strain hardening for a given amount of plastic strain" (Rethwisch, 2008, 262). It is determined based on stress-strain information Klever et al. (2010). Actual stress-strain tests of the tubular in question is needed to determine n_R by curve fitting (Figure 2.8). Equation (2.38) is fitted to the 2-10% strain range. A material with a hardening index of 0 describes a perfectly plastic material. A value of 1 indicates a perfectly

elastic material.

The equation used to curvefit the dimensionless hardening index is given by:

$$\epsilon = \ln(1 + \epsilon_{eng}) \tag{2.36}$$

$$\sigma = e^{\epsilon}\sigma_{eng} \tag{2.37}$$

$$\sigma = C\epsilon^{n_R} \tag{2.38}$$

when

$$C = \left(\frac{e}{n_R}\right)^{n_R}\sigma_{uts} \tag{2.39}$$

where

σ = stress
σ_{eng} = engineering stress
σ_{uts} = ultimate tensile strength
ϵ = strain
ϵ_{eng} = engineering strain
e = Eulers number

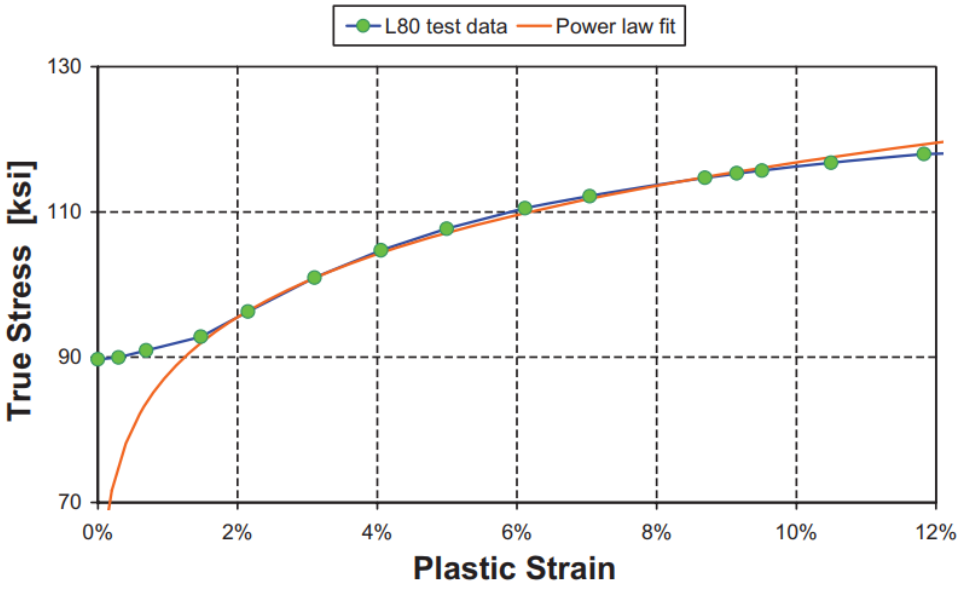

Figure 2.8: A typical Power law fit to actual stress-strain data to determine n_R (Klever et al., 2010).

Stress-strain information is often not available for all tubulars. In these cases ISO (ISO/TR, 2007) recommends the values given in Table 2.3.

Table 2.3: Hardening index factors for different casing grades recommended by ISO (ISO/TR, 2007, 22).

API grade	n_R**-value**
H40	0,14
J55	0,12
K55	0,12
M65	0,12
N80	0,10
L80 Type 1	0,10
L80 Chrome	0,10
C90	0,10
C95	0,09
T95	0,09
P110	0,08
Q125	0,07

Alternatively the hardening index factor can be determined from the correlation:

$$n_R = 0.1693 - 8.12 \times 10^{-7} \sigma_y \tag{2.40}$$

The tensile strength could be measured by testing, or the minimum tensile strength for standard API casings could be used in the model. The latter is more conservative, but due to

absence of proper tests, Table 2.4 given below has been used throughout this thesis.

Table 2.4: API casing grades with their corresponding minimum yield and tensile strength (Bellarby, 2009a, 476).

	Yield Stress		
API Grade	**Minimum [psi]**	**Maximum [psi]**	**Minimum Ult. Tensile [psi]**
H-40	40 000	80 000	60 000
J-55	55 000	80 000	75 000
K-55	55 000	80 000	95 000
N-80	80 000	110 000	100 000
L-80	80 000	95 000	95 000
C-90	90 000	105 000	100 000
C-95	95 000	110 000	105 000
T-95	95 000	110 000	125 000
P-110	110 000	140 000	125 000
Q-125	125 000	150 000	135 000

2.5.1 Combined Loads - Necking

When the tensile stress surpasses the ultimate tensile strength of a ductile material, the cross-sectional area decreases in a localised region of the pipe, Figure (2.9). This phenomenon is called necking and presents the governing failure mechanism for higher values of effective axial tension. The necking region in a stress-strain curve can be seen in Figure 2.1.

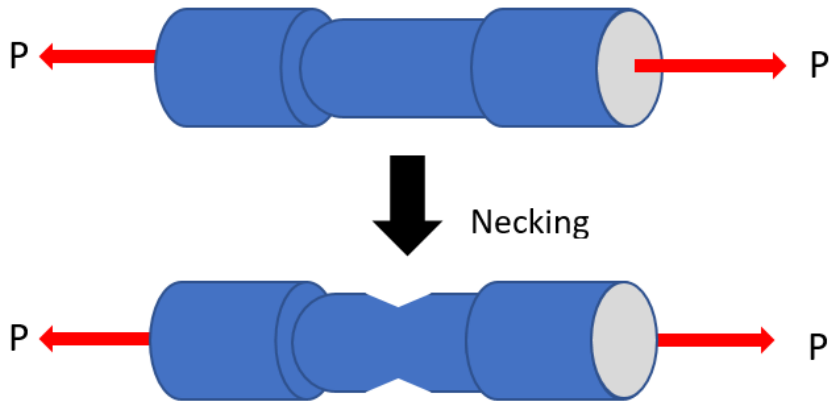

Figure 2.9: Visualisation of necking.

The equation for ductile necking is given by (ISO/TR, 2007, 100)

$$F_{eff} = F_{UTS}\left[1 - k_N\left(\frac{p_i - p_o}{p_{refM}}\right)^2\right]^{\frac{1}{2}} \tag{2.41}$$

where

$$k_N = 4^{(1-n_R)} - 3^{(1-n_R)} \tag{2.42}$$

Boundary between rupture and necking

The boundary between rupture and necking is found by comparing equation (2.26) and equation (2.41). Necking is the dominant failure criterion when (ISO/TR, 2007, 102)

$$\frac{F_{eff}}{F_{UTS}} \geq \frac{3}{2}\frac{p_i - p_o}{p_{UTS}} \tag{2.43}$$

whereas rupture would be the dominant failure criterion with loads below this limit.

2.5.2 Combined Loads - Wrinkling

The second quadrant in Figure 2.3 is comprised of a burst loading in combination with axial compression. For a relatively thick-walled tubular experiencing compression, local buckling or wrinkling can be the governing failure mechanism. Depending on burst and axial compression, the tubular may rupture or wrinkle.

The rupture/wrinkling interaction equation is given by (Klever et al., 2010, 840)

$$\Delta p_{RW} = \min\left[\frac{1}{2}(p_{MRW} + p_{ref,t}), p_{MRW}\right] \tag{2.44}$$

with

$$\Delta p_{MRW} = \frac{2}{\sqrt{3}^{1+n_R}} p_{uts}\sqrt{1 - c_1\left(\frac{F_{eff}}{F_y}\right)^2} \tag{2.45}$$

$$c_1 = \left(\frac{\sigma_y}{e^{f_W} E f_w n_W}\right)^{2n_W} \tag{2.46}$$

$$f_W = \frac{4t}{3(D-t)\sqrt{n_W}} \tag{2.47}$$

$$F_y = \pi t(D-t)\sigma_y \tag{2.48}$$

where

Δp_{RW}	=	differential pressure limit for wrinkling
Δp_{MRW}	=	von Mises differential pressure for wrinkling
F_y	=	yield load
E	=	Youngs Modulus
n_W	=	hardening index for wrinkling

The hardening index (n_W) is curvefitted to the lower strain range in actual stress-strain tests (Uniaxial tensile strength tests). For the axial compression range it can be observed from Figure 2.10, that equation (2.26) is conservative compared to (2.44).

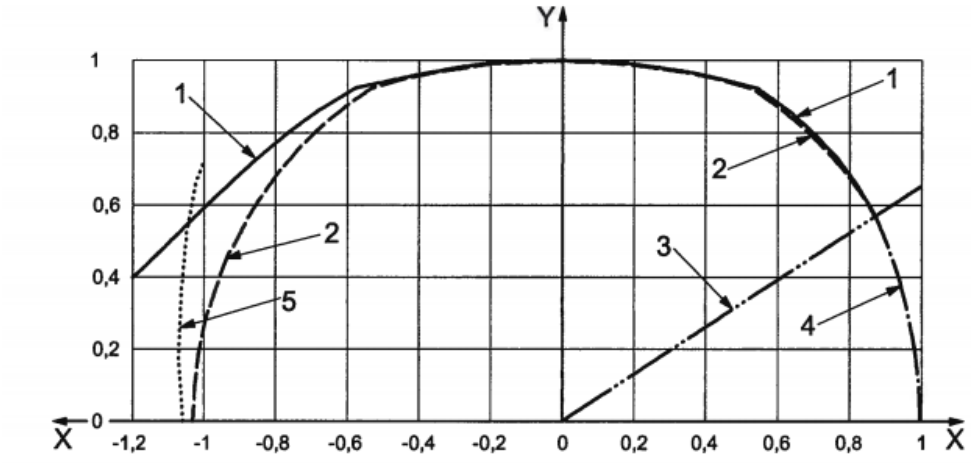

Figure 2.10: Illustration of wrinkling compared with ductile rupture(ISO/TR, 2007, 27).

where

X effective axial tension (F_{eff}/F_{UTS})

Y pressure differential $(p_i - p_o)/p_{ref}$)

1 rupture (exact)

2 rupture (2.26)

3 transition

4 necking (2.41)

5 wrinkling (2.44)

2.6 Casing Wear with burst

A precise casing-wear model is important for well integrity and can improve cost efficiency in casing and tubing design. A model that defines casing wear as the crescent-shape groove that is formed by a rotating tool joint on the inside of the casing wall is given in Appendix C.

Calculating casing wear is not the topic of this thesis, but rather how to include the wear percentage in the improved burst model presented in chapter 3. The paper "Integration of Casing Wear in Casing Design and Stress Analysis Workflow" (Rosland, 2017, 7) proposes the following to include the wear percentage:

$$CW_B = \frac{CW}{100} \times k_{wall} \tag{2.49}$$

where

CW_B = new wall reduction [-]

CW = thickness reduction from casing wear [%]

In effect, the pipe wall reduction factor (k_{wall}) should be replaced by CW_B in the respective models, to account for additional wall loss due to casing wear.

Chapter 3

Wilhelmsen&Bauge - Improved Burst Model

The improved burst model presented in this thesis can improve the design process, by reducing costs and still ensure high safety. The four main elements in the model are

1. **Remove Barlow's equation**

   Barlow's equation was found to obsolete for its theoretical background and for its lack of validity.

2. **Exact von Mises ellipse**

   The model suggest replacing the industry approximate ellipse used in the design limit plot today with the exact von Mises ellipse. This allows external pressure to be included. In addition, this allows the calculated triaxial safety factor to correspond with the triaxial design limit plot.

3. **Pipe wall reduction factor (k_{wall})**

   The model allows the wall tolerance to be specified, as the manufacturing process has improved since the 1960's. Instead of applying the industry practice of 12.5 %, this thesis investigates the implication of a reduction in wall tolerance to 9.4 % and 6.4 %.

4. **Ductile Rupture**

   Ductile rupture is included to visualise the differential pressure necessary to reach rupture and loss of pressure integrity. This allows the engineer to understand the safety margins embedded in the yield formulas. The formula can also be used to ensure appropriate safety factors for different types of wells.

The model includes the industry practice, with Barlow and the approximate von Mises ellipse as well. This is to allow the improved burst model to be compared with the industry practice and to visualise their differences.

It should be noted that the developed model does not include bending and torsional stress in the calculations. Thus, the exact von Mises equation (2.10) is the basis for all calculations regarding the triaxial crtierion in the improved burst model.

3.1 The Software

The ductile rupture equation and von Mises (exact solution) together with the current industry practice has been compiled into a computer software in the app designer environment of MATLAB. The goal has been to make the software as user-friendly and WellCat compatible as possible. WellCat is an ILS often used in current industry practice. The computer software takes tubular properties such as weight, grade, thickness and diameter into account in order to generate the design envelopes for burst in accordance with the improved burst model and the industry practice. Different from WellCat is the option for ductile rupture design limits and exact design limit plots with the von Mises criterion. The exact von Mises can be represented as an ellipse or circle.

The software has the ability to take load lines exported from WellCat (v5000.14) and plot the loads on a design limit plot for both the improved burst model and the industry practice. The improved burst model makes it possible to compare limits and perform casing design on a more realistic basis in regards to true rupture of a tubular casing string. As wrinkling is less conservative than ductile rupture (Figure 2.10), equation (2.44) is not included in the model.

To be able to plot the ductile rupture design limit plot, several properties are needed in order to calculate successfully. Apart from the regular tubular properties, the minimum tensile strength, a burst strength factor (k_a) and a hardening index factor (n_R) must be defined.

The model and software are created as an extension to WellCat. In order to use the software, load cases needs to be simulated in WellCat, and first then can the software be taken into use

in the casing design process.

3.2 User instructions

This section contains a guide for how to use the new software. The software is divided into several tabs and it is recommended to work through the software tab by tab, starting from left to right. The user instruction given below explains each tab separately, starting from the left.

The tabs are named Start, Input Casing Properties, Design Factors, Input Load Data, Casing Wear, Design Limit, Minimum SF, End Design Inputs and End Design Limit Plot. Above the tabs is a menu line as seen in Figure 3.1.

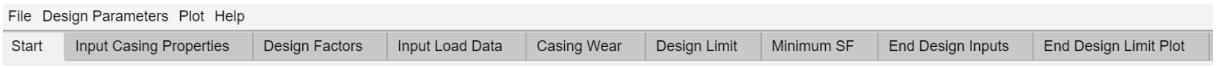

Figure 3.1: Menus and Tabs

3.2.1 Start - Tab

The first thing that should be done after startup is to choose the appropriate software mode. This is done with the following path:

File → Mode → Select one from the listed options.

There are three different modes, dependent on what kind of file type you wish to upload your load case data from. The options are a txt-file or an excel file, both needs a specific layout in regards to load case name and data to upload correctly. The last mode is the “Wellcat Compatible”. This makes it possible to export an excel spreadsheet for axial force data and one for internal and external pressure data directly from WellCat(v5000.14). No alteration of the spreadsheets are needed before importing them to the software.

The chosen mode will appear in the upper right corner (Figure 3.2) in the start tab.

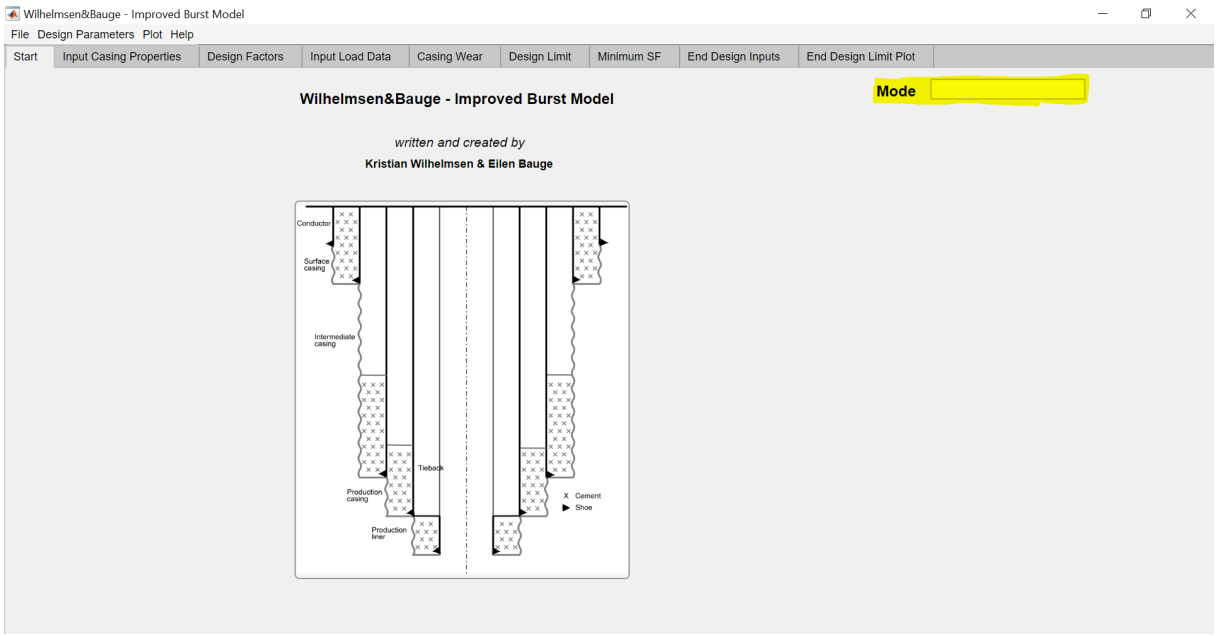

Figure 3.2: Start-Tab

By default, the exact solution of the von Mises criterion is used in the software. If the industry approximation is desired to perform casign design with, the following path can change this option.

File → Preferences → von Mises → Select from list and enable

The drawback of using the exact von Mises solution is that it is not possible to superimpose it with Barlow's equation. Since the coordinate axis are not the same, explained in section 2.3.2.

An option for calculation accuracy is also available. The following path makes it possible to change the default accuracy (medium).

File → Preferences → Calculation Accuracy → Select from list

3.2.2 Input Casing properties - Tab

The next tab is the input casing properties. Under the first label called "Enter Casing Properties", the software needs the casing or tubing grade, OD, ID or thickness and a wall variation factor as indicated in Figure 3.3 . API recommends using 12.5 % for the wall variation factor. This is also the default value in the software. It is now possible to calculate Barlow and the

von Mises failure ellipse for the given casing.

When calculating the von Mises ellipses, by default the Lamé equations (A.1) are used.

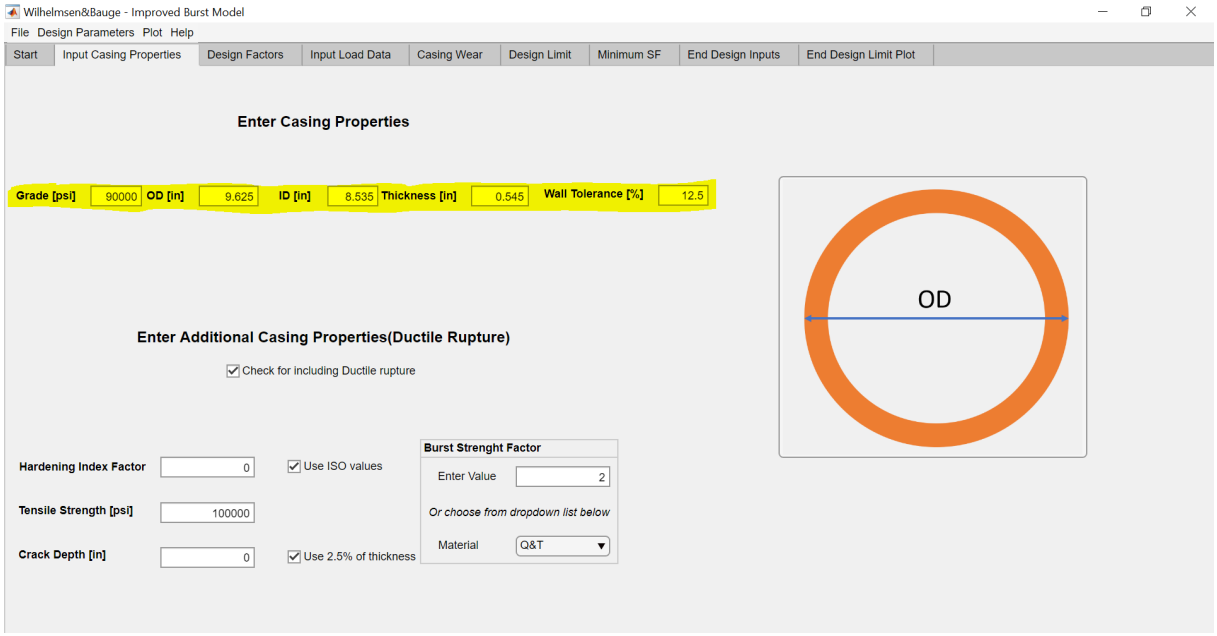

Figure 3.3: Input Casing Properties-Tab

It is often a wish to check how far a casing is from actual rupture, and consequently loss of pressure integrity. In order to use the ductile rupture theory proposed by ISO, the check box for including Ductile Rupture should be checked off.

Several more inputs are needed to calculate true rupture of the pipe.

1. Hardening Index Factor (n_R)
    - There is an option to enter this value or chose values proposed by ISO, equation (2.40).
2. Tensile strength of the pipe (σ_{uts})
    - If the true tensile strength is unknown, the minimum tensile strength should be entered.
3. Crack depth (a_N)
    - There is an option to enter this value or chose 2.5 % of the tubular thickness, which is proposed by the authors.

4. Burst strength factor (k_a)

    - There are two option, either enter your own value or chose from the dropdown list. The options in the dropdown list is limited to either unknown material or Q&T. For an unknown material and Q&T material, ISO recommends 2 and 1 for the burst strength factor respectively (Table 2.2). If the "Enter value" option is used, the dropdown list should show “Non Chosen”.

To get a graphical description of the different properties, the following path could be followed.

Help → Input Parameters → Select from the list.

This will cause a descriptive figure to appear in the “Input Casing Properties” tab as indicated on the right in Figure 3.3.

3.2.3 Design Factors - Tab

In this tab, it is possible to choose your design factor for the respective models. Different companies usually operates with different factors, but an option to use a standard proposed by the authors is possible. This can be done by using the following path.

Design Parameters → Select Standard Parameters for design → Select Casing or tubing.

This will result in design factors for all the models, given by Table 2.1, being filled out automatically.

3.2.4 Input Load Data - Tab

This tab will look different, dependent on what mode is chosen. The WellCat compatible mode is the most advanced, and is therefore explained in detail here.

When WellCat compatible is chosen, the window in Figure 3.4 will appear in the Input Load Data tab.

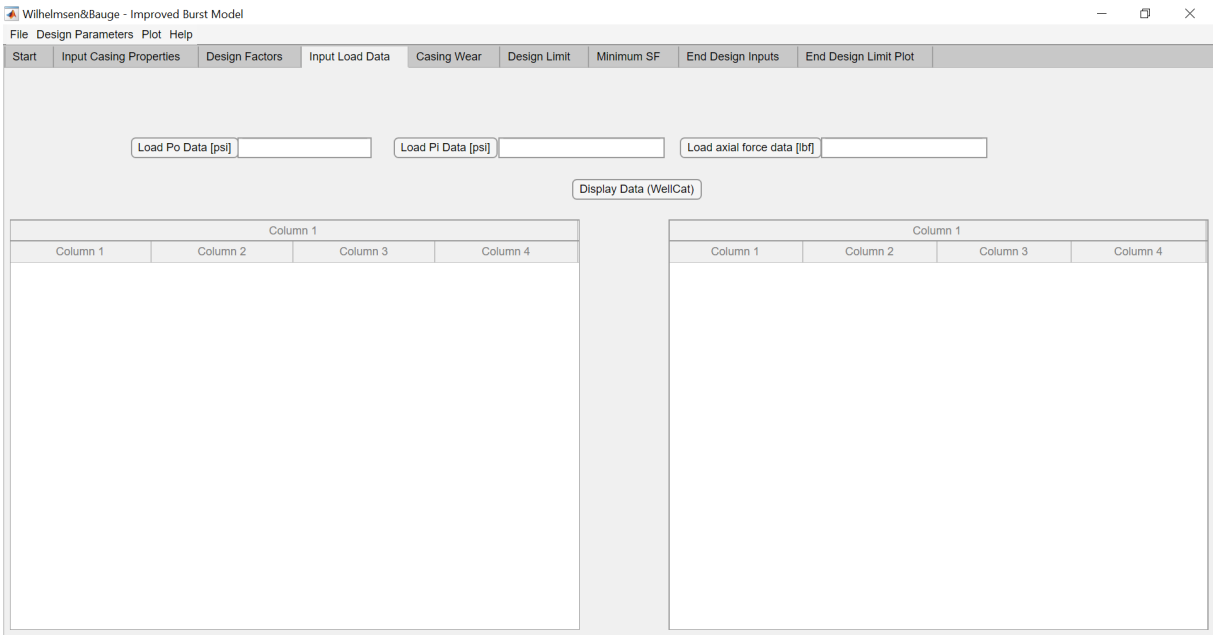

Figure 3.4: Input Load Data-Tab

This tab is used to import your load case data as three separate excel spreadsheets from WellCat. When both axial, external (Po) and internal (Pi) pressure is uploaded, the "Display Data (WellCat)" button should be pushed to check if your data was uploaded correctly. The left table in Figure 3.4 will display differential pressure (Pi-Po). Excel spreadsheets should be located on the desktop (not in a folder on the desktop), before uploading.

3.2.4.1 How to export excel Spreadsheet from WellCat

When all loads are defined in WellCat, the following path should be used.

Results → Multiple loads → Select Axial load, external or internal pressure.

After one of the above options are chosen. The button second from right in Figure 3.5 should be pushed to change from plot to table view. Next the excel icon should be pushed to export the table data to an excel spreadsheet.

Figure 3.5: Button group. Screenshot form WellCat.

3.2.5 Casing Wear - Tab

There is also an option to include a wear factor caused by the rotating drill string. This is found in the casing wear tab (Figure 3.6).

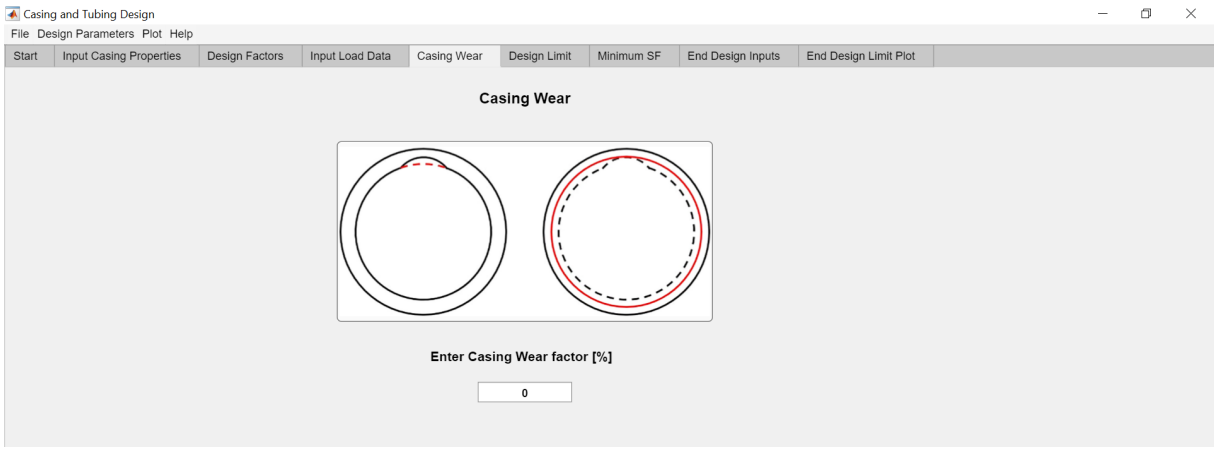

Figure 3.6: Casing Wear Factor tab

The wear factor assumes a uniform wear over the entire casing. The theory behind casing wear used in the software is found in section 2.6.

3.2.6 Design Limit - Tab

The design limit tab will show different windows dependent on your choice of von Mises solution on the start-tab. If no changes were made for this option, the exact von Mises ellipse will be used in the calculations.

To plot the uploaded load case data with the appropriate burst limit formula, the respective formula should be chosen from the list on the right (see Figure 3.7). To compute and show results, the “Calculate&Plot (exact)” button should be pushed. The figure below is only for

illustrative purposes.

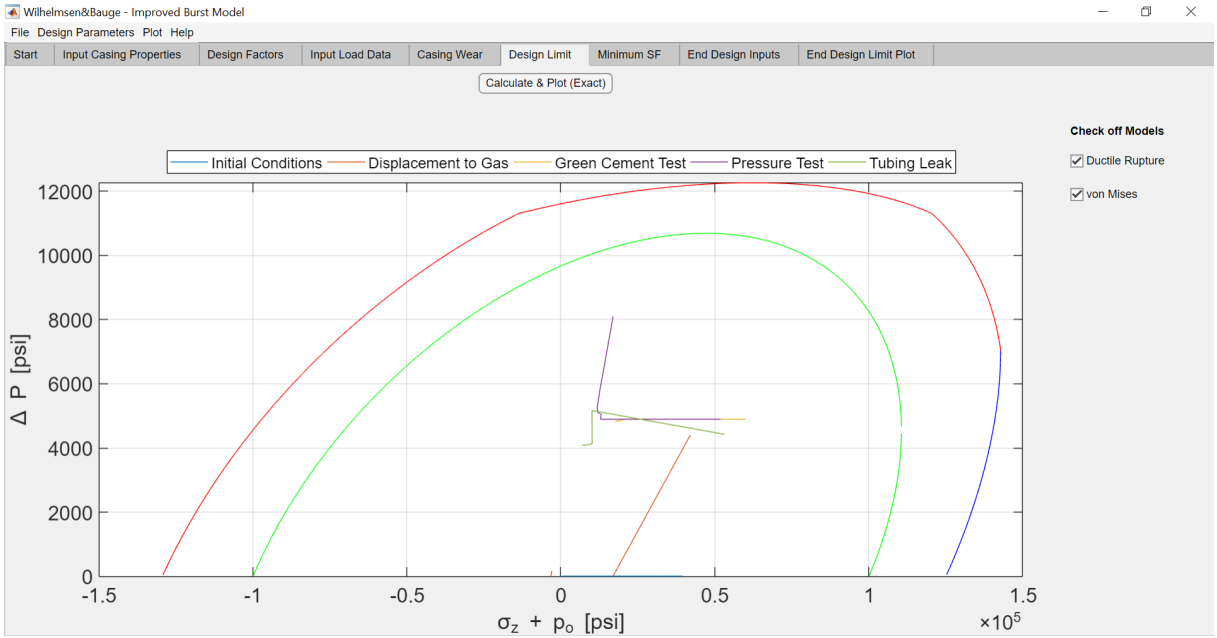

Figure 3.7: Design Limit Tab window when von Mises exact ellipse is chosen.

If the industry approximation is chosen, the window would look like figure 3.8

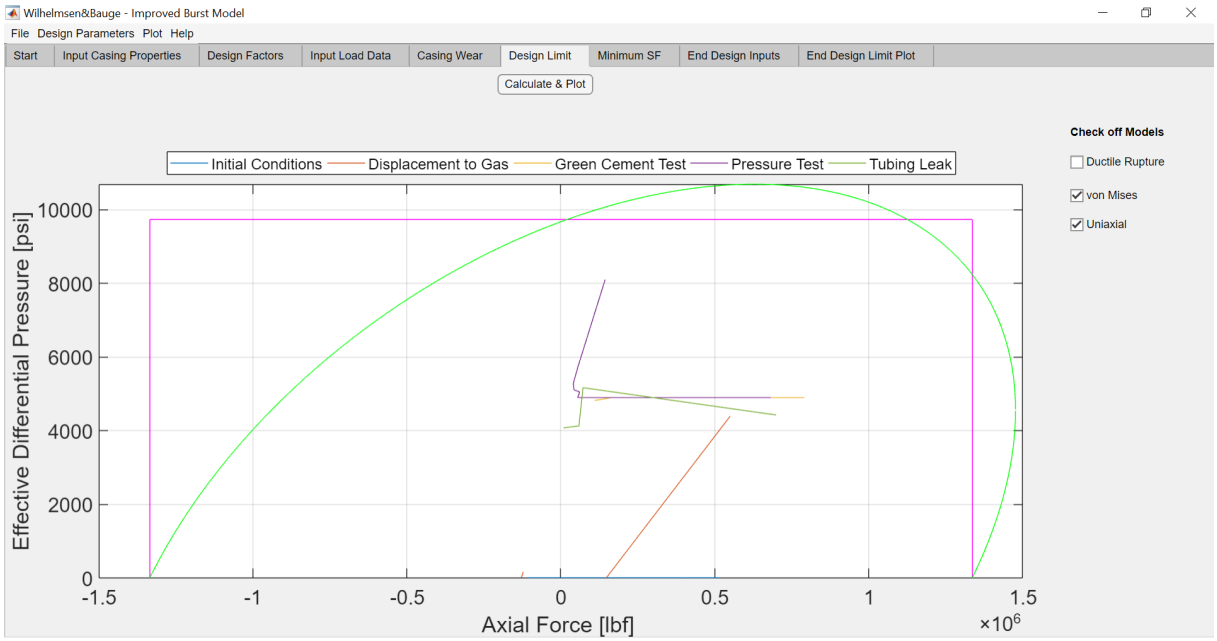

Figure 3.8: Design Limit Tab window when von Mises industry approximation is chosen.

For the "exact ellipse" option, the plot is limited to ductile rupture and von Mises. This is due to the new x-axis variable given as $(\sigma_z + p_o)$. It is not possible to superimpose Barlow's equation on these axis variables, section 2.3.2.

3.2.7 Minimum Safety Factor - Tab

The minimum SF tab will calculate the minimum safety factor for the respective models when the "Calculate minimum Safety Factor" button is pushed. Notice that the Check box for including ductile rupture in the "Input Casing Properties" must be checked off if the minimum safety factors for ductile rupture and necking should be calculated.

In order to calculate safety factors for ductile rupture and necking, several iterations are required, due to the dependence of equation (2.27) and (2.30). Remaining iteration's are indicated in a numeric box on the right side of each heading (Figure 3.9).

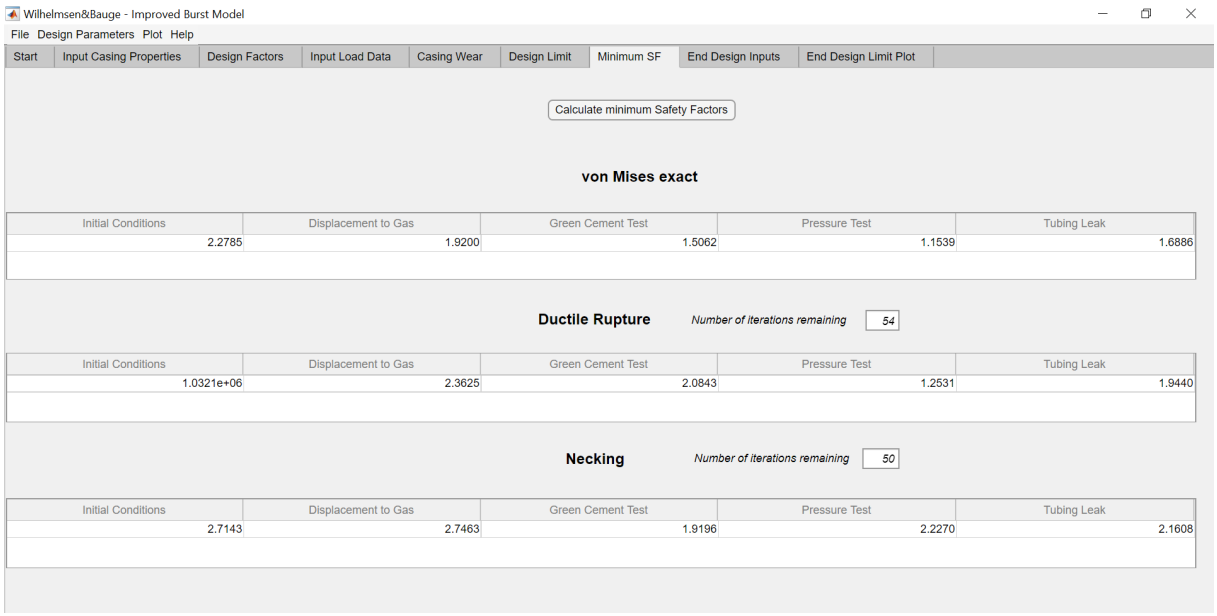

Figure 3.9: Minimum Safety Factor tab

NB! The functionality of this tab works only in WellCat compatible mode.

3.2.8 End Design Inputs - Tab

In the "End Design Inputs" tab is the possibility of gathering all your load cases for each casing string. For each casing string the user has to provide the desired Grade, OD and thickness of the tubular. The load cases are imported in the same manner as for the "input load data" tab. The user also has to provide a name for each tubular. See example of a load case in Figure 3.10. The reason for gathering the load cases for every string in your design is to be able to plot all your cases in a single plot. This will serve as a neat summation of the user's tubular design. This is possible with the use of the von Mises circle (section 2.3.1.1), which is

also exact.

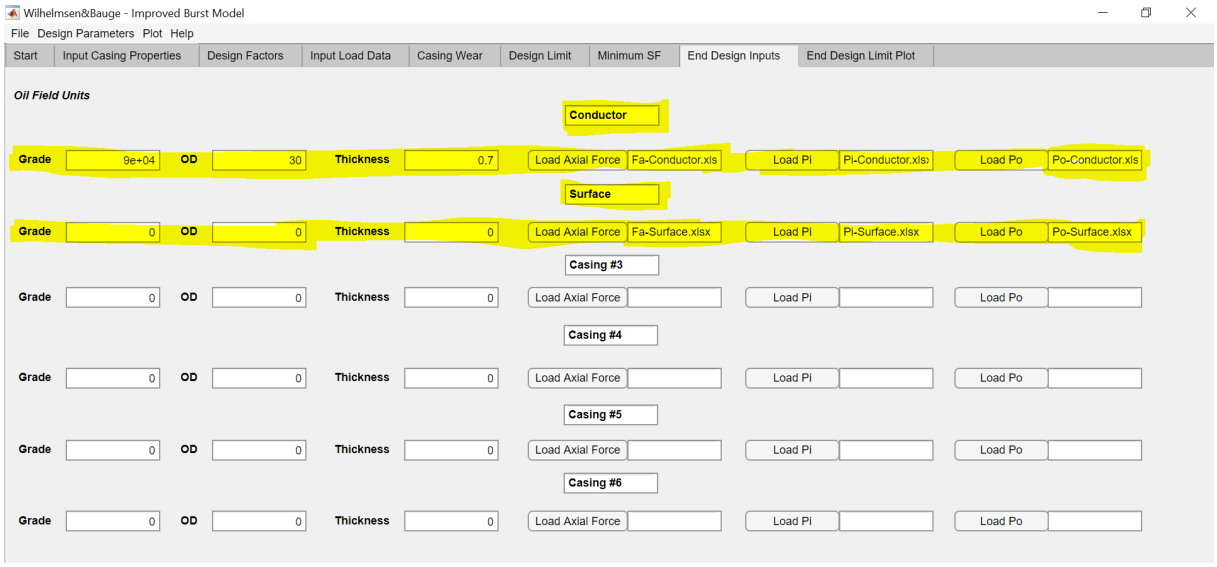

Figure 3.10: End Design inputs tab

NB! The functionality of this tab works only in WellCat compatible mode.

3.2.9 End Design Limit Plot - Tab

When load cases for each tubular is imported in the "End Design Inputs" tab, the results can be graphically represented in a final plot in the "End Design Limit Plot" tab. To show results the "Calculate & Plot" button should be pushed. This will cause the users imported load cases to be plotted. An example is provided in Figure 3.11.

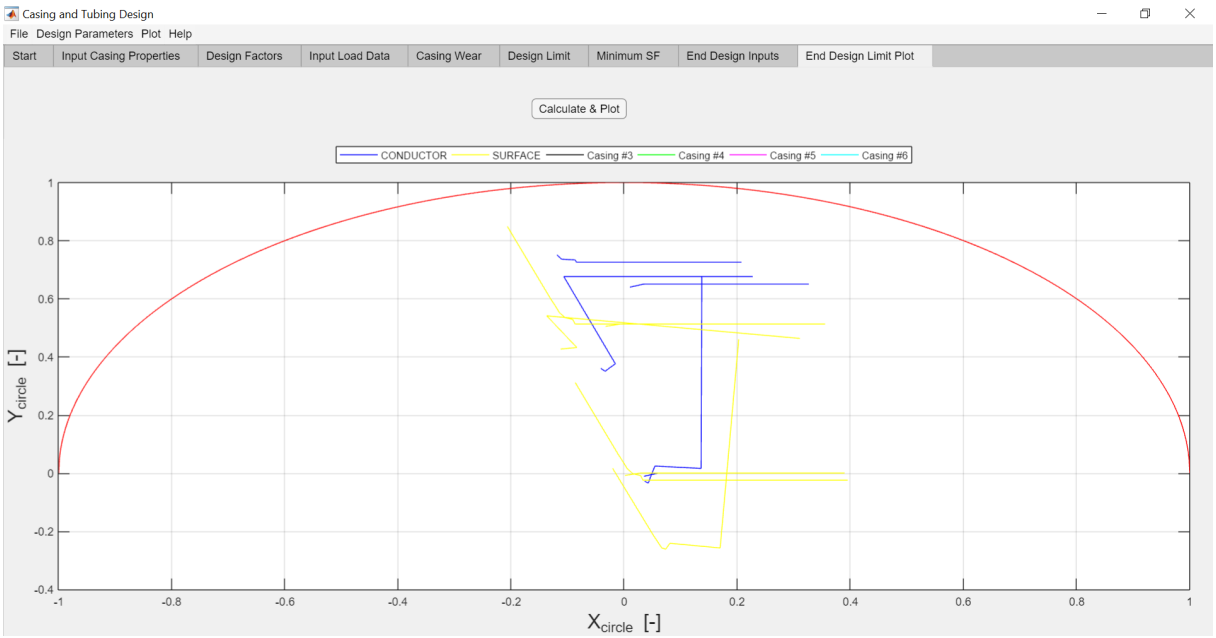

Figure 3.11: End Design Limit Plot tab

NB! The functionality of this tab works only in WellCat compatible mode.

3.2.10 Additional menu options

Plot - Menu

For each plot, there is an option to:

- Show/hide grid
- Limit y-axes to burst area only
- Clear the plot

Help - Menu

For each software mode, a specific standard to the imported files is required in terms of how the data is organised in the file. The software supports excel and txt files. To show a figure of how the data should be organised for the file type in question, the following path should be followed.

Help → Load Data → Select from list

Chapter 4

Results

The theory presented in the previous sections forms the basis for the calculations performed throughout this chapter. First, the presented models were compared with actual test data from ISO. As expected, there was a noticeable difference between the predicted yield pressure and the predicted rupture pressure.

Then, a sensitivity analysis was performed to understand the impact of the different input parameters in the different models. In the end, the Wilhelmsen&Bauge model was compared to the current industry practice using three different case studies. The different case studies were constructed to explore the effect of the improved burst model under varying conditions.

4.1 Comparison of models and pipe rupture data

ISO have conducted 106 pipe rupture tests under capped-end conditions with zero external pressure. The test results have been compared with the predicted values from the models presented in section 2.2 - 2.5. First, the models from ISO will be compared to the test results and then the through-wall yield model will be studied. It should be noted that the minimum wall thickness was specified in the rupture test data given in ISO. Therefore, the embedded wall reduction factors in the models was removed by inserting the values in Table 4.1.

Table 4.1: Input values when the minimum wall thickness is measured.

Parameter	**Value**
Pipe wall reduction factor (k_{wall})	1
Maximum depth of a crack-like imperfections (a_N)	0

4.1.1 ISO models

The percentage difference in predicted rupture pressure to actual pressure for the ISO models, $p_{predicted}/p_{actual} - 1$, is given in Figure 4.1 for different D/t-ratios.

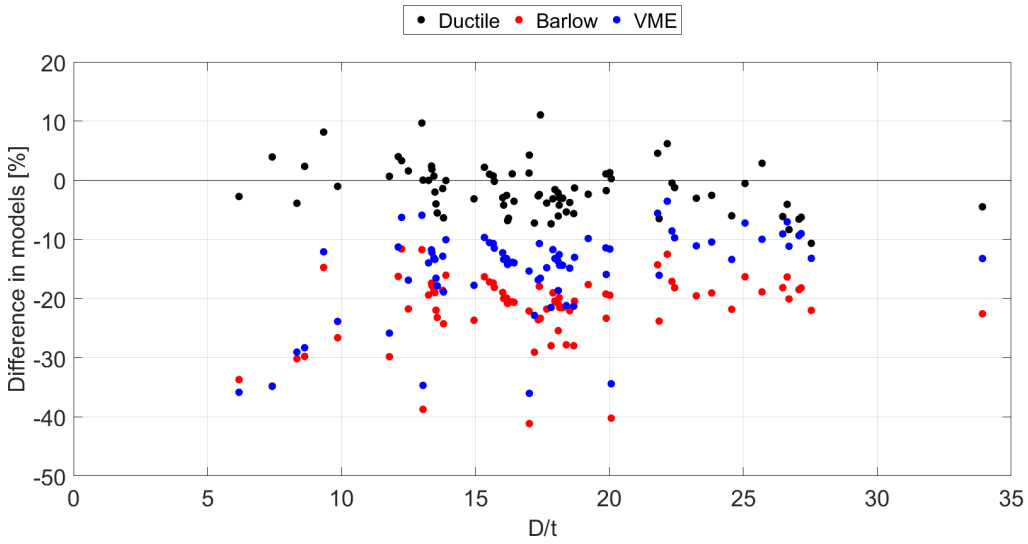

Figure 4.1: Ductile rupture, Barlow and von Mises burst limits compared with measured rupture pressure from ISO.

See Appendix B.1 for a complete plot of all the test data, including equal D/t-ratio.

Table 4.2 gives the mean and standard deviation for all the models, when compared with the percentage difference in predicted to actual pressure.

Table 4.2: Statistical evaluation of ISO models.

Model	**Standard deviation[%]**	**Mean [%]**
Ductile Rupture	4.48	-0.44
Barlow	7.49	-23.75
von Mises	9.13	-17.94

4.1.2 Through-wall yield

A comparison of the ratio of the test results to the through-wall yield model (2.22), $p_{predicted}/p_{i,TWY}$, was performed in Lin et al. (2014). The presented result can be seen in Figure 4.2.

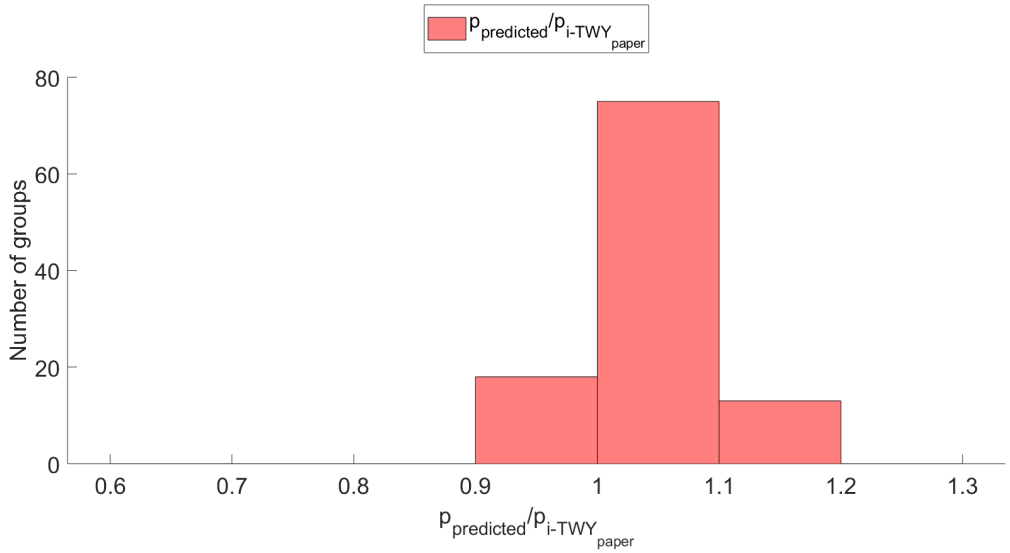

Figure 4.2: Comparison of through-wall yield model performed in Lin et al. (2014).

From Figure 4.2 it can be seen that the model overpredicts the burst limit for only 16.9 % of the 106 test data. Whereas, the ductile rupture model presented above overpredicts the burst limit for 47.2 % of all the test data.

However, the embedded wall reduction factors were included in the through-wall yield model presented in the paper. The error introduced was analysed by reproducing the through-wall yield model, but with the input parameters in Table 4.1 instead. Figure 4.3 demonstrates this effect on the ratio of the test results to the through-wall yield model, with and without the embedded wall reduction factors.

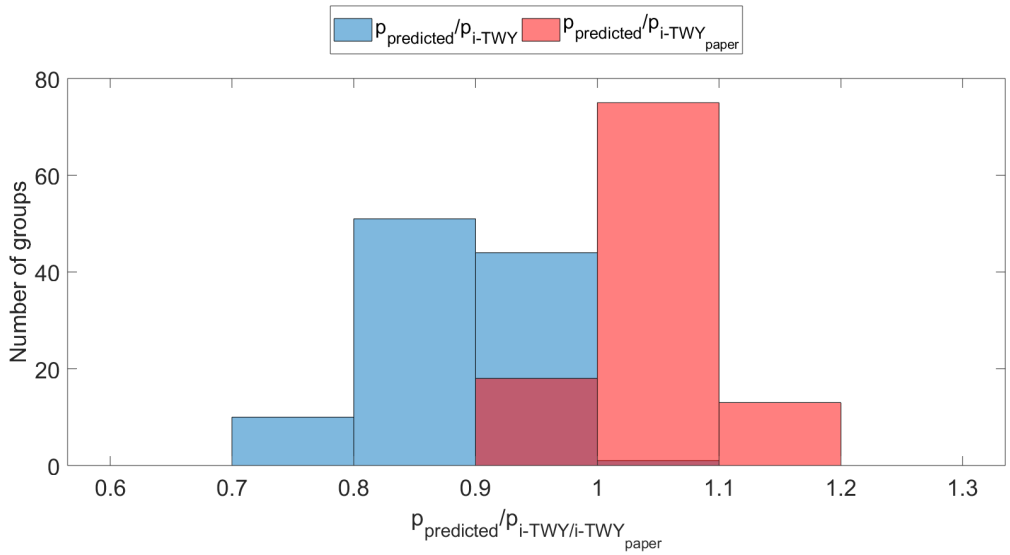

Figure 4.3: Ratio of test result to the through-wall yield model with embedded wall reduction factors ($p_{i-TWY_{paper}}$) and without (p_{i-TWY}).

Figure 4.4 compare the percentage difference in predicted rupture pressure to actual pressure for through-wall yield and ductile rupture. See Appendix F for detailed information about the authors reproduced through-wall yield model.

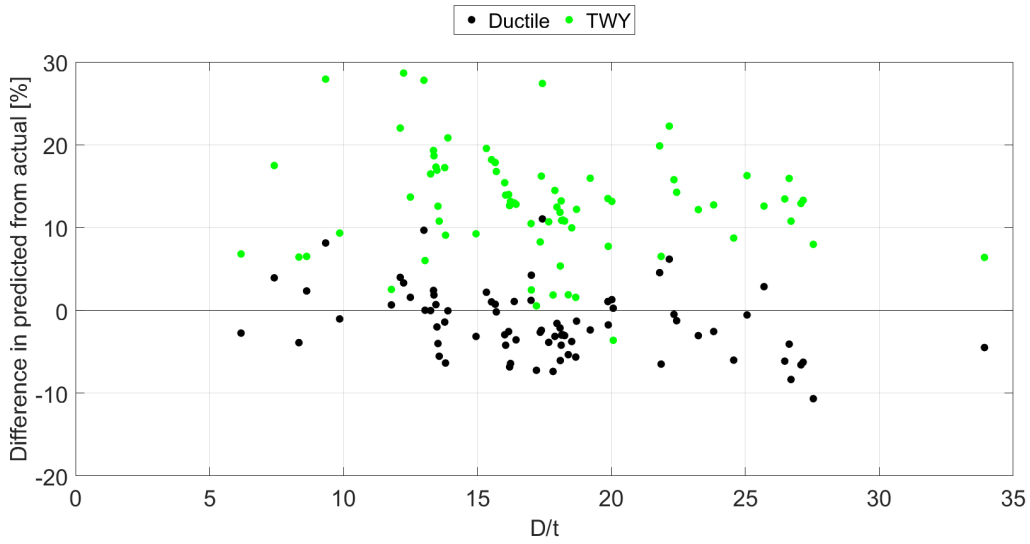

Figure 4.4: Ductile rupture and reproduced calculation of the through-wall yield model compared with the measured rupture pressure from ISO.

Three significant results were observed after analysing the through-wall yield model without the embedded wall reduction factors:

- The through-wall yield model overpredicted the burst limit for 99.1 % of the 106 test data when the embedded wall reduction factors were removed.
- An average overprediction of 12.8 % was obtained for the through-wall yield model without the embedded wall reduction factors.
- The through-wall yield model without the embedded wall reduction factors predicts on average a 14.6 % higher rupture pressure than the ductile rupture model.

4.1.3 Performance of ductile rupture in tension

A small number of tests have been conducted to investigate the burst limiting pressure in combination with tension. Shell is one of the few with such test results published (Cernocky, 2005).

The results given by Shell was based on tests performed on a small pipe section. See Table 4.3 for pipe properties. The test results have been compared with predicted values from the ductile rupture model to investigate the performance of equation (2.26) in combination with tension. A comparison of the ductile rupture model to actual test data is given in Figure 4.5.

Table 4.3: Test pipe properties(Cernocky, 2005, 11).

Pipe Properties	**Value**
OD [in]	0.9
t [in]	0.1065
Grade	C-110
Yield strength [kpsi]	116.1
Tensile Strength [kpsi]	130

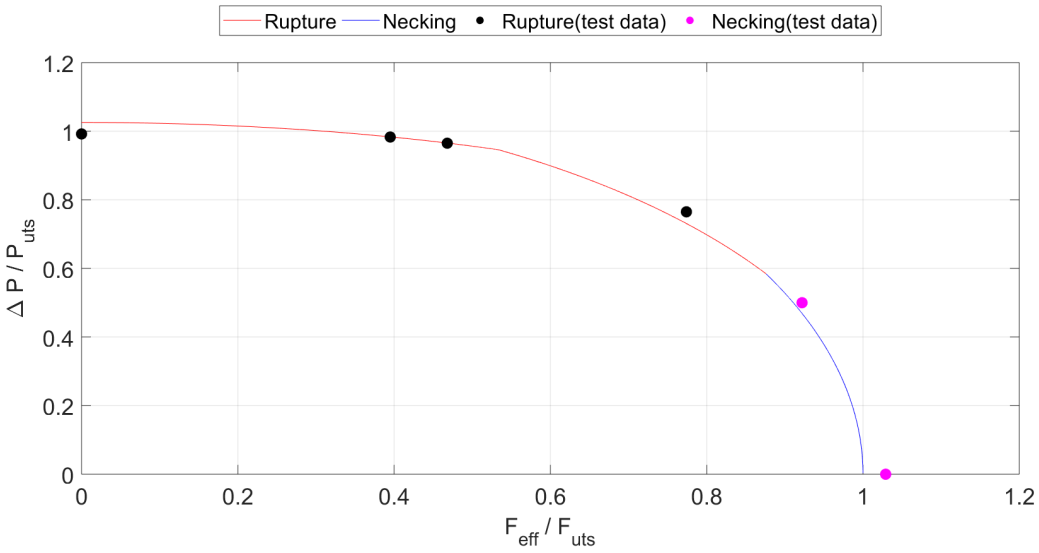

Figure 4.5: Ductile rupture model compared with test results.

The percentage difference in predicted rupture pressure to actual rupture pressure is given in Table 4.4.

Table 4.4: Comparison of ductile rupture and test data in tension.

F_{eff}/F_{UTS}	**Difference in predicted from actual[%]**
Ductile Rupture	
0.00	-3.38
0.40	-0.05
0.47	-0.05
0.77	4.46
Necking	
0.92	1.21
1.03	2.82

4.1.4 Sensitivity analyses

A sensitivity analyses was performed to determine how different values of the input parameters effected the different burst models under a given set of assumptions. External pressure, casing grade, allowable wall thickness variation, hardening index factor and the burst strength factor were analysed to see their effects on the predicted burst pressure limits.

4.1.4.1 Exact and approximate von Mises triaxial yield solution

A sensitivity analysis was performed to see the influence of neglecting external pressure in the approximate triaxial yield criterion (section 2.3.2). The analysis was performed on a thin-wall K-55 casing with an outer diameter of 9 5/8" and a wall thickness of 0.352". The plot contains the exact von Mises solution for different external pressure values together with the approximate von Mises solution, where the external pressures is assumed to be zero (Po = 0).

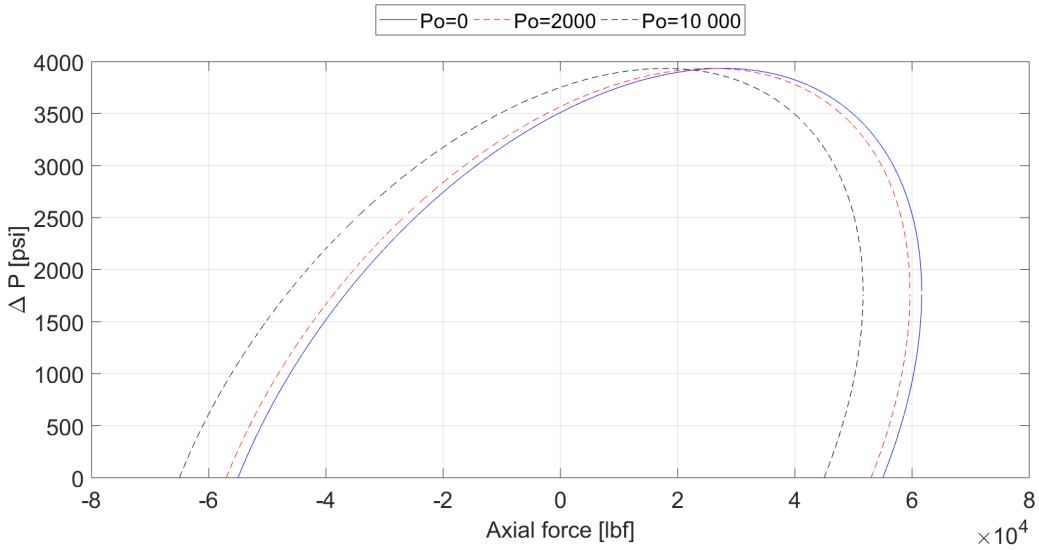

Figure 4.6: Influence of increasing external pressure on the von Mises failure ellipse for a thin-walled pipe.

For the specified casing properties, three significant results were observed for the given range of axial force:

- The error in the approximate von Mises solution resulted in an overprediction of the triaxial yield limit for axial values above 200 000 lbf.
- The error in the approximate von Mises solution resulted in an underprediction of the triaxial yield limit for axial values under 200 000 lbf.

- The exact von Mises solution was shifted further out to the left with increasing external pressure when compared to the approximate solution.

4.1.4.2 Effect of casing grades on ductile rupture

A sensitivity analysis was performed to see the effect casing grades had on the ductile rupture model. Two different casing grades were analysed on a 13 3/8" casing. First, a low casing grade of K-55 was analysed. The predicted yield and rupture pressure can be seen in Figure 4.7. Then, a high casing grade of C-90 was analysed. The predicted yield and rupture pressure can be seen in Figure 4.8. Table 4.5 shows the difference in minimum yield strength and minimum ultimate tensile strength for the different casing grades.

Table 4.5: API casing grades with corresponding minimum yield and ultimate tensile strength.

API Grade	Minimum yield strength [psi]	Minimum ultimate tensile strength [psi]
K-55	55 000	95 000
C-90	90 000	100 000

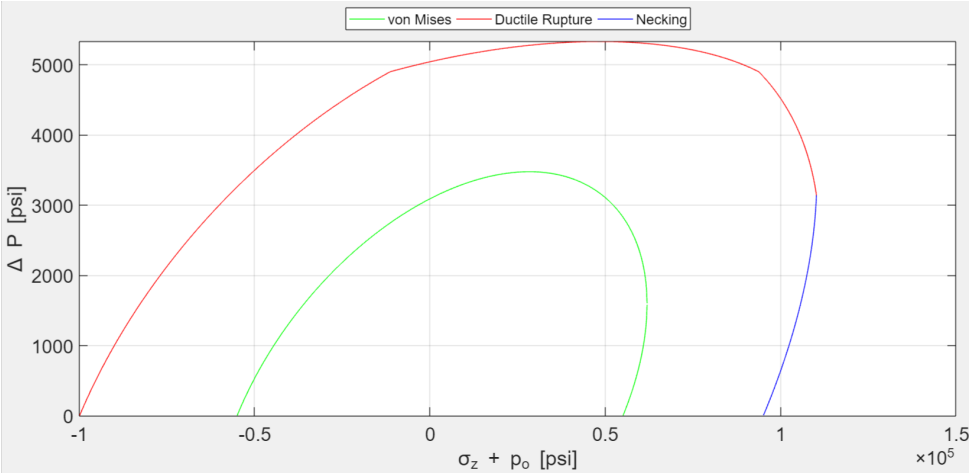

Figure 4.7: A 13 3/8" casing with weight and grade given by 61 ppf and K-55 respectively. The difference between minimum yield strength and ultimate tensile strength = 40 000 psi.

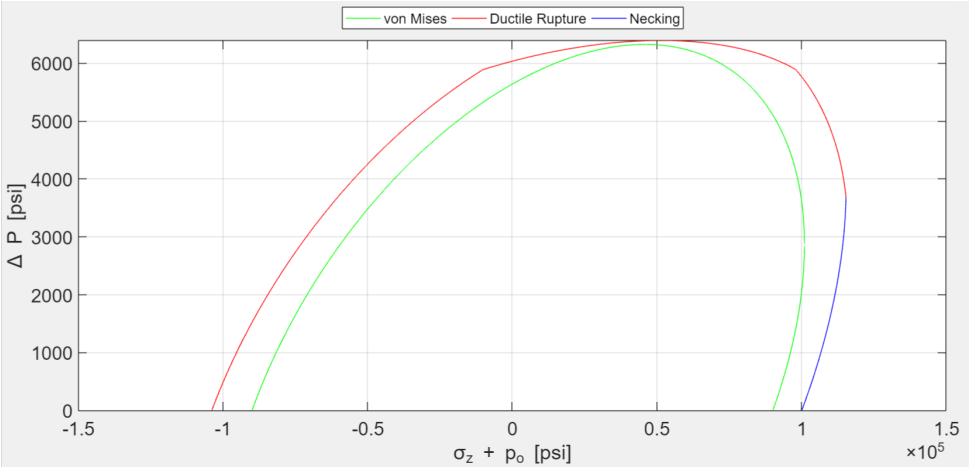

Figure 4.8: A 13 3/8" casing with weight and grade given by 68 ppf and C-90 respectively. The difference between minimum yield strength and ultimate tensile strength = 10 000 psi.

For the specified casing properties two significant results were observed for the given range of casing grades:

- For low grades, where the difference between the minimum yield strength and ultimate tensile strength were large, the plastic strength hardening zone was large.
- High grades on the other hand, had a smaller distance between the two strength parameters and subsequently a small plastic hardening zone.

4.1.4.3 Factor to account for specified manufacturing tolerance of the pipe wall - k_{wall}

The effect the minimum acceptable wall thickness of 87.5 % of the nominal wall thickness, had on the predicted burst limits has been analysed. The results were plotted as the difference in percentage between the models with and without the wall thickness reduction factor k_{wall}.

$$\frac{p_{i(k_{wall}=0.875)} - p_{i(k_{wall}=1)}}{p_{i(k_{wall}=1)}} * 100\%$$

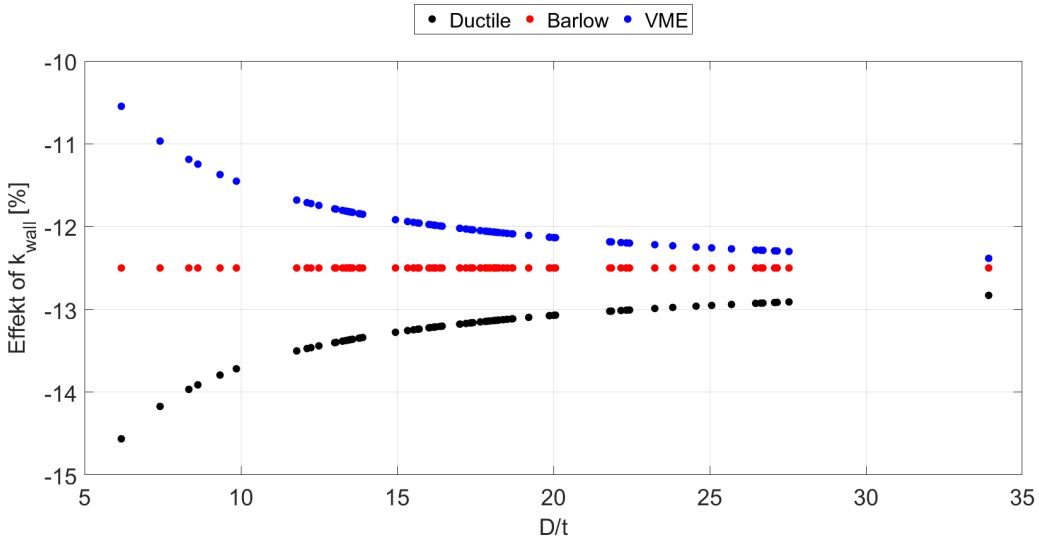

Figure 4.9: Percentage difference with and without k_{wall}.

Three significant results were observed for the given range of diameter to thickness ratio:

- The severity of k_{wall} was highest for ductile rupture, with an average of 13.6 % reduction for the predicted burst limit.
- For increasing D/t-ratio the effect of k_{wall} was decreasing for ductile rupture and increasing for von Mises.
- The API burst limit is a linear equation, hence the effect of k_{wall} was constant and equal to the specified reduction of 12.5 % in pipe wall thickness.

4.1.4.4 Hardening Index Factor - n_R

A sensitivity analysis was performed to see the effect of applying another hardening index factor than the value recommended by ISO. The study was performed on a 9 5/8" production casing with grade C-90 and weight 58.4 ppf, where ISO (Table 2.3) recommended $n_R = 0.1$. The following value have been plotted against the hardening index factor in Figure 4.10.

$$\frac{\Delta p_{(n_R)} - \Delta p_{(n_R=0.1)}}{\Delta p_{(n_R=0.1)}} * 100\%$$

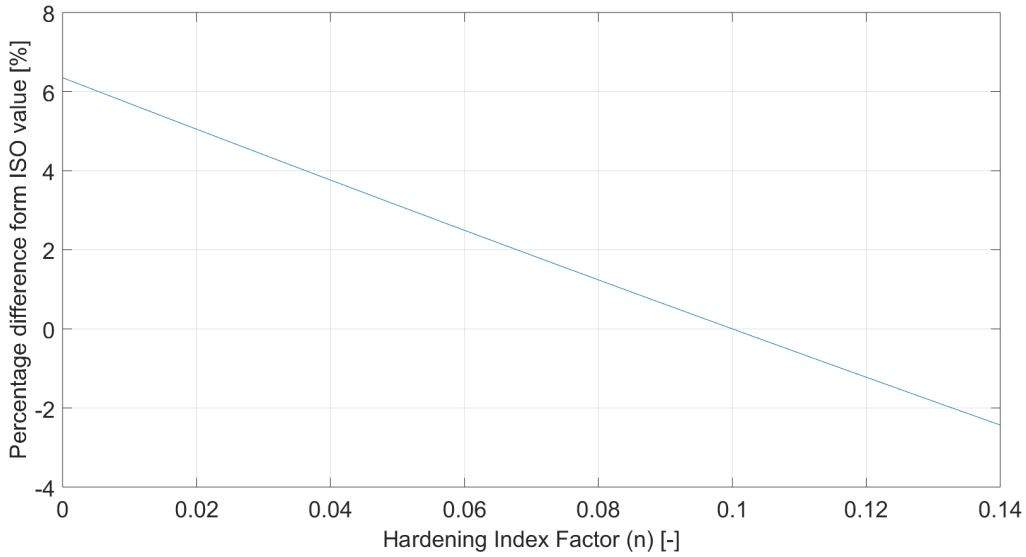

Figure 4.10: Percentage difference in predicted rupture pressure with and without the recommended ISO value for the hardening index factor ($n_R = 0.1$).

Three significant result were observed from Figure 4.10:

- A smaller hardening index factor than the recommended ISO value will overpredict the rupture pressure.
- A higher hardening index factor than the recommended ISO value will underpredict the rupture pressure.
- A difference in hardening index factor of +/- 20 % leads to an -/+ 1.2 % difference in the predicted rupture pressure from ISO.

4.1.4.5 Burst Strength Factor - k_a

To see the effect of variations in the burst strength factor on the predicted rupture pressure, a sensitivity analysis was performed. The study was performed on a 9 5/8" production casing with grade C-90 and weight 58.4 ppf. The result is shown in Figure 4.11.

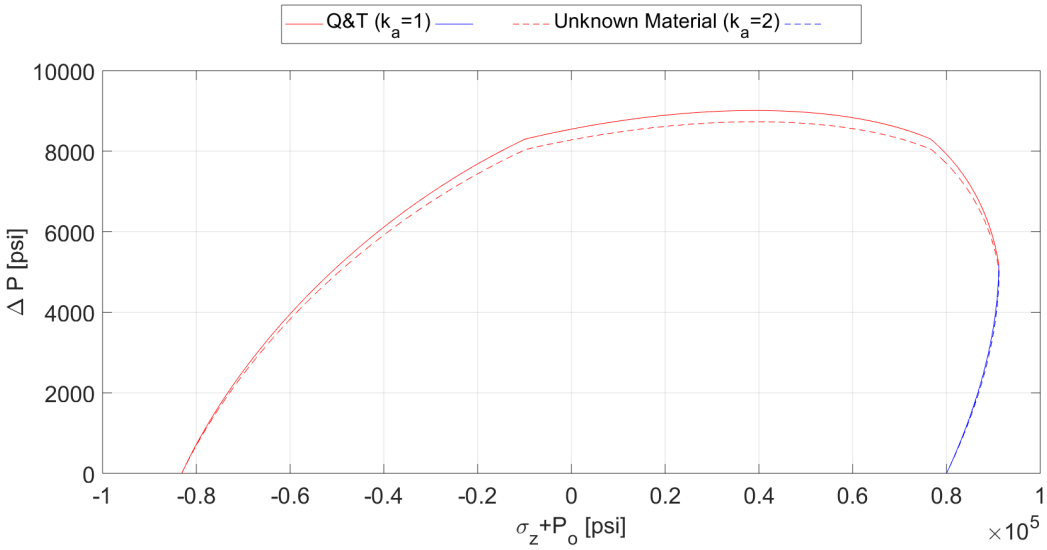

Figure 4.11: Predicted Rupture Pressures dependence on the burst strength factor (k_a).

One significant result was observed from Figure 4.11:

- Increase in the burst strength factor reduced the predicted rupture pressure.

4.1.4.6 Crack Depth - a_N

A sensitivity analysis was performed to see the effect of applying another crack depth factor than the value of 2.5 % used in the calculations performed in this thesis. The crack depth factor is given as a percentage of the wall thickness. The study was performed on a 9 5/8" production casing with grade C-90 and weight 58.4 ppf. The following value have been plotted against different crack depths given as a percentage of the nominal thickness in Figure 4.12.

$$\frac{\Delta p_{i(a_N)} - \Delta p_{i(a_N=0.025*t)}}{p_{i(a_N=0.025*t)}} * 100\%$$

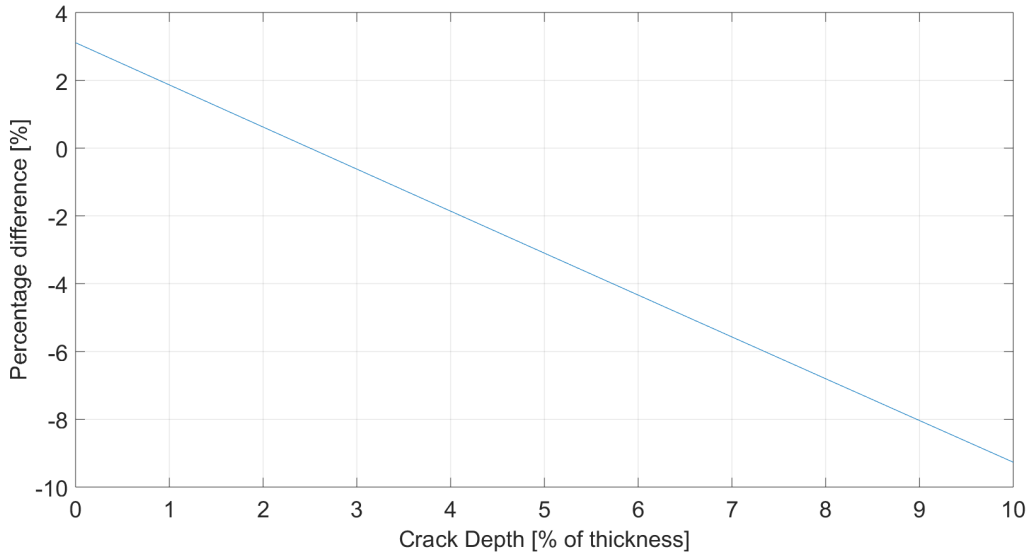

Figure 4.12: Percentage difference in predicted rupture pressure vs. crack depth.

Three significant result was observed from Figure 4.12:

- A smaller crack depth factor than 2.5 % leads to a higher prediction of the rupture pressure.
- A larger crack depth factor than 2.5 % leads to a lower prediction of the rupture pressure.
- A difference in crack depth factor of +/- 20 % from 2.5 % leads to an -/+ 0.6 % difference in the predicted rupture pressure from the one calculated in this thesis.

4.2 Results - Case study

A comparison of the current industry practice and the Wilhelmsen&Bauge model was performed on three case studies. To explore the effect of the improved burst model under varying conditions, the case studies consisted of vertical wells with different water depths, pore and fracture pressures. The water depths were ranging from shallow water to deep water. In other words, the load cases represented typical oil and gas field, in the North Sea to the Gulf of Mexico. The results from the 9 5/8" production casing is presented below. A detailed description regarding casing configuration, mud weight, pore and fracture pressure can be found in Appendix D.

In the analysis, all casings were assumed to be Q&T and the design factors given in Table 2.1 were used for both the improved burst model and the current industry practice. The crack depth factor was assumed to be 2.5 % of the nominal wall thickness and the minimum ultimate tensile strength from Table 2.4 was used. The hardening index factor was applied in accordance with equation (2.40).

The casing design recommended by the different models are summarised in a table for each example well. The Wilhelmsen&Bauge model was divided into three different segments with different wall tolerances. This allowed analysing the specific effect each wall tolerance had on the casing design. For instance, the wall tolerance of 12.5 % currently used in the industry only considered the effect of using the exact triaxial yield limit and the ductile rupture limit. Whereas, a wall tolerance of 9.4 % also considered the effect of reducing the minimum acceptable wall thickness in the exact triaxial yield limit and the ductile rupture limit. Finally, marked in red is the design proposed with the improved burst model, when a reduction in allowable wall tolerance, exact von Mises and ductile rupture were considered.

4.2.1 Shallow water (100 m) - Production Casing

The recommended casing design given by the different models can be seen in Table 4.6 for the production casing.

Table 4.6: Recommended casing design for shallow water well.

Model	Weight[ppf]	Grade	Triaxial yield SF	Burst SF	Rupture SF
Current Industry Practice					
WellCat	40	K-55	1.384	1.294	NA
Wilhelmsen & Bauge model					
kwall = 12.5 %	36	K-55	1.233	NA	1.919
kwall = 9.4 %	36	K-55	1.278	NA	1.992
kwall = 6.4 %	36	K-55	1.322	NA	2.062

The design limit plot for the current industry practice is given in Figure 4.13. Whereas, the design limit plot for the final design with the Wilhelmsen&Bauge model is given in Figure 4.14.

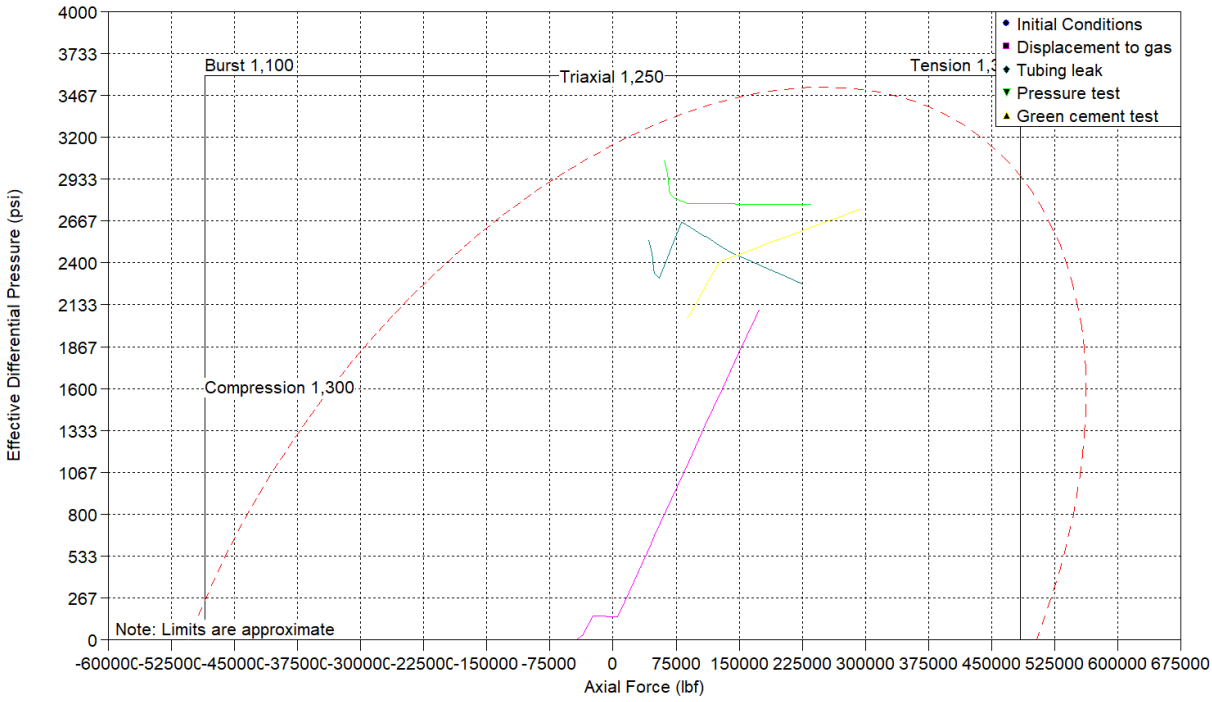

Figure 4.13: Burst load case from the shallow water example plotted with approximate solution of von Mises and the historical API burst limit in WellCat. The weight and grade were 40 ppf and K-55 respectively.

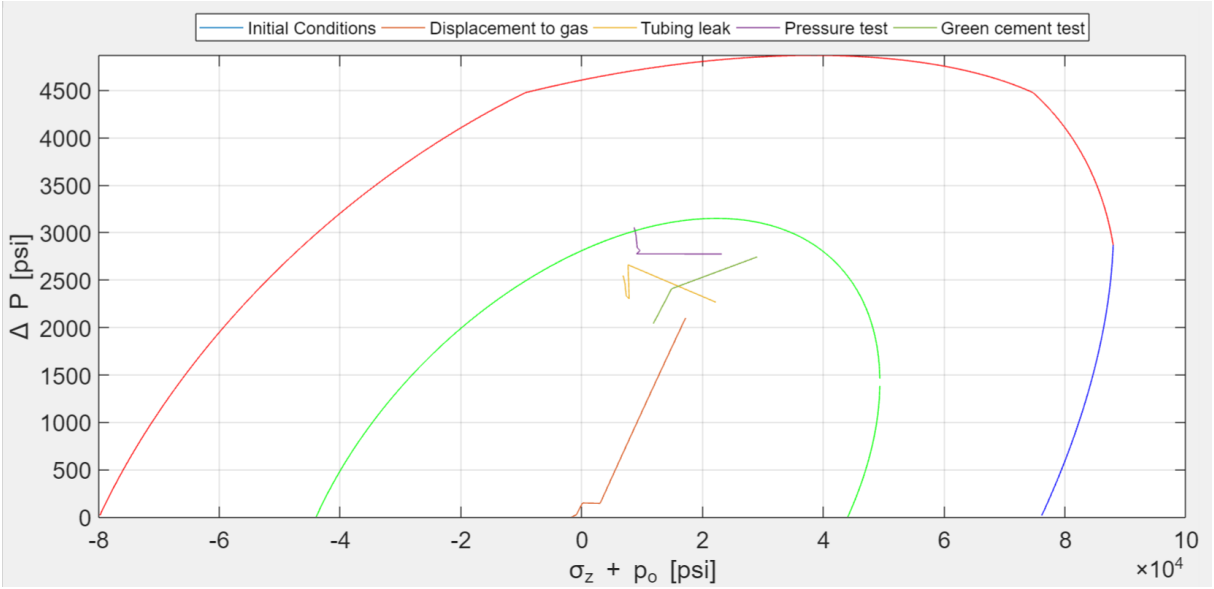

Figure 4.14: Burst load case from the shallow water example well plotted with exact solution of von Mises and ductile rupture. The wall tolerance was chosen as 12.5 %. Weight and grade were 36 ppf and K-55 respectively.

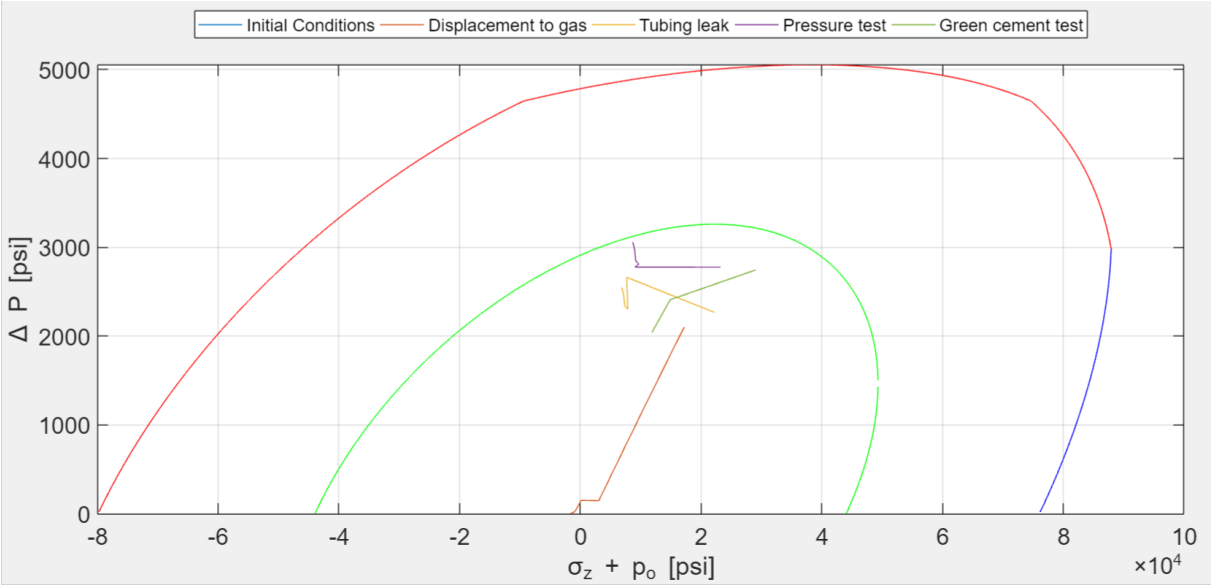

Figure 4.15: Burst load case from the shallow water example well plotted with exact solution of von Mises and ductile rupture. The wall tolerance was chosen as 9.4 %. Weight and grade were 36 ppf and K-55 respectively.

Three significant results were observed from Table 4.6 and Figure 4.13-4.15:

- The historical API burst limit was not dimensioning.
- A casing grad of K-55 resulted in a large plastic strength zone.
- The casing weight was reduced from 40 ppf to 36 ppf by using the improved burst model. Two methods were possible. An elastic design was achieved by applying a wall tolerance of 9.4 %. If the pressure test was allowed to slightly surpass the elastic area, a wall tolerance of 12.5 % could be applied.

4.2.2 Midwater (305 m) - Production Casing

The recommended casing design given by the different models can be seen in Table 4.7 for the production casing.

Table 4.7: Recommended casing design for midwater load case.

Model	Weight[ppf]	Grade	Triaxial yield SF	Burst SF	Rupture SF
Current Industry Practice					
WellCat	58.4	C-90	1.277	1.204	NA
Wilhelmsen & Bauge model					
kwall = 12.5 %	58.4	C-90	1.277	NA	1.357
kwall = 9.4 %	58.4	C-90	1.323	NA	1.409
kwall = 6.4 %	53.5	C-90	1.254	NA	1.332

The design limit plot for the current industry practice is given in Figure 4.16. Whereas, the design limit plot for the final design with the Wilhelmsen&Bauge model is given in Figure 4.17.

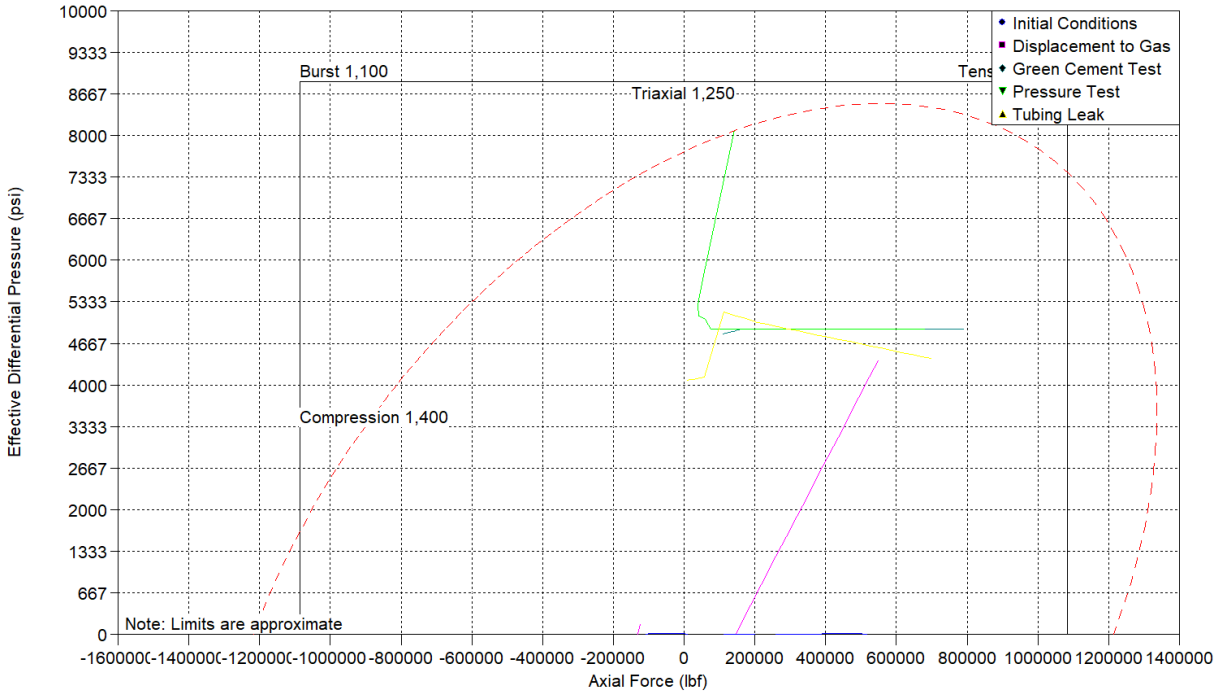

Figure 4.16: Burst load case from the midwater example well plotted with approximate solution of the von Mises and the historical API burst limit in WellCat. The weight and grade were 58.4 ppf and C-90 respectively.

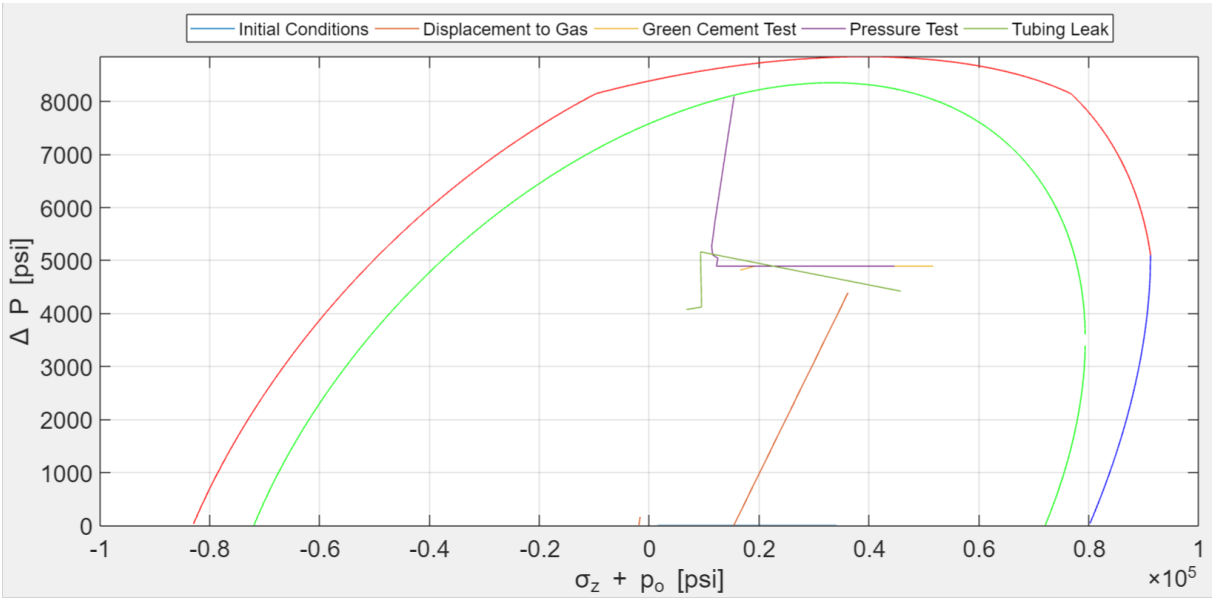

Figure 4.17: Burst load case from the midwater example well plotted with exact solution of von Mises and ductile rupture. The wall tolerance was chosen as 6.4 %. Weight and grade were 53.5 ppf and C-90 respectively.

Three significant results were observed from Table 4.7 and Figure 4.16-4.17:

- The historical API burst limit was not dimensioning.
- A casing grade of C-90 resulted in a small plastic strength zone.
- The casing weight could be reduced from 58.4 ppf to 53.5 ppf by using the improved burst model, with a wall tolerance factor of 6.4 %.

4.2.3 Deepwater (1524 m) - Production Casing

The recommended casing design given by the different models can be seen in Table 4.8 for the production casing.

Table 4.8: Recommended casing design for deepwater load case.

Model	Weight[ppf]	Grade	Triaxial yield SF	Burst SF	Rupture SF
WellCat	59.4	C-90	1.314	1.277	NA
Wilhelmsen & Bauge model					
kwall = 12.5 %	58.4	C-90	1.291	NA	1.407
kwall = 9.4 %	58.4	C-90	1.376	NA	1.462
kwall = 6.4 %	53.5	C-90	1.256	NA	1.383

The design limit plot for the current industry practice is given in Figure 4.18. Whereas, the design limit plot for the final design with the Wilhelmsen&Bauge model is given in Figure 4.19.

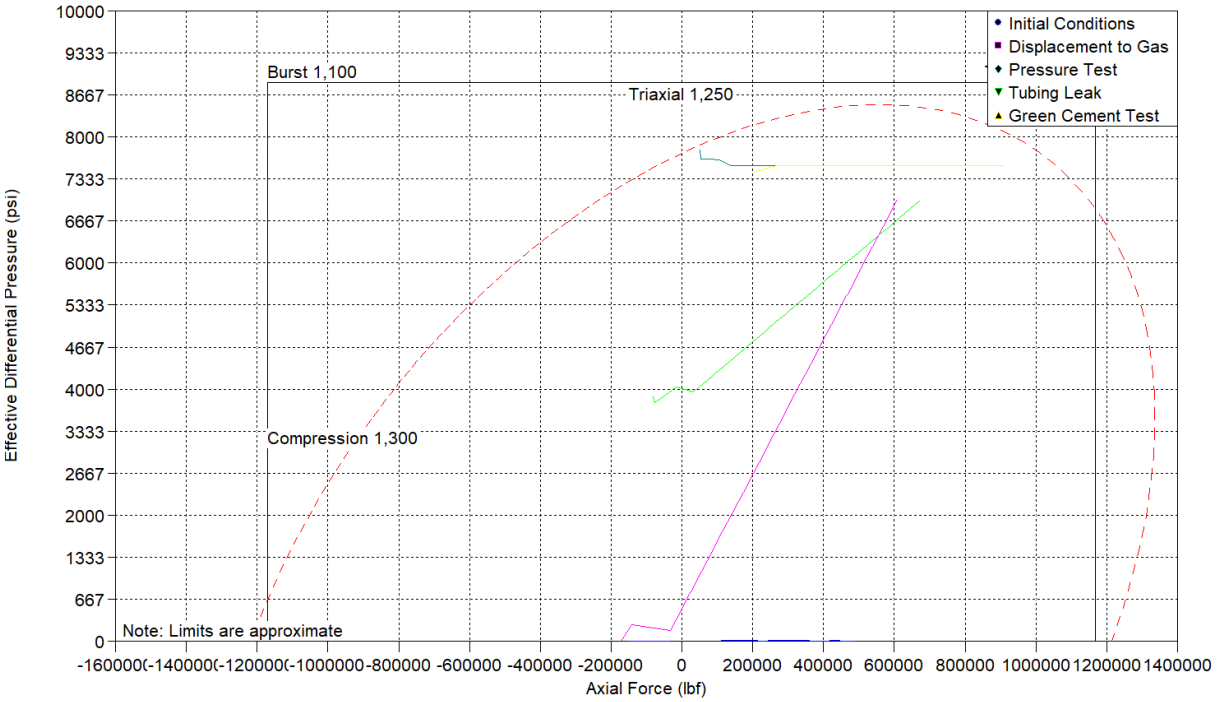

Figure 4.18: Burst load case from the deepwater example well plotted with approximate solution of the von Mises and the historical API burst limit in WellCat. The weight and grade were 59.4 ppf and C-90 respectively.

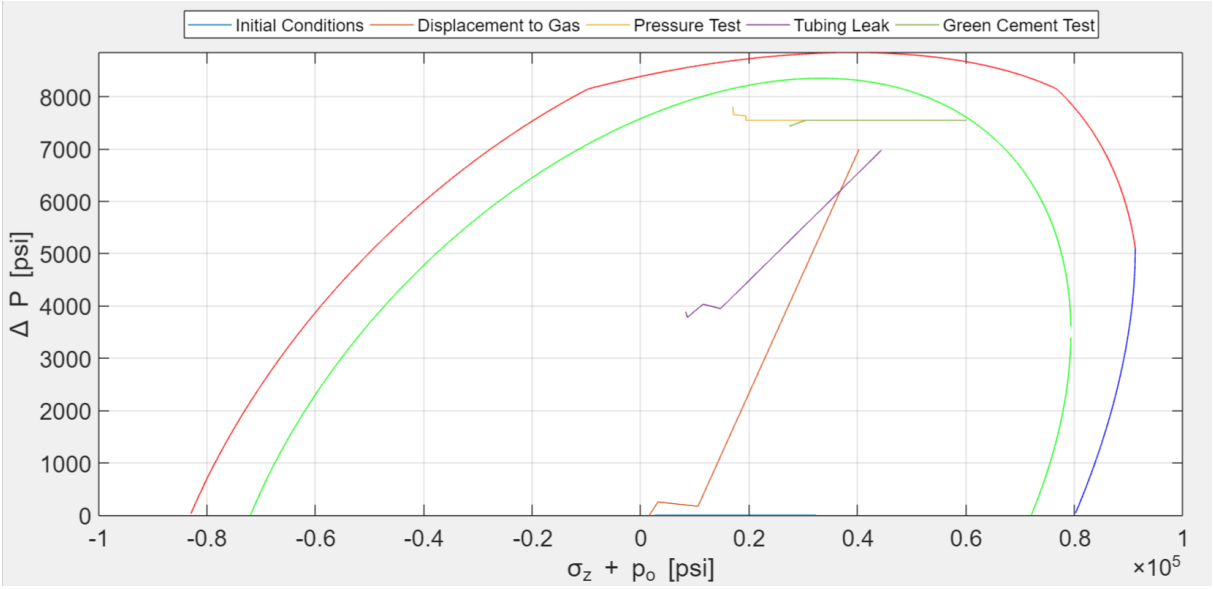

Figure 4.19: Burst load case from the midwater example well plotted with exact solution of von Mises and ductile rupture. The wall tolerance was chosen as 6.4 %. Weight and grade were 53.5 ppf, C-90 and 6.4 % respectively.

Two significant results were observed from Table 4.8 and Figure 4.18-4.19:

- The historical API burst limit was not dimensioning.

- The casing weight was reduced from 59.4 ppf to 53.5 ppf by using the improved burst model, with a wall tolerance of 6.4 %.

4.3 Casing Wear On The Deepwater Well

In the deepwater example the effect of 20 % casing wear have been investigated. As expected, the casing design had to be stronger to ensure pressure integrity with casing wear. For a casing wear factor of 20 %, the casing design for the deepwater well had to increase the casing grade to P-110 as seen in Figure 4.21. Therefore, the recommended casing design for the deepwater well with casing wear was a weight and grade of 53.5 ppf and P-110 respectively. Figure 4.20 illustrates the effect casing wear had on the design limit envelopes. Dotted lines describes 20 % casing wear.

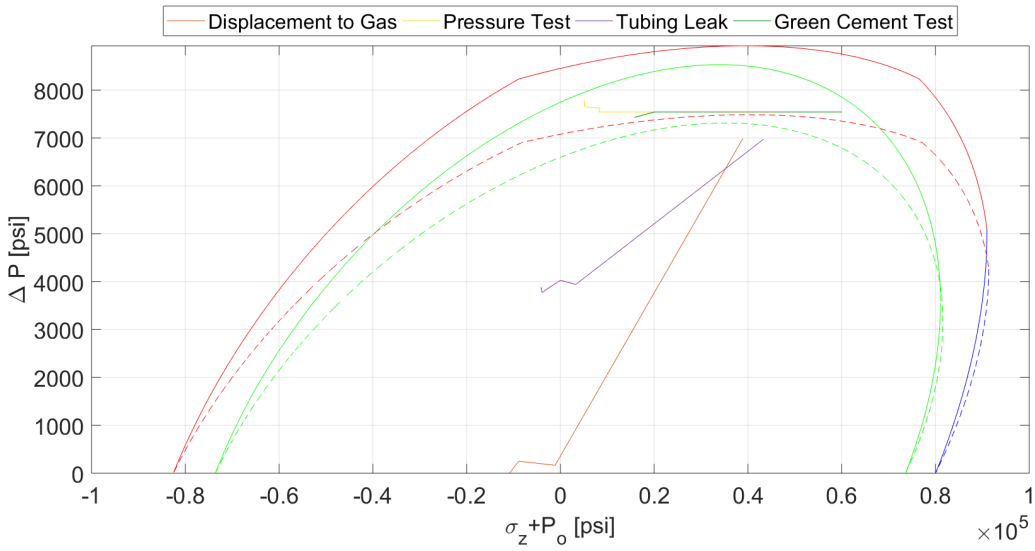

Figure 4.20: The effect of 20 % casing wear on the final deepwater well design.

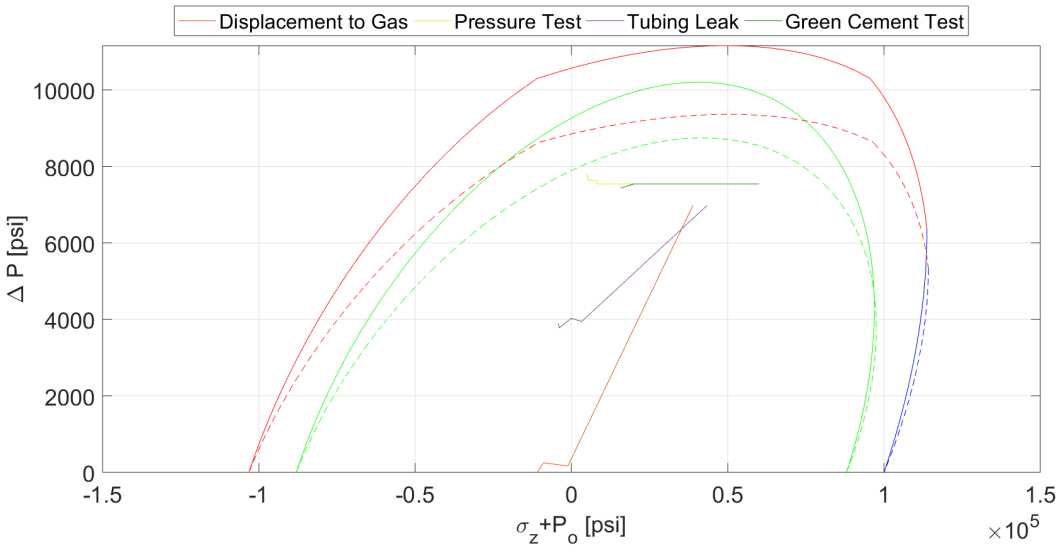

Figure 4.21: The effect of 20 % casing wear on the final deepwater well design when the grade was increased to P-110.

Chapter 5

Discussion

The following chapter will discuss the most important findings in this thesis. First, a discussion of how the Wilhelmsen&Bauge model will change the design from the current industry practice will be presented. Then, the practical applicability of the new burst model will be analysed for three different case studies. In the end, how to use the model correctly will be discussed.

5.1 New Design Elements

Today, the industry is using what is known as a deterministic model (section 2.1.2) in their tubular design process. The use of a deterministic model entails that the worst case/minimum input values are chosen in order to calculate the design limit plot. This results in an underprediction of the casing strength in many cases, as the worst pipe parameters usually not are representative for the whole casing. In addition, design factors up to 1.25 are applied to account for uncertainties downhole.

This conservative approach is still used in the new improved burst model, due to the severe consequences of overestimating the casing strength. Another argument is the industry's low willingness to change. Therefore, the model proposed uses much of what is known to the industry, but in a less conservative way. The four main elements in the improved burst model are discussed below.

1. Remove Barlow's equation

Firstly, the new model proposes to remove Barlow's equation from the design limit plot. The reason is that the equation is only valid under certain conditions and these conditions are never seen in real well applications. For instance, Barlow's equation does not take external pressure into account, but rather assumes it to be zero in the derivation (section 2.2). As a consequence, the predicted yield pressure is conservative. The equation is also uniaxial, meaning that it is not valid in tension or compression. It is well known that the burst pressure limit of a tubular increase with increasing tension and this fact gets lost in Barlow's equation.

2. Exact von Mises Ellipse

Secondly, the new model proposes a new way of plotting the von Mises ellipse. Today, the industry assumes zero external pressure when plotting the triaxial design envelope. This approximation makes the design criterion, "not only approximate, but also inaccurate" (Goodman et al., 2017, 1). Therefore, the improved burst model operates with the exact ellipse proposed in section 2.3.1.2 instead, as it incorporates the external pressure.

The inclusion of external pressure in the von Mises ellipse has a trade-off with the industry practice. The intuitive understanding of the design limit plot gets undermined. The x-axis of the Wilhelmsen&Bauge model consists of $\sigma_z + P_o$, compared to the industry's axial force (F_a). This causes the boundary between tension and compression in the design limit plot to get lost. This might be the reason for why the exact formula has not yet been accepted to the current industry practice. However, this problem can be fixed by adding supporting plots with axial force to accompany the design limit plots.

Most tubulars used in the oil and gas industry today are thin walled. Therefore, it stands to reason that the von Mises equation should use thin walled assumptions. This was considered for the Wilhelmsen&Bauge Model, but as indicated in section 2.2, the assumption for tangential stress (2.2) do not incorporate external pressure. The Lamé equations, based on thick-wall pipe assumptions, were therefore used for both thick and thin wall pipes.

3. Pipe wall reduction factor (k_{wall})

Third, the improved burst model allows the allowable wall tolerance to be specified according to today's manufacturing processes. As presented in section 2.1.2.1, the industry uses a wall tolerance of 12.5 %. Although, the wall tolerance was specified in the 1960's based on the high wall thickness variation during manufacturing of seamless casings. Today on the other hand, the manufacturing process has improved. Hence, applying the same pipe wall reduction factor can be considered conservative and lead to overdesign of casing strings. This design element provides the operator with a tool to analyse and find the most cost-efficient design with regards to allowable wall tolerance and manufacturing costs.

The current industry practice is beneficial for the service companies providing casing strings. They are on paper allowed a significant inaccuracy in their manufacturing process. The buyers of casings, the operating companies, is therefore forced to order thicker casings to uphold industry standards. This means more steel is sold by the service companies, but also more emissions of CO2 from steel production. Therefore, it is highly doubtful that the service companies will give their actual pipe specifications in regard to wall variance without any proper motivation from the operators.

4. Ductile Rupture

Last, the improved burst model includes a true rupture limit. The formula predicts the burst pressure necessary for rupture and loss of pressure integrity. Ductile rupture (2.26) was chosen, as it performed best compared to the measured rupture pressures (Figure 4.4).

The equation is, as far as the authors know, not used in any part of the design process today. Even though a more comprehensive visualisation of the actual casing strength is achieved by including ductile rupture. Most significantly, a more cost-efficient and safer design can be created. This is illustrated in Figure 4.7 and Figure 4.8, where it is clear that the current industry practice overdesign for low grades and underdesign for high grades. In particular, the rupture limit is close to the yield limit for high casing grades. Hence, the design should not allow load lines to reach the yield limit at all. A higher design factor should be considered instead, to ensure a safe distance to the rupture limit. For low grades, on the other hand, the

difference in yield and rupture pressure are normally quite extensive. Essentially, opening up a possibility of designing past yield for non-cyclic load cases.

The ductile rupture equation used in the new model assumes capped-end conditions (section 2.3.2.1). In real well applications, capped-end conditions are rarely experienced. One of the few burst load cases where this is a reasonable assumption is the green cement test (section E.1.2). During this load case the end is free to move since the cement is still in a liquid state. As seen from Figure 4.8, axial tension can cause a higher prediction of the rupture pressure. Therefore, including the additional axial stress generated under capped-end conditions, can lead to an overprediction for non capped-end load cases. The error this causes should be further investigated.

Before the industry can put their trust in the validity of the ductile rupture equation, more test must be performed. Only results from 106 capped-end tests without external pressure and six burst rupture tests in tension have been found in publications. This is inconclusive to confirm the validity of ductile rupture under fixed-end conditions and in combination with axial stress and external pressure. However, ductile rupture performed well for the 106 test results presented in ISO:10400. As it can improve and optimise the design process, it is strongly recommended to confirm the validity of the formula under real well conditions.

Rejected Design Element

From the published results in Lin et al. (2014) the through-wall yield model seemed promising, with even better predictions than the presented ductile rupture model (section 4.1.2). However, the presented results were based on wrong input parameters. The wall reduction factor was applied to the measured minimum wall thickness in the 106 test results from ISO. This lead to a severe reduction in the predictions. Actually, with correct input parameters the model would have over predicted the burst limit in 99.1 % of the 106 test results as seen in Figure 4.4. This implies that the model can lead to severe consequences if used in the design process. Therefore, the through-wall yield model was not included in the improved burst model.

5.2 Case Study

As discussed above, there is a potential for optimising casing design by removing conservative assumptions and include the ductile rupture limit in the design process. This is the motivation behind the improved burst model proposed in chapter 3. The effect of applying the improved burst model on a Q&T production casing will be analysed for three vertical wells with different water depths.

1. Shallow water - 100 m

2. Midwater - 305 m

3. Deepwater - 1524 m

When the improved model is applied on a vertical well, both bending and torsional effects will be minimised. The improved model should therefore be used with care on deviated wells, as the effects of bending and torsional stress should be included in the analysis together with the new design element. It is important to notice that the new design elements still will contribute to an improved design for deviated wells. The implication of the results will therefore be transferable to deviated wells. However, the safety margins will change depending on the magnitude of bending and torsional stress.

As a result of analysing a Q&T casing, a burst factor of 1 instead of 2 can be applied. Consequently, the ductile rupture limit increases as seen in Figure 4.11. It should be noted that the assumptions for the allowable wall tolerance and crack depth parameters used in this thesis is purely based on the authors educated guesses of what a typical manufacture could promise.

In the case study performed the maximum crack depth was set to 2.5 % of the nominal pipe wall thickness. The improved burst limit applied in this section allowed the manufacturing tolerance of the pipe wall to vary between 12.5 %, 9.4 % and 6.4 %.

None of the three case-studies performed where effected by removing the historical API burst limit, Barlow's equation. This can be seen from the design limit plot given in Figure 4.13, Figure 4.16 and Figure 4.18. This result supports the decision to remove the limit in the improved model.

The relevant load cases for burst simulated for each well are displacement to gas (Appendix E.1.1), green cement test (Appendix E.1.2), pressure test (Appendix E.1.3) and tubing leak (Appendix E.2.1). Initial conditions have also been included for reference. Furthermore, the design only considers burst, due to the topic of this thesis.

5.2.1 Shallow Water

A shallow water well (< 150 m) will experience relative low pressures during the well's lifetime, due to the low water column above. For this reason, the formation pressure will be lower compared to the deeper wells studied below. Consequently, the strength requirement is smaller for the casing string.

The well studied in this section assumes a water depth of 100 m. Further well specific details for this case study can be seen in Appendix D.1. As discussed, many low casing grades have a large difference between the minimum ultimate tensile strength and the minimum yield strength. As a result, the material can take larger plastic deformations before rupture occurs. The pipe will expand before rupturing. In this situation, the industry practice can lead to a conservative design.

With this in mind, two casing design routines for the 9 5/8" production casing were run. One in accordance with the industry practice and one in accordance with the Wilhelmsen&Bauge model. The resulting casing grades, weights and safety factors are given in Table 4.6. Figure 5.1 shows a design limit plot from the Wilhelmsen&Bauge model with a 12.5 % allowance in pipe wall thickness. In addition, the weight and grade of the production casing corresponds with the industry practice.

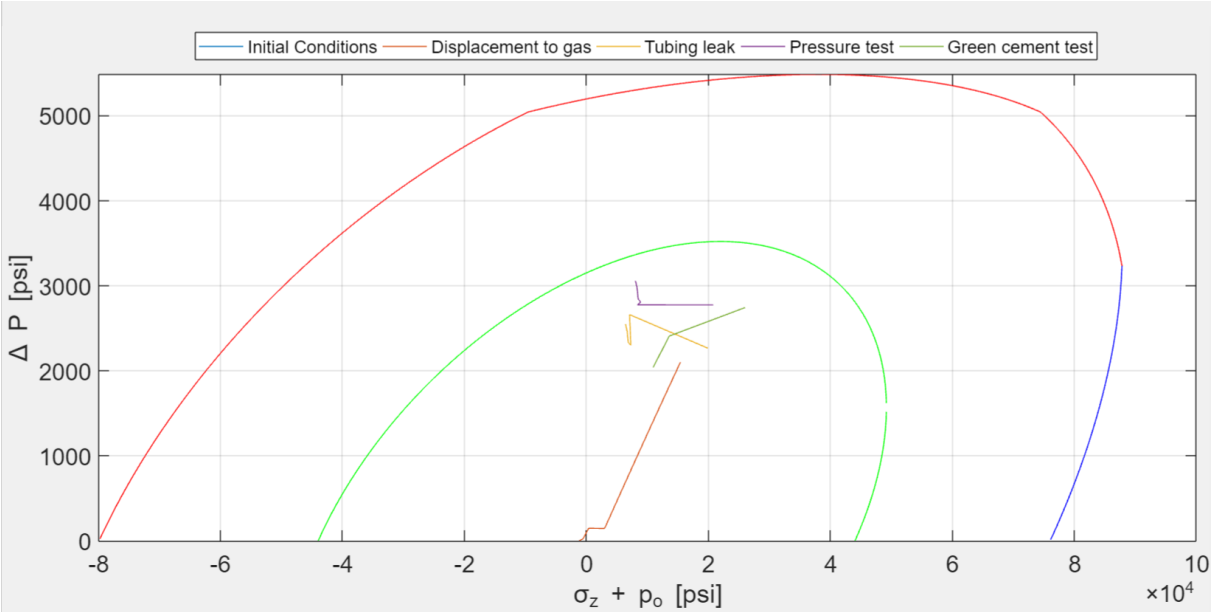

Figure 5.1: Design limit plot for the Wilhelmsen&Bauge model with casing weigh and grade of respectively 40 ppf and K-55. The model has an allowable wall tolerance of 12.5 %.

By analysing the design limit plot in Figure 5.1, one can argue for a less conservative design based on the extra plastic strength area. Accordingly, reducing the casing weight to 36 ppf results in the design limit plot given in Figure 5.2 for the Wilhelmsen&Bauge model.

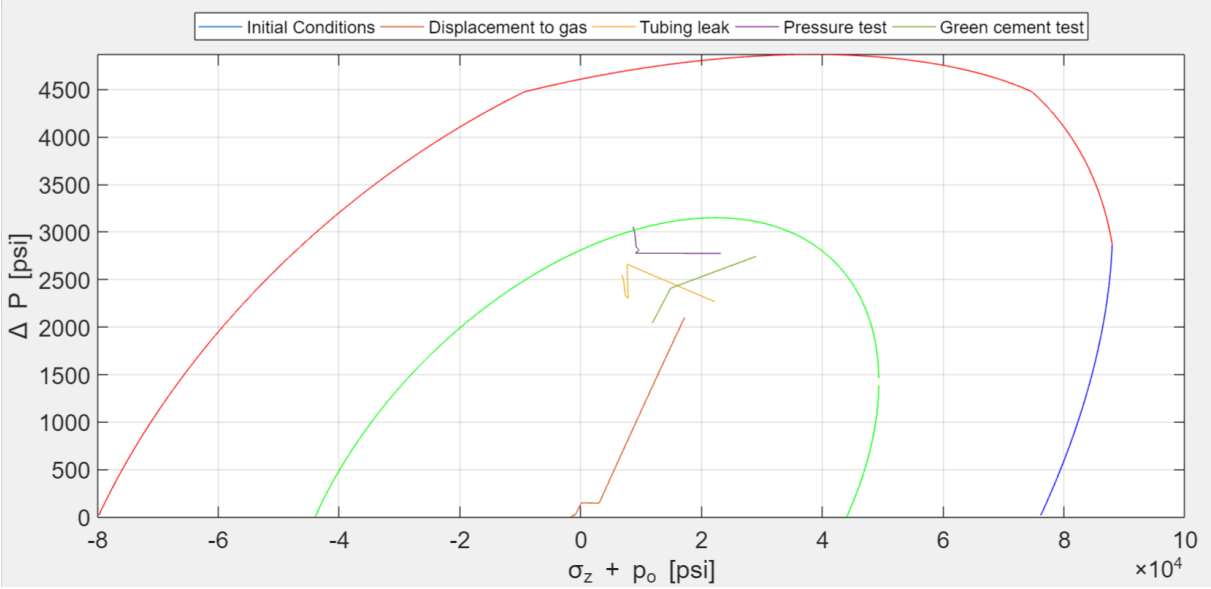

Figure 5.2: Design limit plot for the Wilhelmsen&Bauge model with casing weigh and grade of respectively 36 ppf and K-55. The model has an allowable wall tolerance of 12.5 %.

Normal procedure in casing design is to never surpass the elastic limit, i.e. all load cases must be lower than the triaxial yield criterion. However, the improved burst model allows the engineer to make reasonable choices in the design. In this case study, pressure test is the

only load that will surpass the elastic limit, as illustrated in Figure 5.2. As the pressure test is designed to consider the worst load case, including a safety margin, the well will only experience this stress regime once in its lifetime. Hence, the well will not experience cyclic loading in the plastic region. Therefore, the engineer can suggest a weight reduction as a possibility by argue that it will not jeopardise the pressure integrity of the casing.

Based on this information a reasonable requirement for the allowable tolerance in wall thickness can be estimated for the casing manufacturer. A reduction in the wall tolerance from 12.5 % to 9.4 %, ensures that all the load cases are within the elastic region. No further reduction in grade or casing weight were achieved by reducing the allowable wall tolerance further to 6.4 %. Although, the triaxial safety factor increased from 1.278 to 1.322.

All things considered, the improved burst model allows the casing weight to be reduced from 40 ppf to 36 ppf. Two methods can be used to reach this goal. First, allow the pressure test to slightly surpass the elastic limit to keep an allowable wall tolerance of 12.5 %. Alternatively, reduce the allowable pipe wall tolerance to 9.4 % and keep all the load cases within the elastic region.

5.2.1.1 Exact von Mises circle - Shallow Water

The exact von Mises circle has been utilised for the full casing design for the shallow water well. All of the anticipated load cases for the recommended casing strings are visualised in Figure 5.3.

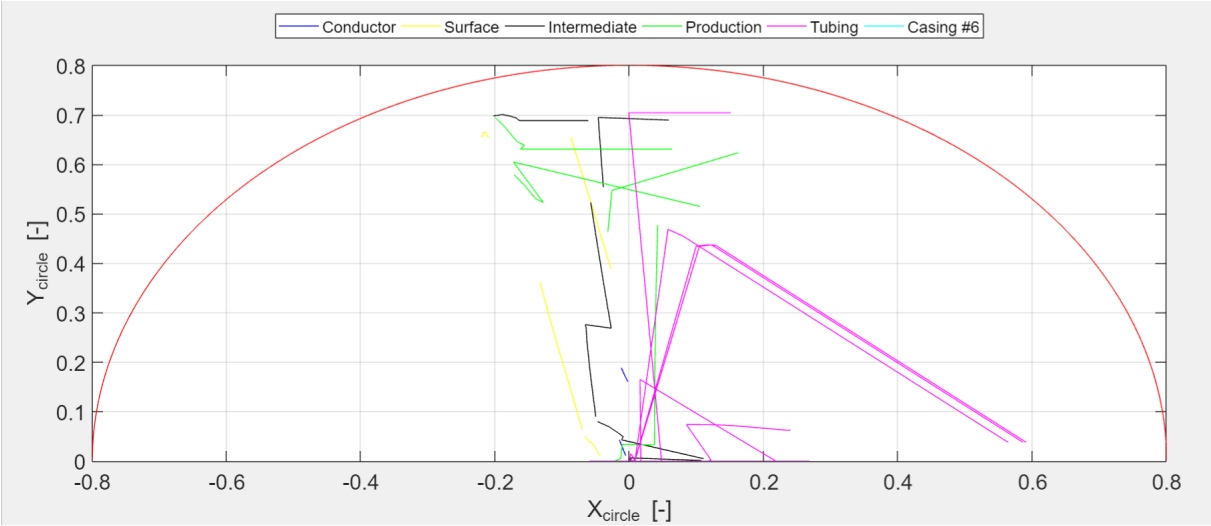

Figure 5.3: End Design limit plot for the shallow well example.

As a result, one can confirm that the chosen design is within the triaxial yield limit for all burst load cases the well will experience. This is the practical application for the exact von Mises circle, to visualise in only one page that the design is safely inside the triaxial criterion. Hence, it can be useful as a summary or a quick overview in a report. As the model do not specify the axis nor load cases, it cannot replace a detailed design process.

5.2.2 Midwater

A midwater well is defined for water depths ranging from 305 m - 1524 m. The annular pressure will usually be larger than for a shallow water well as studied above, due to higher formation pressure. Therefore, the strength requirement for the casing string must be higher. In contrast to the shallow water well, the ductile rupture limit will not affect the design in the same manner. It stems from the fact that the plastic strength area is decreased.

The well studied in this section assumes a water depth of 305 m. Further well specific details can be found in Appendix D.2. Two casing designs for the 9 5/8" production casing were created. First, a design in accordance with the industry practice. Then, a design in accordance with the Wilhelmsen&Bauge model. The industry practice required a weight and grade of respectively C-90 and 58.4 ppf. This can be seen in table 4.7, which summarise the results from the different models. In contrast to the industry practice the improved burst model contained an allowable wall tolerance of 6.4 % instead of 12.5 %. As a result, the burst limit increased in Figure 5.4 compared to Figure 4.16.

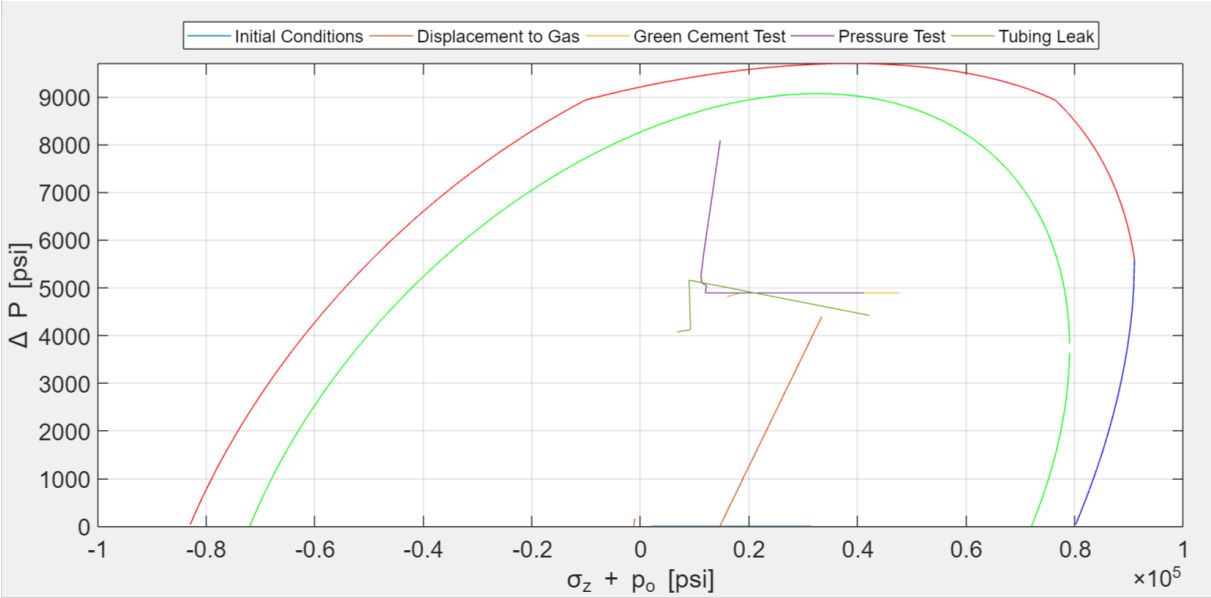

Figure 5.4: Design limit plot for the Wilhelmsen&Bauge model with casing weigh and grade of respectively 58.4 ppf and C-90. The model has an allowable wall tolerance of 6.4 %.

By analysing the design limit plot in Figure 5.4, one can argue for a less conservative design based on this extra strength area. A reduction in casing weight from 58.4 ppf to 53.5 ppf results in the design limit plot given in Figure 4.17.

As seen from Figure 4.17 the load lines is fairly close to the ductile rupture limit. Therefore, an increased design factor should be considered. As seen from Table 4.7 the safety factor towards ductile rupture is 1.332. To be on the safe side one can choose a more robust design than given in Figure 4.17. For instance, going back to the weight and grade of 58.4 and C-90 respectively. The safety factor towards rupture and loss of pressure integrity is then increased to 1.357, when an allowable wall tolerance of 12.5 % is applied. The corresponding design limit plot is given in Figure 5.5. A further increase in the rupture safety factor can be achieved by reducing the wall tolerance. However, in this load case a safety factor towards rupture of 1.357 was considered sufficient.

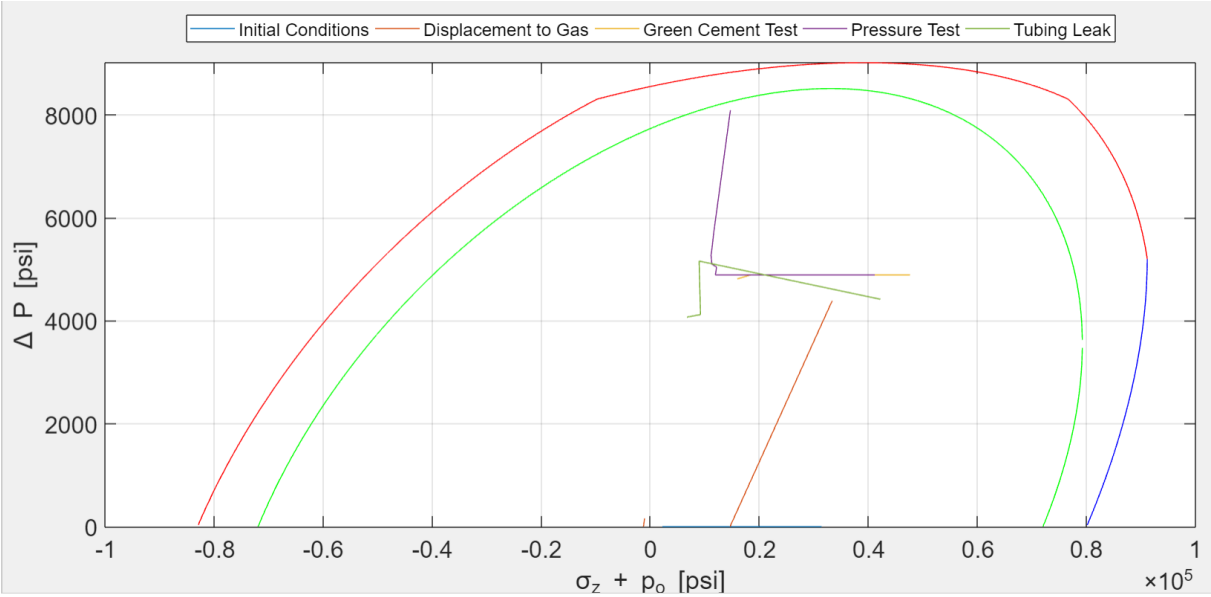

Figure 5.5: Design limit plot for the Wilhelmsen&Bauge model with casing weigh and grade of respectively 58.4 ppf and C-90. The model has an allowable wall tolerance of 12.5 %.

As seen from Figure 5.5, the plastic strength zone is small and it is therefore not recommended to design outside yield.

5.2.3 Deepwater

A deepwater well (1524 m < Well Depth < 2133 m) will cause a high pressure in the annulus for each casing cemented in place, due to the high water column above.

The well studied in this section assumes a water depth of 1524 m. The second element proposed in the improved burst model, is to use the exact von Mises ellipse. As Figure 4.6 indicates, the von Mises ellipse shifts to the left when external pressure is taken into account. The figure also indicates that relatively high external pressures are required to move the ellipse notably, meaning that the industry inaccuracy is most significant for loads with high external pressure.

First the production casing is designed in accordance with industry practice. Then, a second design is carried out using the Wilhelmsen&Bauge model.

The figure below shows a design limit plot from WellCat for the 9 5/8” production casing in the deepwater example well. As indicated by the plot, the load case pressure test crosses the

von Mises ellipse. Most likely would many casing design engineers have chosen a more robust casing in this example, by either increasing the weight, grade or even both. However, it should be noted that the exact triaxial safety factor calculated in WellCat (Figure 5.7) in fact is larger than the required design factor of 1.25. Hence, the approximate von Mises ellipse used in the ILS can easily lead to overdesign.

The inaccuracy in the design limit plot used in the industry is one of the elements that the Wilhelmsen&Bauge model corrects. This can be seen from the load line crossing the triaxial design limit in Figure 5.6, wheras the load line is within the triaxial limit in Figure 5.8. Both figures represent the same conditions, but are performed with the different models.

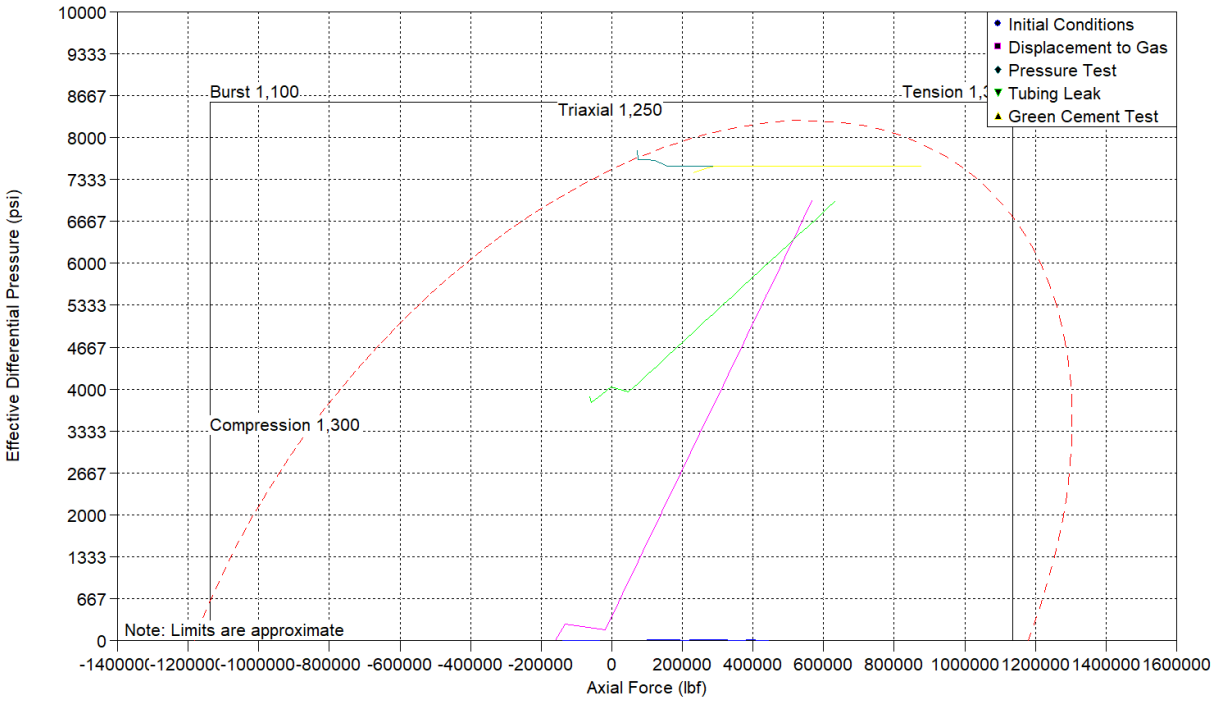

Figure 5.6: Burst load cases from deepwater example well plotted with approximate von Mises. The weight and grade are 58.4 ppf and C-90 respectively.

Load Minimum Safety Factors - Green Cement Test - 9 5/8" Production Casing

	String Section	MD Interval (m)	Pipe OD/Weight/Grade	Connection Name/OD/Grade	Minimum Absolute Safety Factor				
					Triaxial	Envelope	Burst	Collapse	Axial
1	1	1546,04-5229,42	9 5/8", 58,400 ppf, C-90	<N/A>	1,289	N/A	1,291	100+	1,671
2									

Figure 5.7: Minimum safety factors for the 9 5/8" production casing. Limiting load is green cement test.

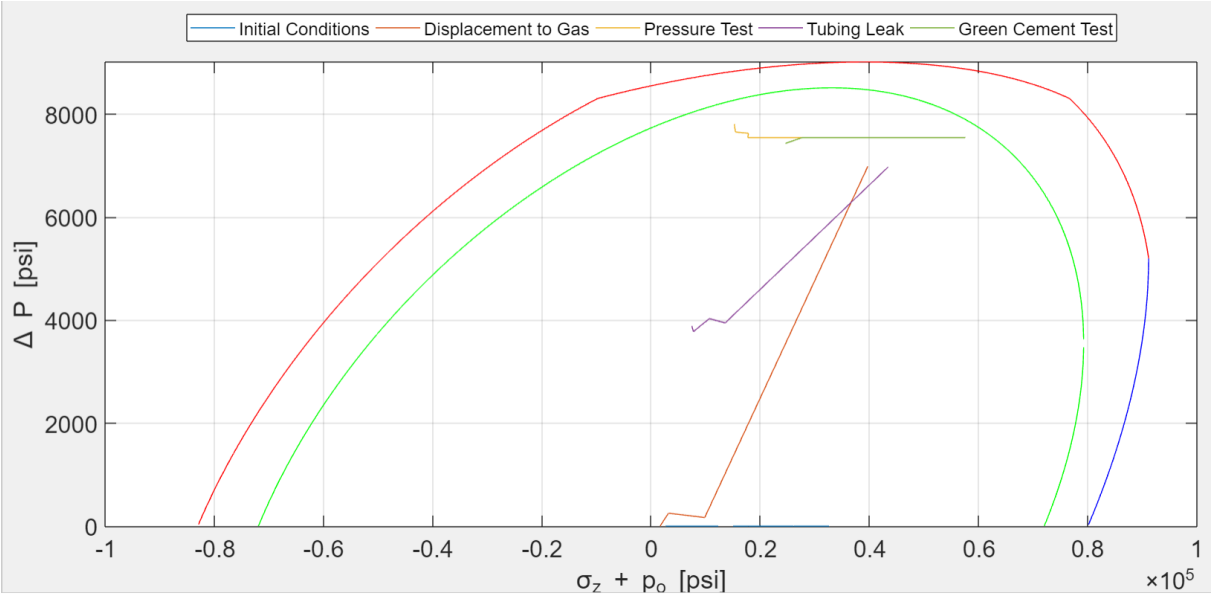

Figure 5.8: Design limit plot for the Wilhelmsen&Bauge model with casing weigh and grade of respectively 58.4 ppf and C-90. The model has an allowable wall tolerance of 12.5 %.

By using the Wilhelmsen&Bauge model a less conservative, but still safe design is obtained. A reduction in casing weight from 59.4 ppf to 58.4 ppf can be achieved by only plotting the exact von Mises ellipse.

As expected will a reduction in the wall tolerance increase the triaxial safety factor in the improved burst model, as seen in Table 4.8. By reducing the wall tolerance to 6.4 % (k_{wall} = 0.936) makes it possible to reduce the casing weight to 53.5 ppf.

Due to the high casing grade used in the design, the difference between yield strength and minimum tensile strength is small. This causes the ductile rupture prediction to be relatively close to the yield condition. Based on figure 5.8, design passed yield is not recommended in this thesis.

5.2.3.1 Casing Wear on Deepwater

As expected, casing wear causes the design envelopes to shrink as seen in Figure 4.20. It is important to notice that the load lines also should shift, due to their dependence on axial stress, which in turn is dependent on the cross sectional area and wall thickness in different regions of the pipe. However, as a uniform casing wear model has been used in the Wilhelmsen&Bauge model this effect is not accounted for.

It should be noted that 20 % wear is only an example. The real wear percentage must be calculated using a casing wear model.

5.3 Engineering basis

The industry has for many years put their trust in the von Mises/Lamé ellipse. The model has served them well for many years, but it is time for an update. The new model, ductile rupture, seems to perform well under testing (Figure 4.1) with only a mean underprediction of 0.44 % from the actual rupture pressure. However, as the comparison was performed without design factors the underprediction will increase accordingly in real well application (section 2.1.3). This is to account for unexpected risks and uncertain estimations of downhole parameters, such as temperature deration of yield.

As discussed above, the meaning behind this thesis is to improve the casing and tubing design for burst. The results from the example wells presented shows that the summation of each contribution from the proposed measures in the new model, can save both money for the industry and the earth from CO_2 pollution by the reduction of steel. However, it is important to not use the model without knowing the ramification of the model inputs. This is why a sensitivity analysis (section 4.1.4) for the model parameters have been performed.

The estimation of the hardening index factor (n_R) is described in section 2.5. Such tests costs both time and money, and its understandable that the industry would not perform such test for each tubular used. Therefore the ISO recommended values can be used in the improved burst model. The sensitivity analysis of the hardening index factor (section 4.1.4.4) indicates that the predicted burst rupture strength is not highly sensitive to the index factor. These results also back the assumption that doing uniaxial tensile tests to estimate the hardening index factor can in many cases be neglected without causing inaccurate results.

However, the sensitivity analysis shows that the allowable wall tolerance influences the predicted yield and rupture pressure the most. Therefore, it can be profitable for the operators

to set stricter requirements for the casing manufacturers. This can lead to a more optimised design, with lower embedded safety margins in the burst limits.

As illustrated in Figure 4.11, a Q&T casing will increase the ductile rupture limit. As the burst strength factor decreases from 2 to 1. Therefore, it can be profitable to use a Q&T casing.

Chapter 6

Conclusion

- The historical API's burst limit, Barlow's equation, should be removed from the design process. The burst limit is one-dimensional and not valid under normal well conditions.
- The wall variance allowance of 12.5 % used in the industry today is conservative. The tolerance was constructed from the wall variance in manufacturing of seamless casings in the 1960's.
- The improved burst model allows the engineer to set the wall tolerance in the design process. By reducing the established wall tolerance of 12.5 % in the current industry practice, steel costs can be cut. Designing with a wall tolerance of 6.4 % instead, allowed a steel weight reduction from 58.4 ppf to 53.5 ppf for the deepwater example well.
- Design limit plots in ILS contains the approximate von Mises ellipse. The ellipse is approximate because it neglects external pressure. The exact von Mises equation is used to calculate the triaxial safety factor in ILS. As a consequence, the calculated triaxial safety factor does not correspond with the triaxial design limit plot in ILS.
- An error is introduced in ILS by plotting the approximate ellipse. The error is proportional to the external pressure and shifts the approximate ellipse to the right. A deepwater well, due to high external pressure, is more prone to this error.
- The deepwater well studied in this thesis was affected by the approximate ellipse used in ILS. The assumption of zero external pressure caused the dimensional load case

to appear outside the triaxial design limit. Even though, the calculated triaxial safety factor actually was within the industry requirements. This confirmed that the error in ILS's design limit plot can lead to overdesign.

- The improved burst model plots the exact von Mises ellipse in the design limit plot. By including external pressure, overdesign of casing strings can be avoided.

- The exact von Mises circle can show load cases relative to the von Mises yield criterion from an entire well. As a result, the final casing design for the whole well can be represented in a single plot, as a summary.

- ISO have conducted 106 pipe rupture tests under capped-end conditions. Ductile rupture gives a good prediction of the rupture pressure with only a mean difference from the measured rupture pressure and standard deviation of - 0.44 % and 4.48 % respectively. Whereas, the yield models predicts deformation of pipe and not loss of pressure integrity.

- Low casing grades usually have a higher difference between the minimum yield strength and the minimum ultimate tensile strength. As a result, designing on the boarder of the elastic limit or slightly past can be considered for non-cyclic load cases.

- High casing grades usually have a small difference between the minimum yield strength and the minimum ultimate tensile strength and subsequently a small plastic zone. To maintain a safe casing design a higher safety factor towards yield should be considered.

- Only six published pipe rupture test in combination with tension were found. The ductile rupture predication gave a mean difference from the measured rupture pressure and standard deviation of 0.25 % and 3.22 % respectively. This supports the accuracy of the ductile rupture model, but the number of tests is insufficient to conclude anything without further testing.

- The improved burst model allowed cost savings for two of the three case studies analysed. The new design methodology reduced the steel weight from 40 ppf to 36 ppf for the shallow water well. For the midwater well no further reduction in the steel weight was recommended. In addition, the improved burst model allowed the steel weight to reduce from 59.4 ppf to 53.5 ppf for the deepwater well.

- The improved burst model is more environment-friendly than the ILS, as it can reduce the required steel produced and consequently CO_2 emissions.

Chapter 7

Further Work

- Burst testing should be executed for the full burst and tension quadrant.
- Include pipe buckling and bending in the Wilhelmsen&Bauge model.
- Improve triaxial safety factor calculations in the Wilhelmsen&Bauge model by including shear stress induced by bending in deviated wells.
- Include the collapse model proposed by Klever&Tamano in the Wilhelmsen&Bauge software.
- Create a probabilistic model of the ductile rupture equation including calculation of burst uncertainty.
- Include connection safety factors in the Wilhelmsen&Bauge model.
- Investigate the effects of temperature on burst strength.
- Test for pipe with casing wear of varying degrees.
- Test for different degree of temperature deration for different casing grades.
- Investigate other casing wear models and implement the most promising in the improved burst model.

Abbreviation

API	American Petroleum Institute
DF	Design Factor
ILS	Industry Leading Software
MASP	Maximum Allowable Surface Pressure
OCTG	Oil Country Tubular Goods
Q&T	Quenched&Tempered
RPM	Revolutions per Minute
SF	Safety Factor
TVD	True Vertical Depth
WOB	Weight on Bit
WV	Wear Volume

Nomenclature

W_f	=	Wear factor $[10^{-5}/psi]$
Δp_{MRW}	=	von Mises differential pressure for wrinkling
Δp_{RW}	=	Differential pressure limit for wrinkling
ϵ	=	Strain
ϵ_{eng}	=	Engineering strain
ρ_{cement}	=	Density of cement
$\rho_{fm,min}$	=	Minimum formation pressure gradient
ρ_g	=	Density of gas
$\rho_{mud,dt}$	=	Density of mud, deteriorated
ρ_{mud}	=	Density of mud
σ	=	Stress
σ_θ	=	Tangential stress for a thin-walled cylinder
σ_a	=	Axial stress
σ_b	=	Bending stress
σ_{eng}	=	Engineering stress
σ_e	=	Equivalent stress
σ_r	=	Radial stress
σ_{uts}	=	Ultimate tensile strength
$\sigma_{y,min}$	=	Minimum yield strength
σ_y	=	Yield strength
τ	=	Torsional stress
a_N	=	Maximum depth of a crack-like imperfection
CW	=	Thickness reduction from casing wear [%]
CW_B	=	New wall reduction [-]
D	=	Outside diameter

d	=	Inner diameter; d = (D-2t)
d_{ax}	=	Axial distance while reciprocation [ft]
d_{rco}	=	Total reciprocation distance [ft]
d_{rot}	=	Rotational distance while reciprocation [in]
D_{tj}	=	Tool-joint outer diameter
d_{wall}	=	Inside diameter based on k_{wall}t; d_{wall} = D-2k_{wall}t
E	=	Youngs Modulus
e	=	Eulers number
F_a	=	Axial force
F_y	=	Yield load
F_{eff}	=	Effective axial load
f_{umn}	=	Minimum tensile strength
k_a	=	Burst strength factor
k_{wall}	=	Pipe wall reduction factor (k_{wall} = 0.875)
L_p	=	Length of drillpipe
L_{stk}	=	Stroke length [ft]
L_{tj}	=	Length of tool joint [ft]
MD_{end}	=	End depth of operation [ft]
MD_{srt}	=	Start depth of operation
n_R	=	Hardening index for rupture
n_w	=	Hardening index for wrinkling
p_i	=	Inner pressure
p_M	=	von Mises pressure
p_{frac}	=	Formation fracture pressure
$p_{i,th}$	=	Tubing head pressure
p_{iAPI}	=	Internal pressure at yield for a thin pipe
p_{ir-New}	=	Internal pressure for through-wall yield
p_{iYOE}	=	Internal pressure at yield for an open-end thick pipe
p_o	=	Outer pressure
$p_{ref,T}$	=	Tresca pressure
r_i	=	Inner radius
r_o	=	Outer radius

S_{op}	=	Number of operational steps
SF_{ft}	=	Side force per ft of drillpipe [lbf/ft]
SF_{TJ}	=	Side force acting on the tool joint [lbf]
t	=	Nominal wall thickness
z_{shoe}	=	Casing shoe, vertical depth
z_{TOC}	=	Top of cement, vertical depth
$z_{wiperplug}$	=	Wiper plug vertical depth
d	=	Inner diameter; d = D-2t
L	=	Length
T	=	Operational time [hrs]

Bibliography

Bellarby, J. (2009a). *Well completion design*, volume 56. Elsevier.

Bellarby, J. (2009b). *Well Completion Design*, volume 56. Elsevier.

Byrom, T. G. (2015). *Casing and Liners for Drilling*. Elsevier.

Cernocky, V. A. P. P. R. W. E. (2005). Combined axial tension/compression and internal pressure testing of mini-pipe specimens in h2s environment to determine three dimensional (triaxial) stress states which produce crack initiation failure: Explanation of the new test fixture, mini-pipe specimen, and preliminary test results. *Society of Petroleum Engineers*.

Goodman, M. A., Kalil, I. A., McSpadden, A. R., Coker, O. D., et al. (2017). New tubular design ellipse with backup pressure. In *SPE Bergen One Day Seminar*. Society of Petroleum Engineers.

Hall, R., Malloy, K. P., et al. Contact pressure threshold: An important new aspect of casing wear. In *SPE Production Operations Symposium, year = 2005, organization = Society of Petroleum Engineers*.

Hall Jr, R., Garkasi, A., Deskins, G., Vozniak, J., et al. (1994). Recent advances in casing wear technology. In *SPE/IADC Drilling Conference*. Society of Petroleum Engineers.

Hill, R. (1998). *The mathematical theory of plasticity*, volume 11. Oxford university press.

ISO/TR, . (2007). *Petroleum and Natural Gas Industries - Equations and calculations for the properties of casing, tubing, drill pipe and line pipe used as casing or tubing, edition 1*. ISO.

Kazanowski, P. and Dickson, R. (2012). Evaluation of process mechanism and parameters for automated stretching line.

Klever, F. et al. (2010). Formulas for rupture, necking, and wrinkling of oil country tubular goods under combined loads. *SPE Journal*, 15(03):834–855.

Klever, F., Stewart, G., et al. (1998). Analytical burst strength prediction of octg with and without defects. In *SPE Applied technology workshop on risk based design of well casing and tubing*. Society of Petroleum Engineers.

Lin, Y., Deng, K., Sun, Y., Zeng, D., Liu, W., Kong, X., and Singh, A. (2014). Burst strength of tubing and casing based on twin shear unified strength theory. *PloS one*, 9(11):e111426.

PA, K. (2013). *Mechanics Lecture Notes: An introduction to Solid Mechanics*. The University of Auckland.

Rethwisch, W. C. D. (2008). *Fundamentals of materials science and engineering: An integrated approach*. John Wiley Sons, Inc.

Rosland, A. S. M. F. A. H. A. (2017). Integration of casing wear in casing design and stress analysis workflow. *Society of Petroleum Engineers*.

Samuel, R., Kumar, A., Gonzales, A., Marcou, S., Rød, A. M., et al. (2016). Solving the casing wear puzzle using stiff string model. In *IADC/SPE Drilling Conference and Exhibition*. Society of Petroleum Engineers.

Wilhelmsen, E. B. T. R. (2017). Analysis of industry standards and practice for casing and tubing design.

Appendix A

Additional Information

A.1 Thick-walled cylinders

A.1.1 Lamé's equation

Lame's equations for the radial and tangential stress components as a function of pressure (Bellarby, 2009b, 515):

$$\begin{aligned}\sigma_r &= \frac{r_i^2 r_o^2 (p_o - p_i)}{r_o^2 - r_i^2}\frac{1}{r^2} + \frac{p_i r_i^2 - p_o r_o^2}{r_o^2 - r_i^2} \\ \sigma_\theta &= -\frac{r_i^2 r_o^2 (p_o - p_i)}{r_o^2 - r_i^2}\frac{1}{r^2} + \frac{p_i r_i^2 - p_o r_o^2}{r_o^2 - r_i^2}\end{aligned} \tag{A.1}$$

Lamé's equation at the inner wall (r=r_i)

$$\begin{aligned}\sigma_r &= -p_i \\ \sigma_\theta &= \frac{p_i(r_o^2 + r_i^2) - 2p_o r_o^2}{r_o^2 - r_i^2}\end{aligned} \tag{A.2}$$

A.1.2 Axial stress

$$\Delta\sigma_z = \begin{cases} \frac{p_i r_i^2 - p_o r_o^2}{r_o^2 - r_i^2} & \text{capped ends, both} & \text{free ends, one or both} \\ 0 & \text{open ends, one or both} & \text{free ends, one or both} \\ \nu(\sigma_\theta + \sigma_r) & \text{open or capped ends} & \text{fixed ends, both} \end{cases} \tag{A.3}$$

Appendix B

Test Data

B.1 Complete data set of 106 pipe rupture test from ISO

The complete data set of 106 pipe rupture test from ISO (ISO/TR, 2007, 108) are compared with the different models in Figure B.1.

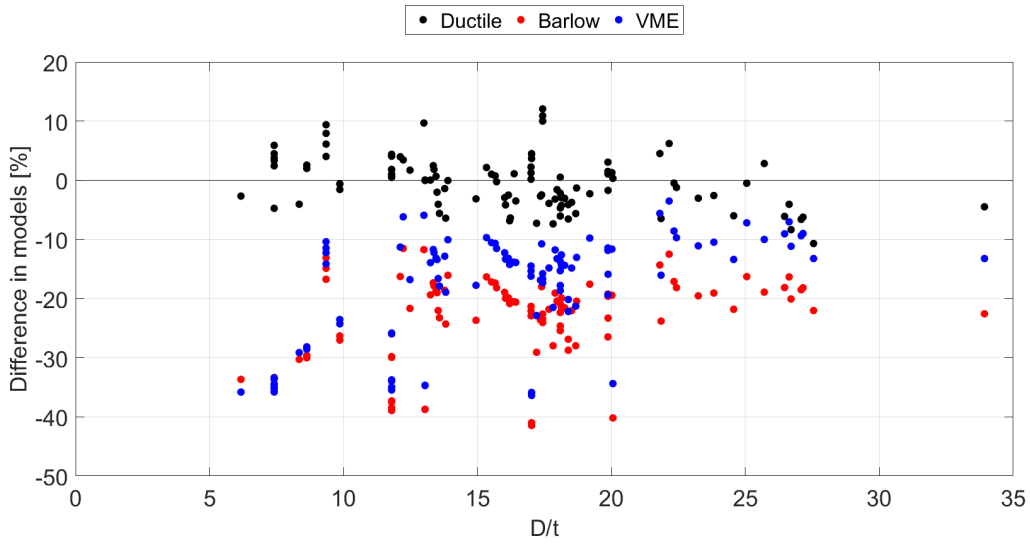

Figure B.1: Ductile Rupture, Barlow and von Mises burst limits compared with test results

The data presented in Figure 4.1 contain less data points to better visualise the trend. The data was sorted as follows:

- Test results with equal D/t-ratio and pipe parameters were merged to one datapoint, by taking the average of the measured rupture pressures.
- Test result with equal D/t-ratio and different pipe parameters was removed.

B.2 Tresca vs. von Mises

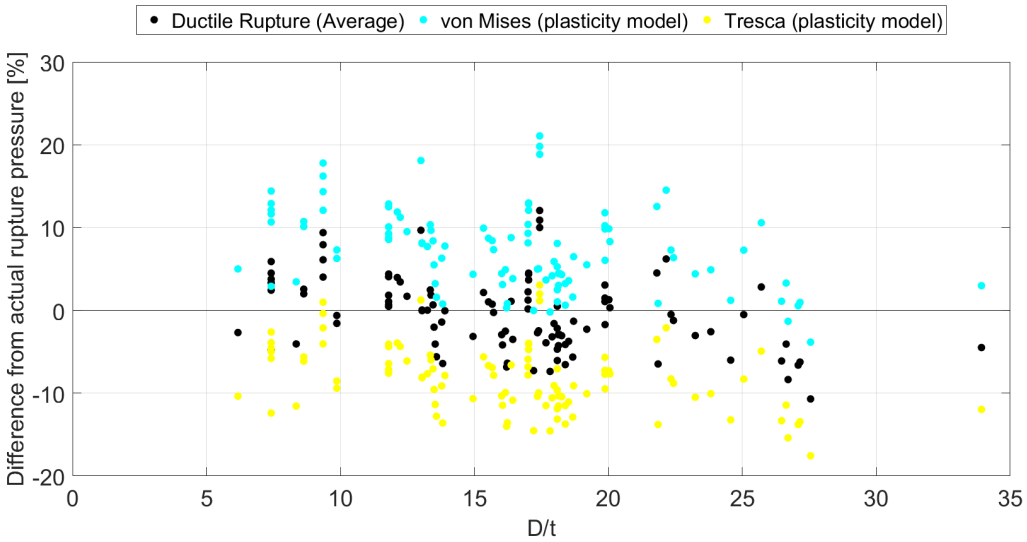

Figure B.2: Percentage difference from actual burst pressure predicted by Tresca criterion, von Mises criterion and an average of both criterion's

The rupture tests has also been used to investigate the use of an average value of the Tresca and von Mises plasticity models in the ductile rupture equation. The percentage difference in predicted value from actual burst pressure is plotted for each model(figure B.2). The findings is summarised in table B.1

Table B.1: Statistical evaluation of Tresca, von Mises and the average assumption

Model	**Standard deviation [%]**	**Mean [%]**
Tresca	4.0475	-8.2362
von Mises	4.9163	7.3470
Average	4.4765	-0.4446

Appendix C

Casing Wear

C.1 Casing Wear

A precise casing-wear model is important for well integrity and can improve cost efficiency in casing and tubing design. A new model to predict casing-wear by using stiff-string analysis instead of the conventional soft-string model is proposed by Samuel et al. (2016). The model aims to reduce the existing uncertainties in casing wear prediction. As the stiff-string model estimates more accurate side forces, and can predict the contact position of the drillstring at any given depth in the casing (Samuel et al., 2016, 2).

C.1.1 Casing Wear Model

The new casing wear model is based on the work performed by Hall Jr et al. (1994), as part of the joint-industry project DEA-42. This model defines casing wear as the crescent-shape groove, Figure C.1, that is formed by a rotating tool joint on the inside of the casing wall, Figure C.2.

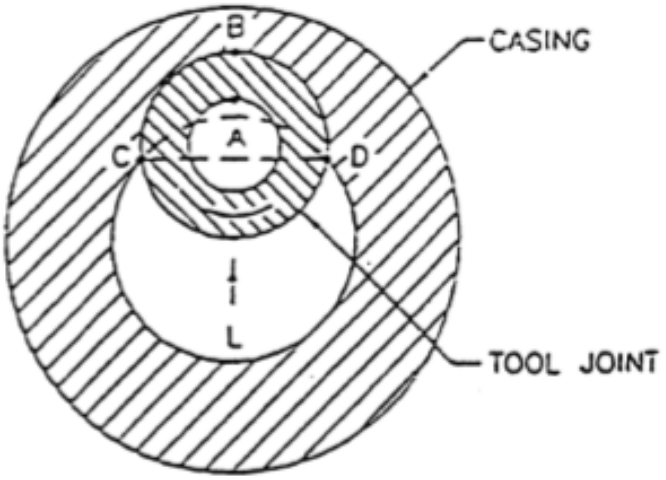

Figure C.1: Cross-Section of Crescent-Shaped Wear Groove, (Hall Jr et al., 1994, 2)

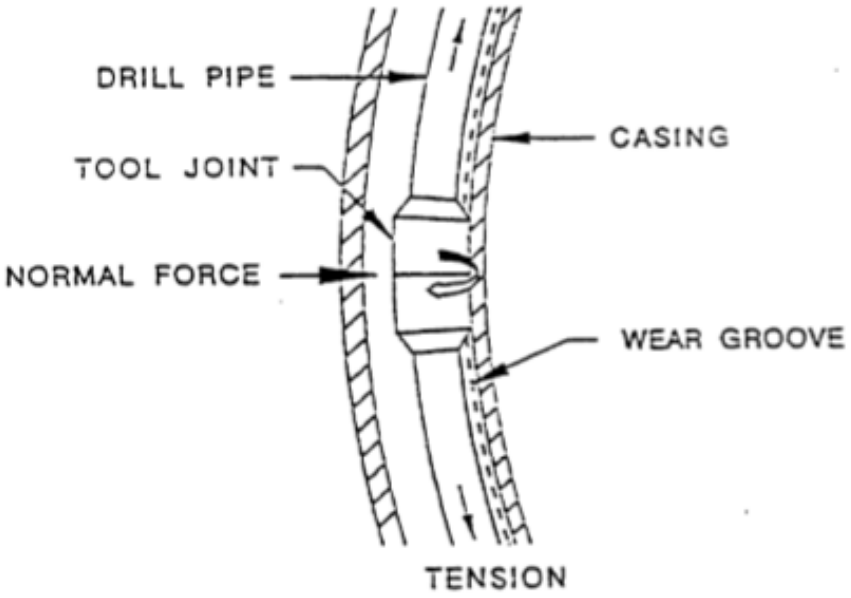

Figure C.2: Casing-wear at dogleg, (Hall Jr et al., 1994, 2)

The fundamental assumption behind the model is that "the volume worn away from the casing or riser wall is proportional to the frictional work done on the inner wall by the tool-joint (Hall et al., 1)".

The new model focuses on predicting wear caused by five major operations:

1. Drilling and backreaming

2. Rotating off-bottom
3. Sliding
4. Reciprocation

1. Drilling and backreaming

For the operations drilling and backreaming equation (C.1) is used to estimate the casing wear, (Samuel et al., 2016, 3).

$$WV = W_f \times SF_{tj} \times \pi \times D_{tj} \times RPM \times 60 \times T \times \frac{L_{tj}}{L_p} \tag{C.1}$$

where

WV = wear volume $[in^3/ft]$
W_f = wear factor $[10^{-5}/psi]$
SF_{tj} = side force acting on the tool joint [lbf]
D_{tj} = tool joint outer diameter [in]
T = operational time [hrs]
L_{tj} = length of tool joint [ft]
L_p = length of drillpipe [ft]

Both drilling and backreaming will have a varying contact between the tool-joint and the inner casing wall, as the drill string moves down/up the wellbore. This effect is considered in equation (C.1) by applying the ratio of tool joint length to the length of the drillpipe, L_{tj}/L_p. The average side force exerted on the casing from the tool joint is calculated from equation (C.2), assuming there is no pipe-body contact (Samuel et al., 2016, 3).

$$SF_{tj} = SF_{ft} \times \frac{L_p}{L_{tj}} \tag{C.2}$$

where

SF_{ft} = side force per feet of drillpipe [lbf/ft]

To calculate the casing wear the side force (C.2) and wear volume (C.1) are calculated in steps of 30 ft to simulate the drillstring movement. The incremental wear volume for each operational step is added cumulatively to get the total wear volume. The number of operational

steps are given by equation (C.3), by rounding up to the nearest whole number.

$$S_{op} = \frac{|\, MD_{end} - MD_{srt} \,|}{30ft} \tag{C.3}$$

where

S_{op} = number of operational steps
MD_{end} = end depth of operations [ft]
MD_{srt} = start depth of operation [ft]

The proposed modelling approach in (Samuel et al., 2016) divide the operational steps into segments of 10 ft to improve the accuracy. The increased number of point analysed along the wellpath will reduce the risk of under predicting the dogleg severity and subsequently the side force. As a result, the wellbore curvatures between the survey points are more easily detected. Figure C.3 shows how the wellpath geometry can mask the dogleg severity between the survey points i and j.

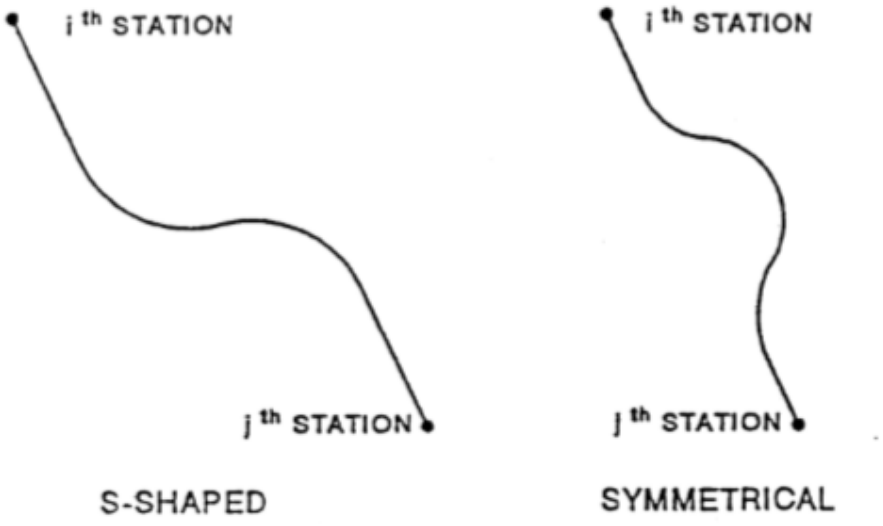

Figure C.3: Undetected dogleg, (Hall Jr et al., 1994, 4)

2. Rotating off-bottom

When the drillstring is rotated off-bottom without movement along the wellbore, casing wear can be estimated by neglecting this effect in equation (C.1). This is done by setting $L_{tj}/L_p = 1$. The calculation procedure is similar to that of drilling and backreaming, except that the calculation are performed over the entire operation length resulting in only one calculation step.

3. Sliding

In a sliding operation without rotation equation (C.4) is used to estimate the casing wear (Samuel et al., 2016, 3) along the total sliding distance, d_{sld}, given by equation (C.5).

$$WV = W_f \times SF_{tj} \times d_{sld} \times 12 \times \frac{L_{tj}}{L_p} \tag{C.4}$$

$$d_{sld} = MD_{end} - MD_{srt} \tag{C.5}$$

The calculation procedure is equal to that of drilling and backreaming, by dividing the sliding distance into segments by equation (C.3). For a sliding operation were rotation is applied, the wear volume can be calculated from equation (C.1).

4. Reciprocation

Reciprocation can be performed in the field to keep a gauge open-hole section or to clean the wellbore. The wear resulting from this operation can be estimated from equation (C.6). The total reciprocation distance, d_{rcp} are given by equations (C.7)-(C.9)

$$WV = W_f \times SF_{tj} \times d_{rcp} \times \frac{L_{tj}}{L_p} \tag{C.6}$$

$$d_{rcp} = \sqrt{d_{ax}^2 + d_{rot}^2} \tag{C.7}$$

$$d_{ax} = L_{stk} \times 12 \tag{C.8}$$

$$d_{rot} = \pi \times D_{tj} \times RPM_r \times t_s tk \tag{C.9}$$

where

d_{rcp} = total reciprocation distance [ft]

d_{ax} = axial distance while reciprocation [ft]

d_{rot} = rotational distance while reciprocation [in]

L_{stk} = Stroke length [ft]

Appendix D

Load cases - well information

D.1 Shallow water well

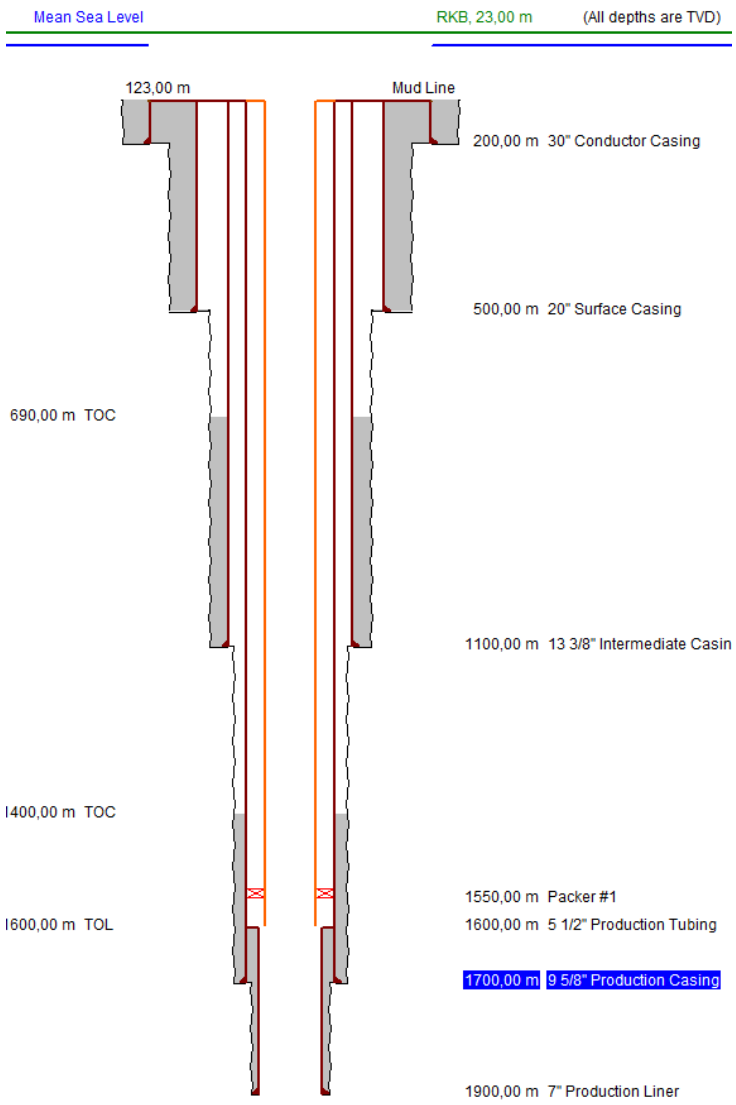

Figure D.1: Well sketch for the shallow water load case

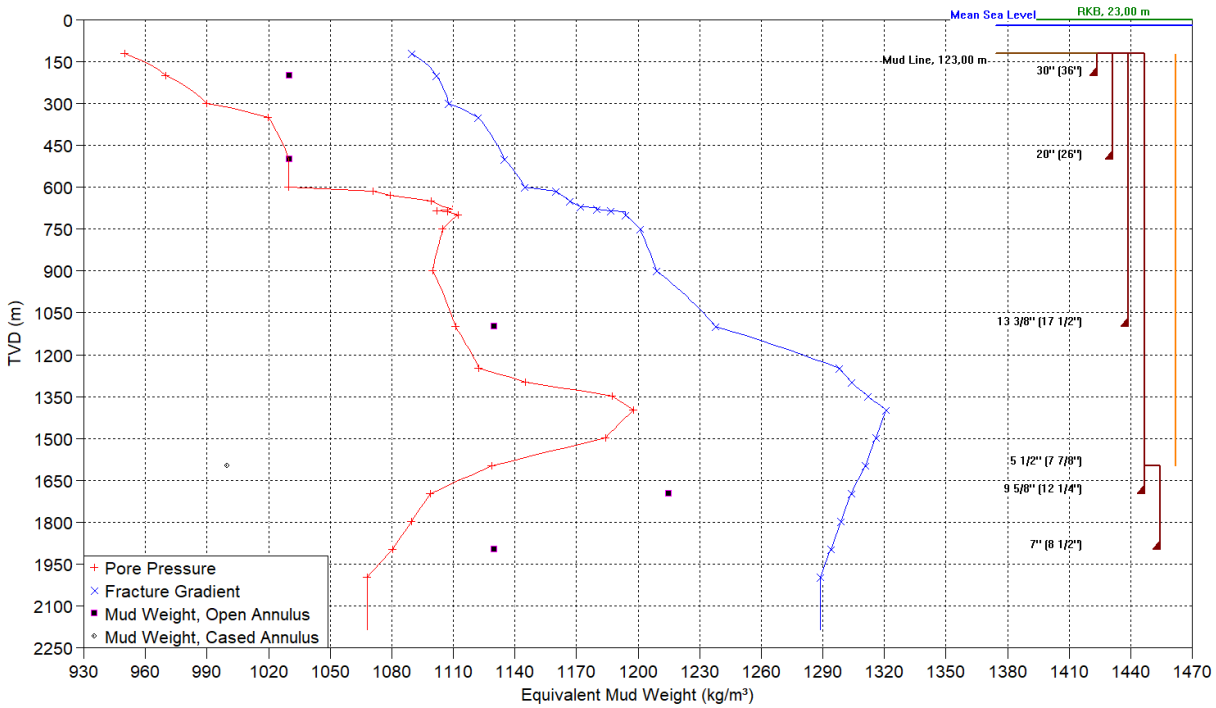

Figure D.2: Pore,Mud weight and fracture plot for shallow water load case

D.2 Midwater well

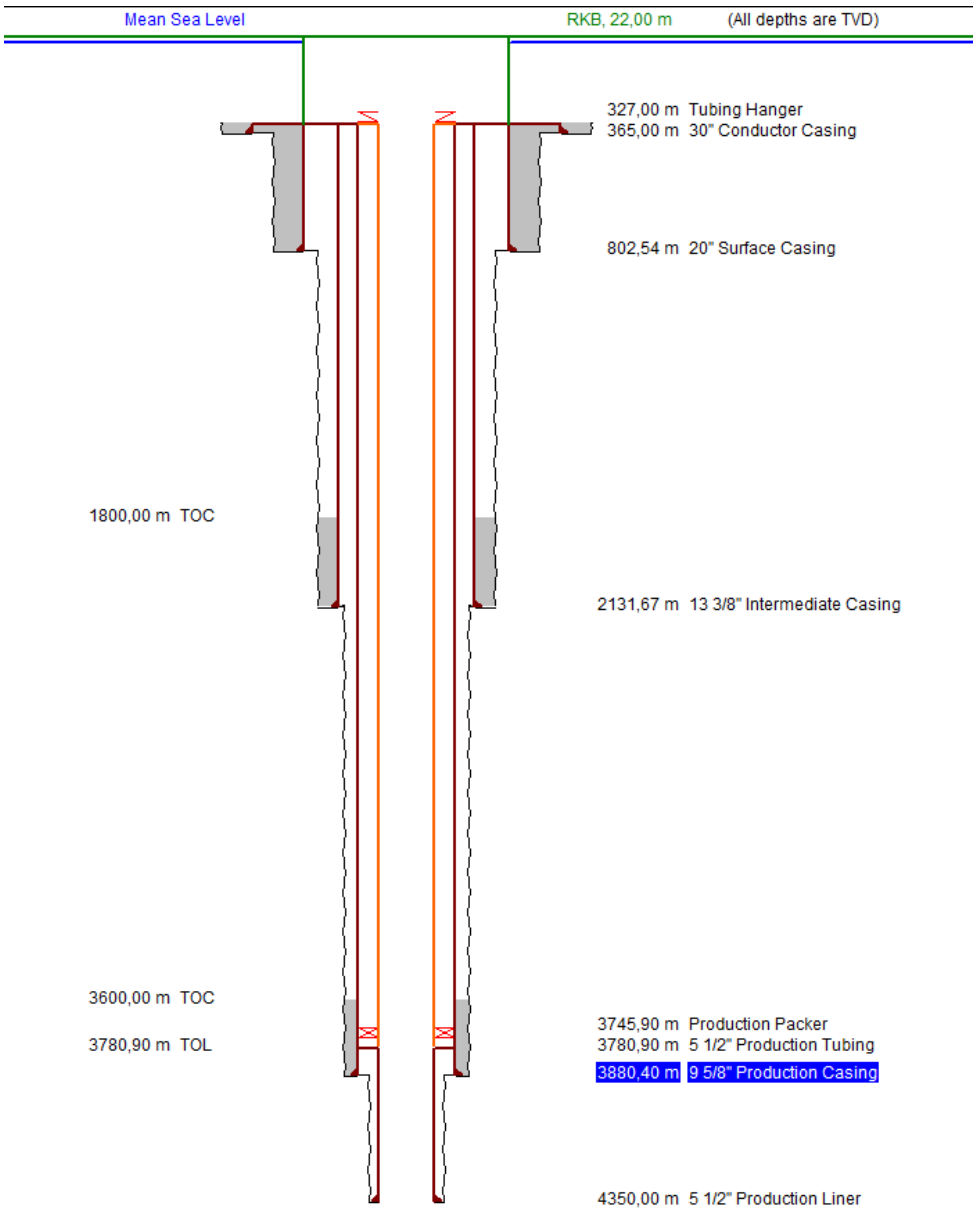

Figure D.3: Well sketch for the midwater load case

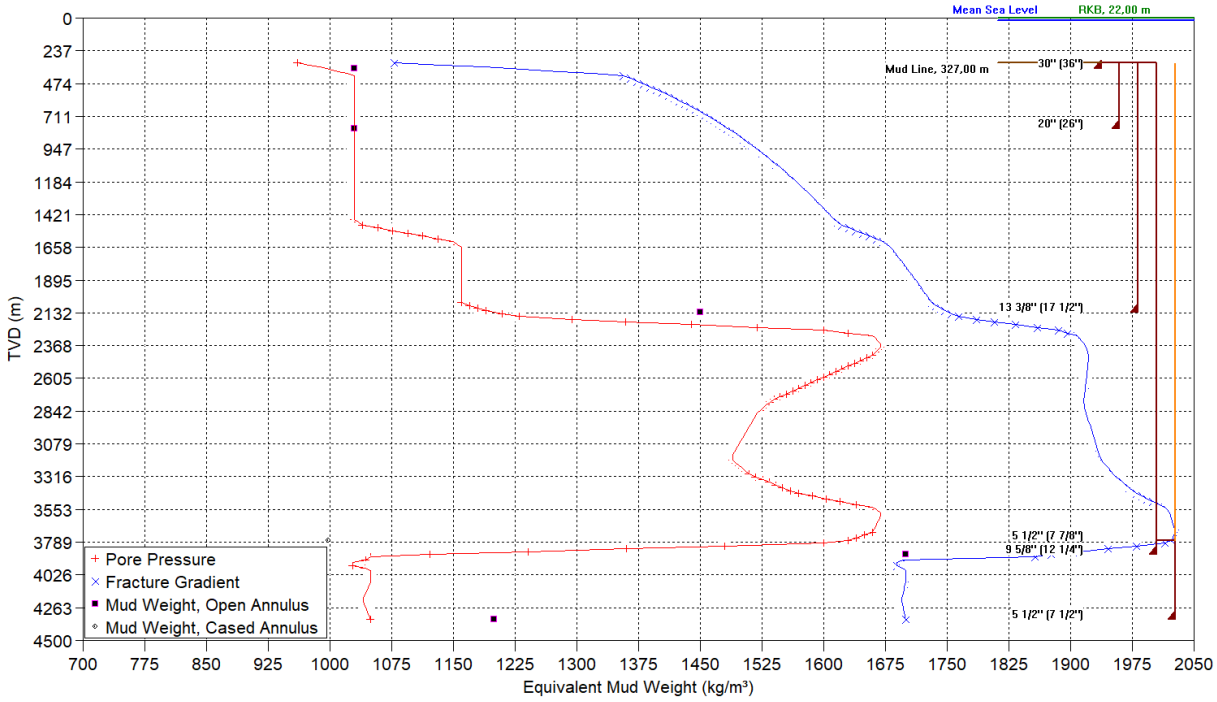

Figure D.4: Pore,Mud weight and fracture plot for the midwater load case

D.3 Deepwater well

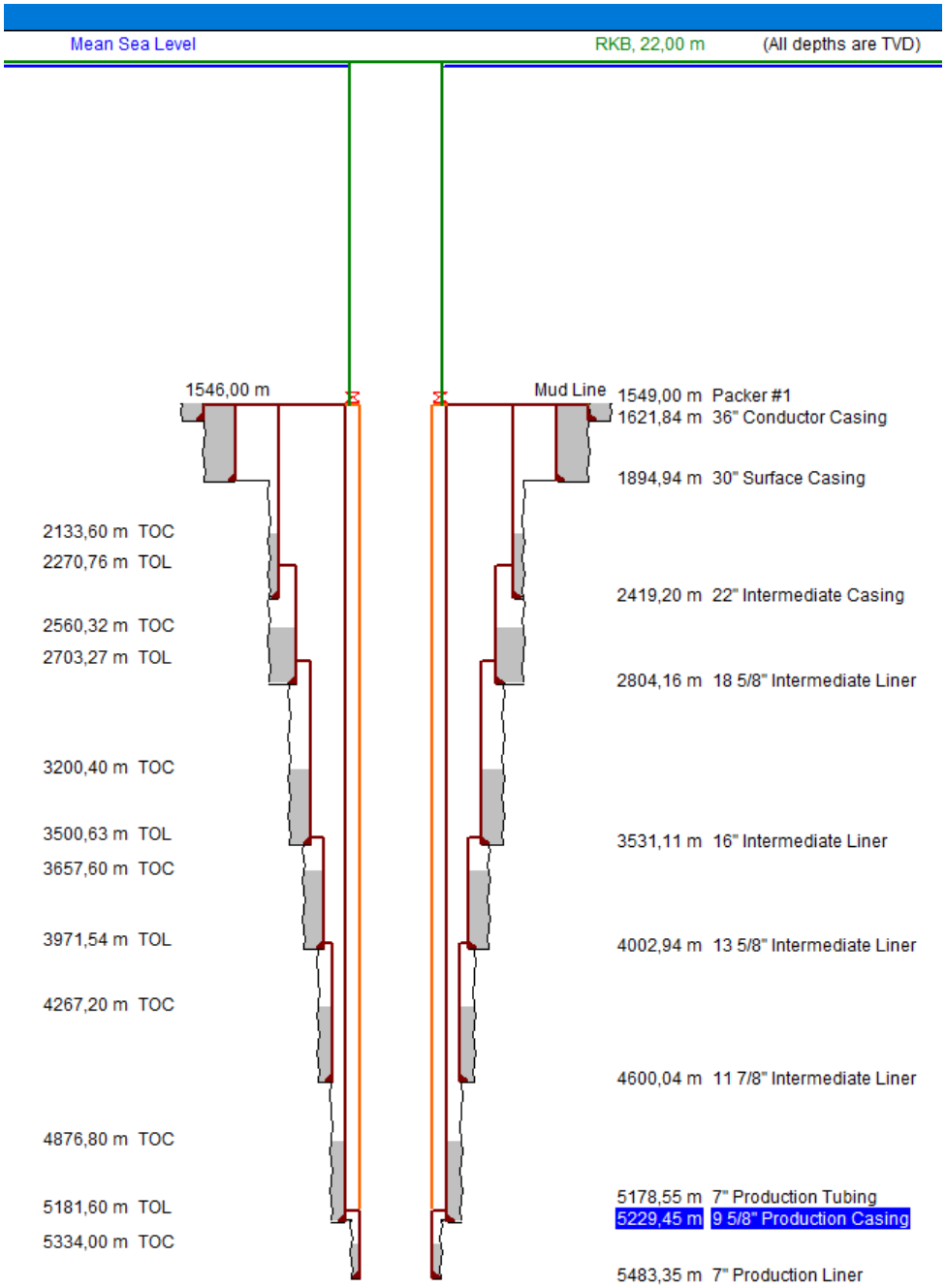

Figure D.5: Well sketch for the deepwater load case

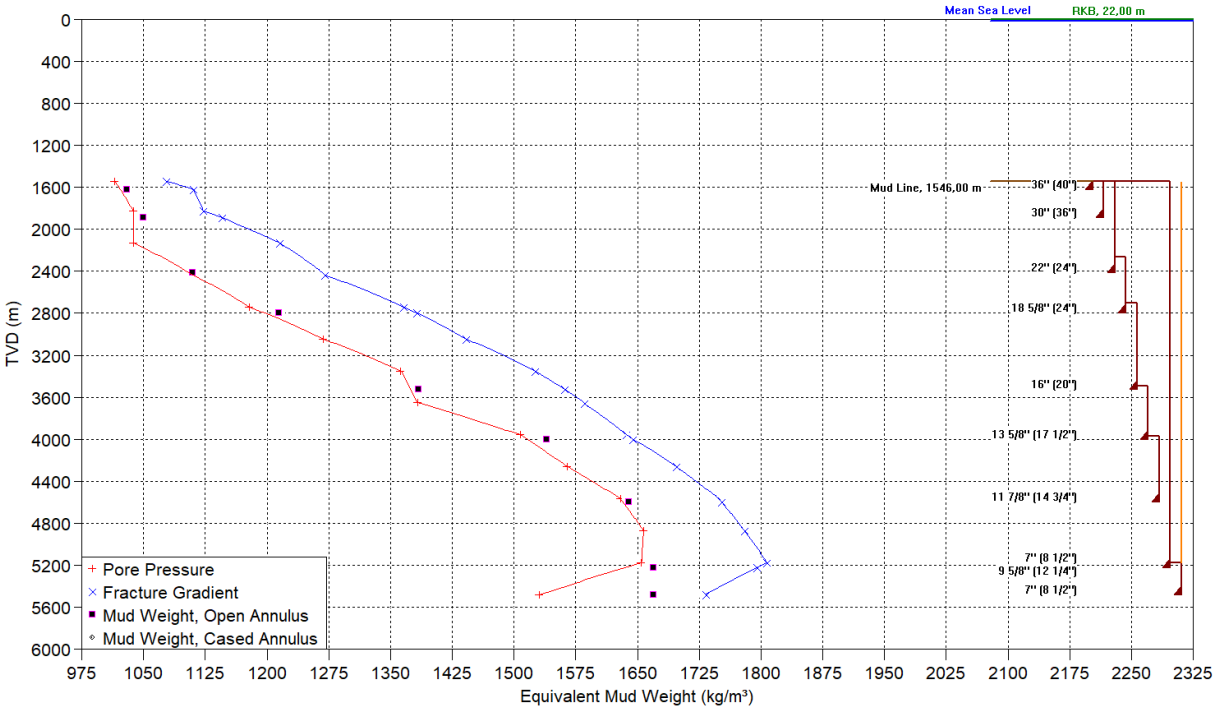

Figure D.6: Pore,Mud weight and fracture plot for the deepwater load case

Appendix E

Burst Load Cases

E.1 Drilling Loads

The loads simulated to perform a proper casing design in regards to burst are described in this section. The descriptions and corresponding figures are gathered from (Wilhelmsen, 2017, 33-58)

E.1.1 Displacement to Gas

Displacement to gas is a critical burst load for the casing strings. The load case is most relevant for the intermediate and the production casing, where the sections are drilled with a BOP. The load case simulates the entire casing filled with gas, from the casing shoe all the way up to the wellhead. The max pressure is linked to the fracture pressure at the casing shoe. This is the highest pressure the formation can hold before the fluids starts leaking off to the formation, and it will therefore also be the highest burst pressure for the casing during drilling. The burst pressure for the production casing is calculated by the inner and outer pressure in equation (E.1).

$$\begin{aligned} p_i(z) &= p_{frac} - \rho_g g(z_{shoe} - z) && \text{for} \quad z \leq z_{shoe} \\ p_o(z) &= \rho_{mud} g z && \text{for} \quad z \leq z_{TOC} \\ p_o(z) &= \rho_{fm,min} g z && \text{for} \quad z \geq z_{TOC} \end{aligned} \tag{E.1}$$

where

p_{frac} = fracture pressure at the shoe

ρ_g = gas density

ρ_{mud} = mud density

$\rho_{fm,min}$ = minimum formation pressure gradient

z_{shoe} = casing shoe, vertical depth

z_{TOC} = top of cement, vertical depth

WellCat simulates the gas gravity as a function of pressure and temperature data. The model also simulates a discontinuity at TOC, where formation pore pressure is applied in the cemented section. Figure E.1 visualizes how the different pressures are acting.

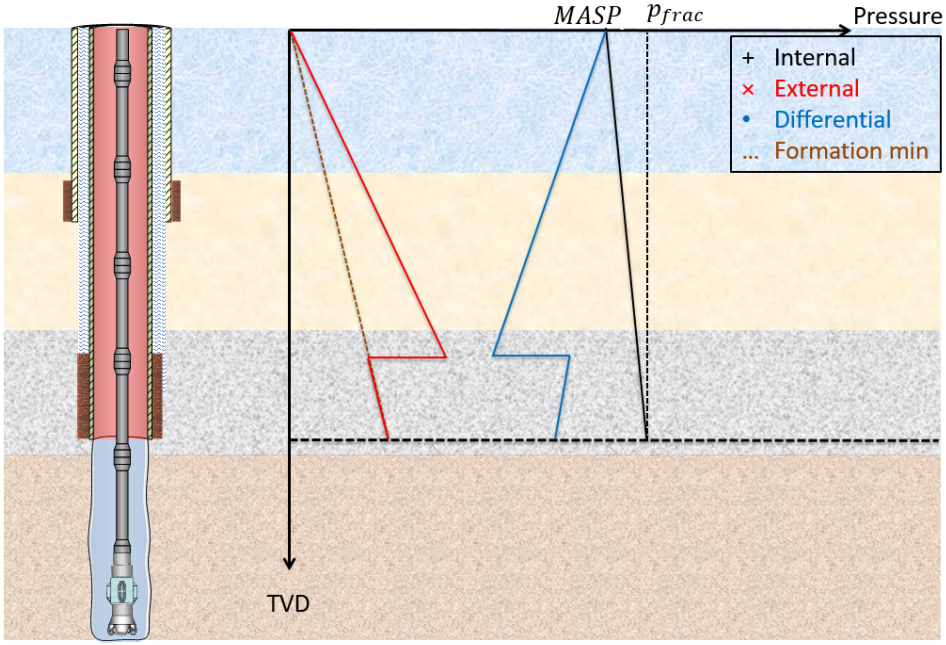

Figure E.1: Displacement to Gas

E.1.2 Green Cement Test

Green cement test has its name from when the test is performed - before the cement is set up. This load case simulates both a burst and axial load. The test is identical with any pressure test, except the cement is still in liquid state with high density fluid column. The pressure simulates the maximum anticipated burst pressure given by WDP for the production casing, defined as the Maximum Expected Kill Pressure (section **??**). For the previous set casing strings, the applied pressure is given by the Section Design Pressure, often defined by the displacement to gas load case plus a safety factor of 35 bar.

The motivation behind the green cement test is to save time. The pressure test has to be done while the cement is still in liquid state. Then, no micro annulus will be created. The time aspect will also be short enough to assume the mud has not deteriorated. The green cement test is often performed maximum one hour after the plug is bumped for the primary cement job.

The burst pressure for the production casing is calculated using the inner and outer pressure in equation (E.2).

$$\begin{aligned} p_i(z) &= WDP + \rho_{mud} g z && \text{for} \quad z \leq z_{wiperplug} \\ p_o(z) &= \rho_{mud} g z && \text{for} \quad z \leq z_{TOC} \\ p_o(z) &= \rho_{mud} g z_{TOC} + \rho_{cement} g (z - z_{TOC}) && \text{for} \quad z \geq z_{TOC} \end{aligned} \tag{E.2}$$

where

ρ_{cement} = cement density

$z_{wiperplug}$ = wiper plug, vertical depth

Figure E.2 visualizes how the different pressures are acting.

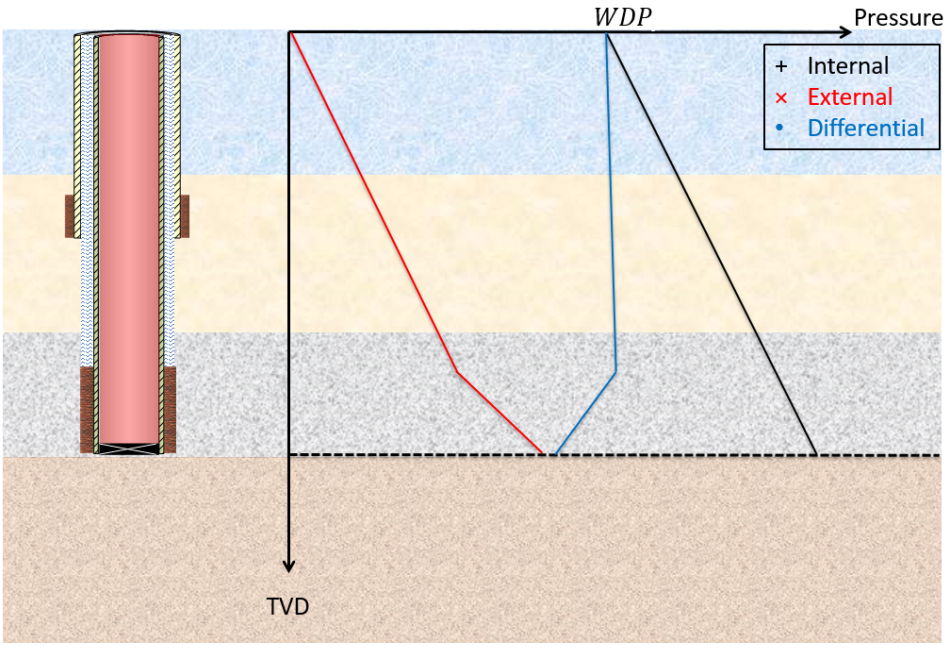

Figure E.2: Green Cement Test

E.1.3 Pressure Test

Pressure test is a burst load performed in the same manner as the green cement test. The difference is that the pressure test is performed after the cement is set. The green cement test is preferred as the initial pressure test method. Sometimes it is not possible to conduct a pressure test while the cement is still in its liquid state, and an ordinary pressure test must be performed instead.

The burst pressure for the production casing is calculated by the inner and outer pressure in equation (E.3).

$$\begin{aligned} p_i(z) &= WDP + \rho_{mud} g z \quad \text{for} \quad z \leq z_{wiperplug} \\ p_o(z) &= \rho_{mud} g z \quad \text{for} \quad z \leq z_{TOC} \\ p_o(z) &= \rho_{fm,min} g z \quad \text{for} \quad z \geq z_{TOC} \end{aligned} \tag{E.3}$$

The model also simulates a discontinuity at TOC, where formation pore pressure is applied in the cemented section. Figure E.3 visualizes how the different pressures are acting.

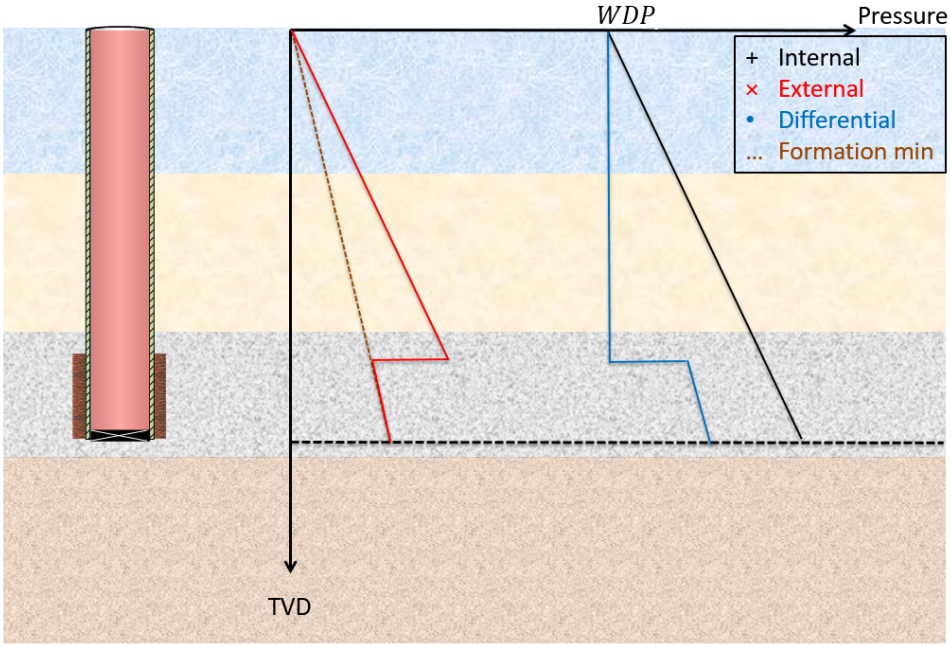

Figure E.3: Pressure Test

E.2 Production Load

E.2.1 Tubing Leak

Tubing leak can be critical for both the tubing and the production casing. The load case is parted in two scenarios; tubing leak below tubing hanger and tubing leak above production packer. Both the tubing and the production casing is evaluated according to these scenarios.

E.2.1.1 Tubing Leak below Tubing Hanger

The most critical collapse case the tubing can experience during an operation, is a leak below the tubing hanger. Tubing leak has been simulated with both oil and gas production. Thus, two alternative equations for inner pressure is presented. Tubing leak will cause high annulus pressure which lead to a critical collapse load on the tubing. The inner and outer pressures are calculated from equation (E.4):

$$\begin{aligned} p_i(z) &= p_r - \rho_g g(z_r - z) \quad \text{for} \quad z \leq z_r \\ p_i(z) &= p_r - \rho_o g(z_r - z) \quad \text{for} \quad z \leq z_r \\ p_o(z) &= p_{i,th} + \rho_a g z \qquad \text{for} \quad z \leq z_{packer} \end{aligned} \tag{E.4}$$

where

$p_{i,th}$ = inner pressure at tubing head

Figure E.4 visualizes how the different pressures are acting on the tubing:

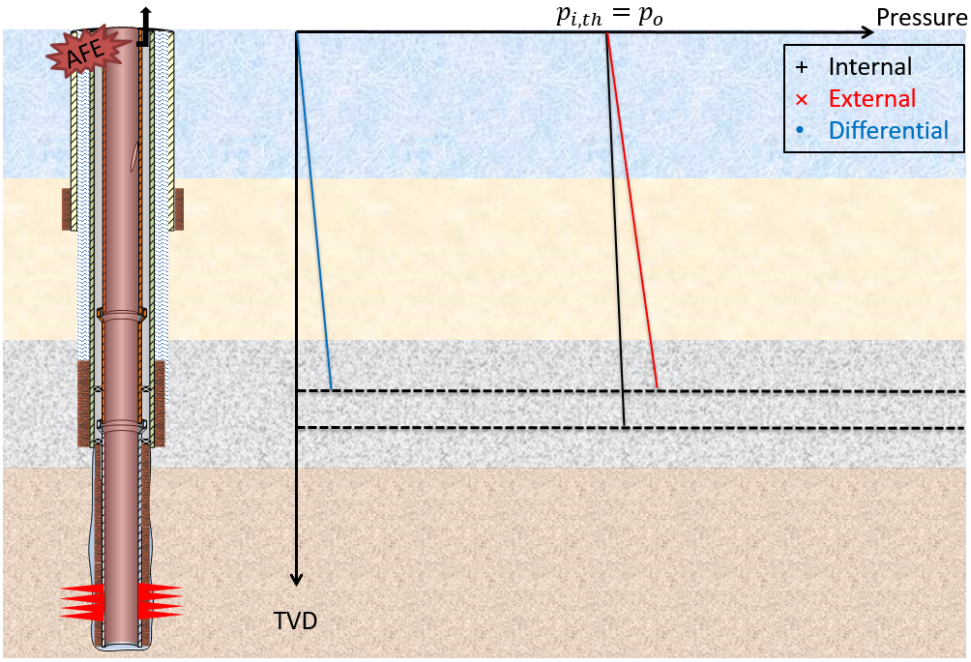

Figure E.4: Tubing Leak below tubing hanger, differential pressure acting on tubing

Tubing leak below the tubing hanger will further cause a burst load on the production casing. The most critical burst load will be with deteriorated mud as the external pressure above TOC. The burst pressure is calculated from equation (E.5):

$$\begin{aligned} p_i(z) &= p_{i,th} + \rho_a g z \quad \text{for} \quad z \leq z_{packer} \\ p_o(z) &= \rho_{mud,dt} g z \quad \text{for} \quad z \leq z_{TOC} \\ p_o(z) &= \rho_{fm,min} g z \quad \text{for} \quad z \geq z_{TOC} \end{aligned} \tag{E.5}$$

where

$\rho_{mud,dt}$ = deteriorated mud density

Figure E.5 visualizes how the different pressures are acting on the production casing:

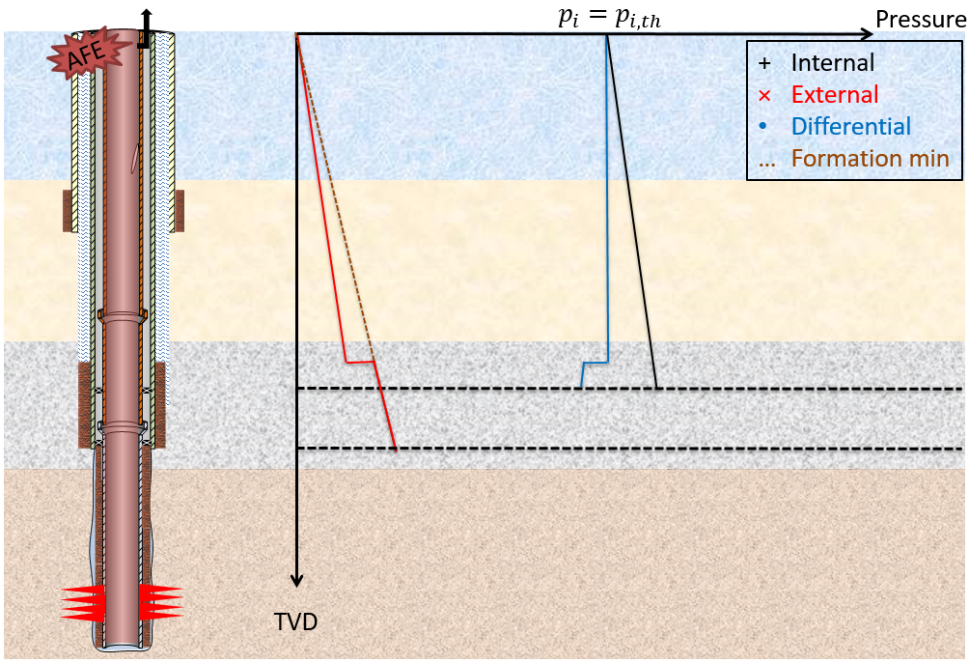

Figure E.5: Tubing Leak below tubing hanger, differential pressure acting on production casing

During production, the thermal expansion of steel will cause compression forces in the tubing. The increase in annular pressure causes a collapse load in the lower part of the tubing. The tubing will experience a reverse-ballooning effect, that will add to compressive forces from the thermal expansion of steel. Helical buckling and doglegs will induce local bending forces. If tubing leak occurs, it is inevitable to replace the tubing as the integrity of the primary barrier envelope is lost. However, the analysis of axial loads is helpful to evaluate packer forces.

Appendix F

Through-wall yield

The chosen input parameters and calculated values for the model with the 106 data sets from ISO were not reported in the paper Lin et al. (2014). Therefore, the reproduced calculations are performed by educated guesses of the input parameters, given in table F.1.

Table F.1: Input values used in calculations of the reproduced through-wall yield model

Parameter	**Value**
Factor to account for specified manufacturing tolerance of the pipe wall (k_{wall})	0.875
Maximum depth of a crack-like imperfections (a_N)	$0.005 \times t_{min}$
Burst strength factor (k_a)	2

To check that the reproduced model is representative for the data presented in (Lin et al., 2014), a comparison is done to the reproduced model with the input parameters given in Table F.1. Figure F.1 shows the difference in the presented results from Lin et al. (2014) and the reproduced model.

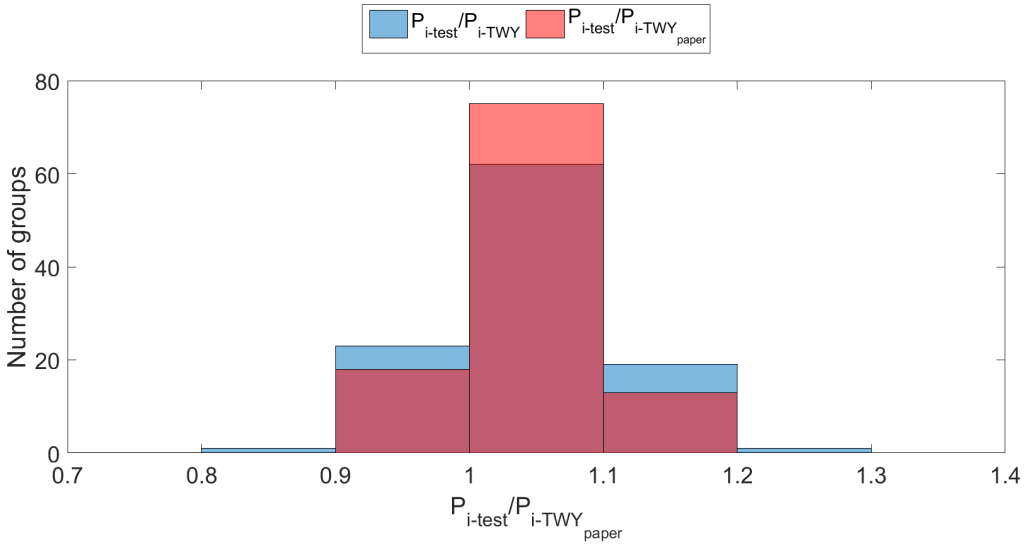

Figure F.1: The ratio of test result to the through-wall yield model presented and the reproduced through-wall yield model.

From Figure F.1 it can be seen that the reproduced model has a larger variance in the predicted rupture pressure than the model presented. However, as the reproduced model is reasonable close to the presented calculations, it was accepted to perform further investigations.